MESOPOROUS SILICA MATERIALS IN ASYMMETRIC CATALYSIS AND SELECTIVE FUNCTIONALIZATION

by

Tomohiro Seki

A thesis submitted to the Department of Chemistry

In conformity with the requirements for

the degree of Doctor of Philosophy

Queen's University

Kingston, Ontario, Canada

(February, 2013)

Abstract

This thesis describes the synthesis and application of three types of selectively functionalized mesoporous materials. In the first section, periodically ordered mesoporous organosilicas (PMOs) are prepared that have the axially chiral bidentate phosphine ligand 2,2'-Bis(diphenylphosphino)-1,1'-binaphthyl (BINAP) embedded in the wall structure. Asymmetric hydrogenation of β-ketoesters under high-pressure hydrogen gas and hydrogen transfer reduction were carried out using Ru catalysts resulting from these materials. In the next chapter, our new methodology to selectively functionalize the internal/external surface of SBA-15, a mesoporous silica whose pore diameter is ~8 nm, by blocking the pore surface with reloaded Pluronic P123® micelles is presented. Multiple tests were attempted to validate the efficiency of the methodology including nitrogen adsorption, quantitative analysis by solid state NMRs, fluorescence measurements, elemental analysis and XPS. Eventually SS NMR proved to be the most appropriate. Finally, chapter four describes ordered organic materials in catalysis, namely star-shaped polymers containing chiral core-gels synthesized from chiral 1,1'-binaphthalene-2,2'-diol (BINOL) and 1,1'-binaphthalene-2,2'-diamine (BINAM). The kinetic resolution of 1-phenyl ethanol was carried out expecting to see differential affinity of the chiral core-gel to one enantiomer of the substrate in hydrogen transfer oxidation reaction.

Acknowledgements

Statement of Originality

(Required only for Division IV Ph.D.)

I hereby certify that all of the work described within this thesis is the original work of the author. Any published (or unpublished) ideas and/or techniques from the work of others are fully acknowledged in accordance with the standard referencing practices.

(Tomohiro Seki)

(February, 2013)

Index

List of Figures

List of Tables

List of Schemes

List of Abbreviations

Å	angstrom
A.C.S.	American Chemical Society
Ac	acetyl
AcOH	acetic acid
AIBN	azobis(isobutyronitlire)
Anal. Calc.	analysis calculated
APTES	3-aminopropyl triethoxysilane
Ar	aryl
ASNC	arrays of silica nano channels
atm	atmosphere
ATRP	atom transfer radical polymerization
BET	Brunauer Emmett Teller
BINAP	2,2'-bis(diphenylphosphine)-1,1'-binaphthyl
BINAM	2,2'-diamino-1,1'-binaphthyl
BINOL	1,1'-bi-2-naphtol
BINOL-DMA	1,1'-bi-2-naphthyl dimethacrylate
BJH	Barrett Joyner Halenda
Bn	benzyl
nBu	n-butyl
bpy	2,2'-bipyridyl
br	broad

c	centi
ºC	Degree Celsius
cal	calorie
cat	catalyst
cc	co-condensed
CD	circular dichroism
CN	cyano
Co.	company
cod	1,5-cyclooctadiene
CP	cross-polarization
Cp	cyclopentadiene
Cp*	1,2,3,4,5-pentamethylcyclopentadiene
CTAB	cetyltrimethylammonium bromide
CLSM	Confocal Laser Scanning Microscopy
Cy	cyclohexane
D	diameter
d	day, doublet
Δ	delta, chemical shift
DCE	dichloroethane
de	diastereomer excess
DMB	1,4-dimethoxybenzene
DME	dimethoxyethane
DMF	N,N-dimethylformamide

DOE	Department of Energy (United States)
DSC	differential scanning calorimetry
dppf	1,1'-bis(diphenylphosphine)ferrocene
e^-	electron
EA	elemental analysis
ECPA	ethyl alpha-chlorophenylacetate
ee	enantiomeric excess
EGDMA	ethyleneglycoldimethacrylate
EI	electron impact
EO	ethylene oxide
eq.	equivalent
Et	ethyl
Et_2O	diethyl ether
EtOAc	ethylacetate
EtOH	ethanol
ESI	electron spray ionization
ESR	electron spin resonance spectroscopy
em	emission
ex	excitation
F127	poly(ethyleneoxide)$_{106}$–poly(propyleneoxide)$_{70}$–poly(ethyleneoxide)$_{106}$
FDU	Fudan University material
FID	free induction decay, flame ionization detector

FSM	folded sheets mesoporous materials
FT-IR	Fourier Transform infrared spectroscopy
g	gram
GC	gas chromatography
GNP	gold nano particles
GNR	guns and roses
GPC	gel permeation chromatography
h	hour, hextet
Hz	hertz
HBpin	pinacol borane
HETCOR	heteronuclear correlation
HMBC	heteronuclear multiple bond correlation
HMDS	hexamethyldisilazane
HT	hydrogen transfer, high tension
HTREM	high resolution transmission electron microscopy
HSQC	heteronuclear single quantum correlation
ICP-MS	inductively couples plasma mass spectroscopy
IMD	1,3-imidazole
iPr	isopropyl
J	coupling constant, joule
k	rate constant, kilo
K	Kelvin
KIT	Korea Advanced Institute of Technology material

L	litre
LA	Lewis acid
λ	wavelength
λ$_{ex}$	excitation wavelength
LB	Lewis Base, lactobacillus
M	molar, mega
m	multiplet, metre, milli, meta
MAS	magic angle spinning
MALS	multiangle light scattering
MCM	Mobil® crystalline material
Me	methyl, worst windows OS
MeCN	acetonitrile
MeOH	methanol
min	minute
MMA	methylmethacryate
mol%	mol percent
MPTMS	3-aminopropyltrimethoxysilane
MS	mass spectroscopy
n	nonatet, nano
NMR	nuclear magnetic resonance
NOE	nuclear overhauser effect
º	degree
OTf	triflate

P	pressure
p	pentatet, para
P123	poly(ethyleneoxide)$_{20}$-poly(propyleneoxide)$_{70}$-poly(ethyleneoxide)$_{20}$
Pd/C	palladium on carbon
PG	protection group
Ph	phenyl
pMMA	poly-methylmethacrylate
ppb	percent per billion
ppm	percent per million
Pr	propyl
psi	pressure per square inch
py	pyridine
q	quartet
re-	reloaded
rpm	rotations per minute
rt	room temperature
rxn	reaction
S	surface area
s	second, singlet
SBA	Santa Barbara material
SDA	structure directing agent
SDP	styryldiphenylphosphine
SEC	size exclusion chromatography

SET	single electron transfer
SFC	supercritical fluid chromatography
t	triplet
TBDMS	tertiarybutyldimethylsilyl
TBDMSCl	tertiarybutyldimethylsilylchloride
TBS	TBDMS, Tokyo broadcasting system telecision
tBu	tertiary butyl
tBuOH	tert-butyl alcohol
TEM	transmission electron spectroscopy
TEOS	tetraethylorthosilicate
THF	tetrahydrofuran
TMB	1,3,5-trimethylbenzene
TMEDA	N,N,N',N'-tetramethylethylenediamine
TMS	trimethylsilyl
TMSCl	trimethylsilylchloride
TMSOEt	ethoxytrmethylsilane
TOF	time of flight, turn over frequency
tol	toluene
TON	turn over number
UV	ultraviolet
V	volume, volt
vol%	volume percent
W/O	water in oil

wt%   weight percent

XPS   x-ray photoelectron spectroscopy

XRD   x-ray diffraction

XANES   x-ray Auger induced spectroscopy

Chapter 1

General Introduction

1.1   Mesoporous Materials

There are many types of natural and unnatural porous solids known, some of which are used extensively in industry as catalysts, absorbents and ion exchangers.[1-5] Among the porous solids in both natural and artificial materials, mesoporous silicas are those with pore diameters are in the range of 2 to 50 nm.[6] When prepared under appropriate conditions, materials with controlled and periodically ordered pores result, which provides opportunities for reaction or interaction with varieties of molecules that cannot access the smaller pores of zeolites.[7, 8] Therefore many applications of mesoporous materials as catalysts, separation/sensing materials, and absorbent have been reported in the last few decades For many of these materials, not only the size of the pores, but also the apertures of the pores are periodically ordered on this type of materials, hence applications as a support of metals, clusters, and supramolecules toward functional materials in electronics and photonics are also expected.[9-13] To realize such applications, fine control of pore size, pore geometry, particle morphology, and functionality on the internal/external pore surface is likely necessary.[14-18]

The history of mesoporous silicas began in 1971, when a synthesis of low-bulk density silica gels was first reported.[19] However there was not any description of meso structure or porosity, therefore analysis and study of this low-bulk density silica as a mesoporous material was not carried out. Indeed two decades later, in the 1990s,[20-24] the synthesis of mesoporous silicas employing a surfactant templating method was reported and these seminal reports marked the beginning of enormous interest in mesoporous materials that continues to the present day. Among these, MCM-41[21] and SBA-15[24] are the most commonly prepared and employed mesoporous silicas.

1.2   Synthesis of Mesoporous Silicas

1.2.1 Folded Sheets Material

The first modern report of the synthesis of a mesoporous silica material was a material which was synthesized from kanemite (a layered silicate salt) by treatment with alkyl trimethylammonium salts (CnTMA$^+$: n = 12 – 20), thus exchanging the interlayer sodium ions with ammonium groups. The resulting hybrid material was calcined to yield a new porous material which had a 1000 m^2g^{-1} surface area and about 2 nm pores.[20] The pore diameter and narrow distribution was found to be adjustable in the range of 2 to 4 nm by selecting the length of alkyl chains of ammonium surfactants. An ordered

hexagonal structure and one dimensional straight channels were able to be constructed by

optimizing the synthetic conditions. These materials were called FSM-16,[22] which stood

for "Folded Sheets Mechanism", since the material was believed to be prepared by

folding of the silicate sheets of kanemite by the added surfactants resulting eventually in

the observed mesoporous structure.[25] TEM analyses of the material revealed that the

thickness of the walls in the final material was the same as that of the each layer of

starting silicate material, kanemite. (Figure 1-1)[22]
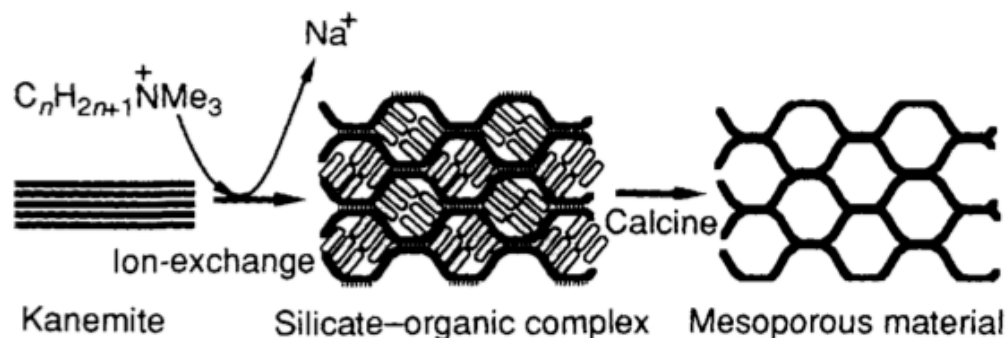
Figure 1-1. Schematic model for the formation of FSM-16[22]

However, even though the thickness of the silicate sheets did not change, the

same group reported later that most of the silicate sheets of kanemite were decomposed

and re-condensed on the surface of the surfactant micelles, such that the mechanism of

formation of the mesoporous materials shown in Figure 1-1 is not accurate, and the true

mechanism is the same as that proposed for formation of MCM-41 (described below)

under basic conditions.[25] Further evidence for the role of kanemite merely as a source of

3

silica is that under acidic conditions, where the silicate sheets were maintained and silica

monomers not generated, a tetragonal, rather than hexagonal mesoporous structure was

obtained (Figure 1-2).[26] According to Chen and co-workers, materials synthesized from

kanemite, even under basic conditions, have higher thermal stability than MCM-41,

which may imply that the original structure of the silicate sheets is retained to some

extent.[27]
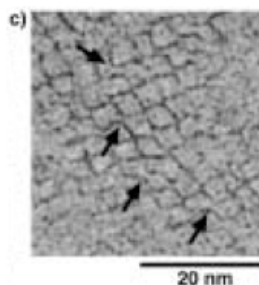
Figure 1-2. TEM image of Folded Sheet Material synthesized under acidic condition[26]

1.2.2 MCM-41 and Surfactant Templating

MCM-41,[17, 23] which stands for Mobil Crystalline Material # 41, was reported by

Mobil at almost the same time as FSM-16. MCM-41 was also synthesized in the presence

of cationic ammonium salts, but in this case, using tetraalkyl orthosilicate as the silica

source. As mentioned above, this is currently one of the most popular and versatile

mesoporous silica materials and in fact many applications of MCM-41-type materials

have been reported.[2, 18, 28-39] The pore diameters could be adjusted by changing the length

of alkyl chain of the surfactant, changing the temperature,[40] and also by the addition of mesitylene (1,3,5-trimethylbenzene) or auxiliary organic compounds as swelling agents, such that pores in the range of 2 to 10 nm could be obtained.[23] TEM images and XRD studies demonstrated the long-range hexagonal structures of these mesoporous silicas. Cubic MCM-48, and lamellar MCM-50 were subsequently reported.[41] (Figure 1-3)[42]

The first suggested mechanism for the synthesis of MCM-41 was different from that of FSM-16. In MCM-41, it was proposed that lyotropic liquid crystals formed from surfactants in aqueous media, and were expected to be templates for the final mesoporous structure (Figure 1-5).[23] Thus, the mesoporous structure would be expected to be significantly affected by the structure of the micelles, which are generated when the concentration of the surfactant becomes higher than the *critical micelle concentration* (CMC).[18]
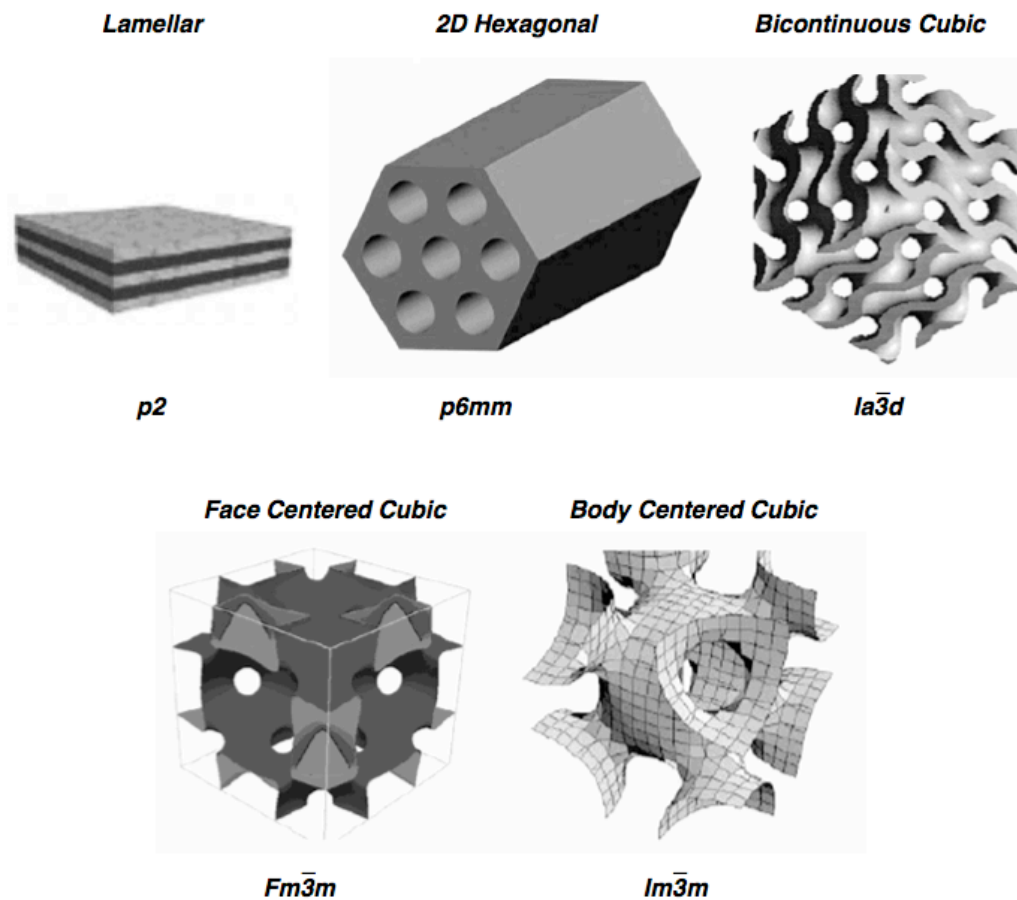
Figure 1-3. Schematic structures of pore geometries[42]

The concept is then that the shape of the micelle aggregates would be transferred to the silica as condensation progress on the micelles, such that the meso structure is maintained even after the surfactants are removed. Subsequently, however, it was reported that mesoporous silicas could be easily synthesized from micelle solutions whose concentrations were significantly lower than that needed for generation of the lyotropic liquid crystal phases. Hence, the so-called *lyotropic liquid crystal templating* (LLCT) mechanism is not widely recognized as the actual mechanism of formation,

although when the synthesis of mesoporous silica is actually performed above concentrations needed for the formation of liquid crystalline phases, mesoporous materials do in fact result.[43] In order to differentiate these conditions from typical conditions under which mesoporous silicas are made, the term "true liquid crystal templating" is used.

A recent example of mesoporous silica materials that are synthesized via a true liquid crystal templating process comes from the labs of MacLachlan and co-workers, who reported free-standing mesoporous films with chiral nematic structures (Figure 1-4).[44] The chiral nematic liquid crystal template employed was nano-crystalline Cellulose (NCC) as a suspension in acidic aqueous acetone. To that solution, a soluble silica source $Si(OMe)_4$ (tetramethylorthosilicate, TMOS) or $Si(OEt)_4$ (TEOS) was added, and the chiral nematic structure of the NCC template was replicated and maintained in the mesoporous silica even after the cellulose template was removed by calcination. Interestingly, the wavelength of the reflected light of the film can be tuned by changing the ratio of silica source to the NCC template, thus the color of the film can be controlled over the range of visible spectrum.
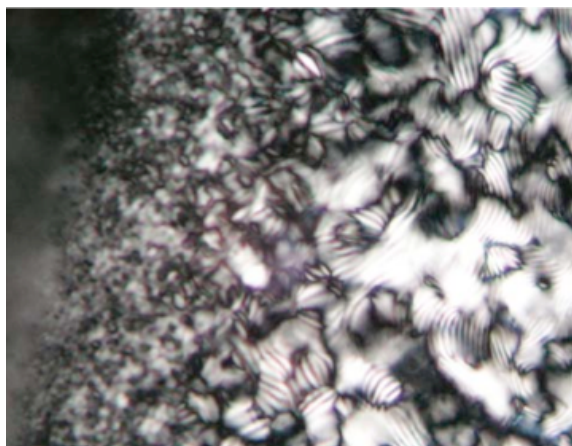
Figure 1-4.   Chiral nematic phase structure[45]

In cases where concentrations of surfactant are too low to promote the complete formation of liquid crystal phases, it is generally accepted that the early stages of silica condensation actually helps the formation of liquid-crystal-like meso-structured aggregates of micelles such that considerably lower concentrations of the surfactant are needed.[46] In cases where highly concentrated micelle solutions are employed,[43] hexagonally packed rods of micelles were observed prior to the addition of the silica source. This is not the case when low concentrations of surfactant are employed (Figure 1-5).[47]
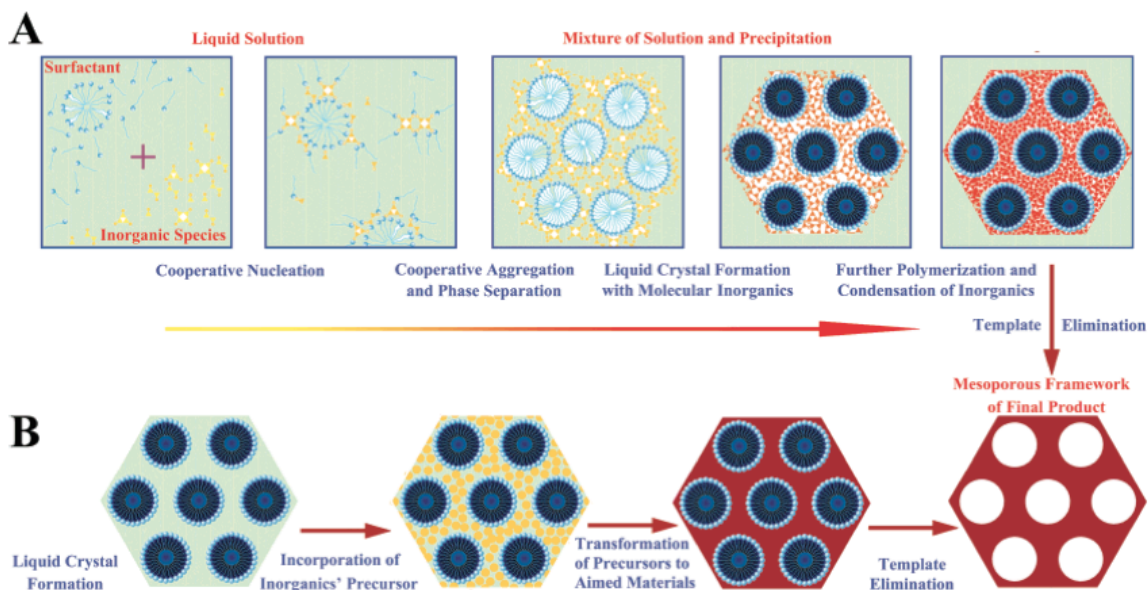
Figure 1-5. Cooperative (A) and true liquid crystal templating mechanism (B)[47]

As noted, the LLCT mechanism is not typically in effect for most mesoporous silicas syntheses, including MCM-41 that is synthesized with low concentrations of C_{16}TMA in solution. ^{14}N-NMR analysis has been shown to be a valuable tool to reveal that liquid crystal phases do not exist in the early stages of the synthesis under low dilution conditions. Instead, it is believed that the anionic silicates and the cationic ammonium head moieties of randomly aligned rod-type micelles interact to fulfill charge matching requirements and generate rod-shaped hybrid components, followed by concerted condensation of those silicates between particles resulting in the formation of hexagonally packed meso-structured material, generally called *as-synthesized* material.[48] (Figure 1-6)
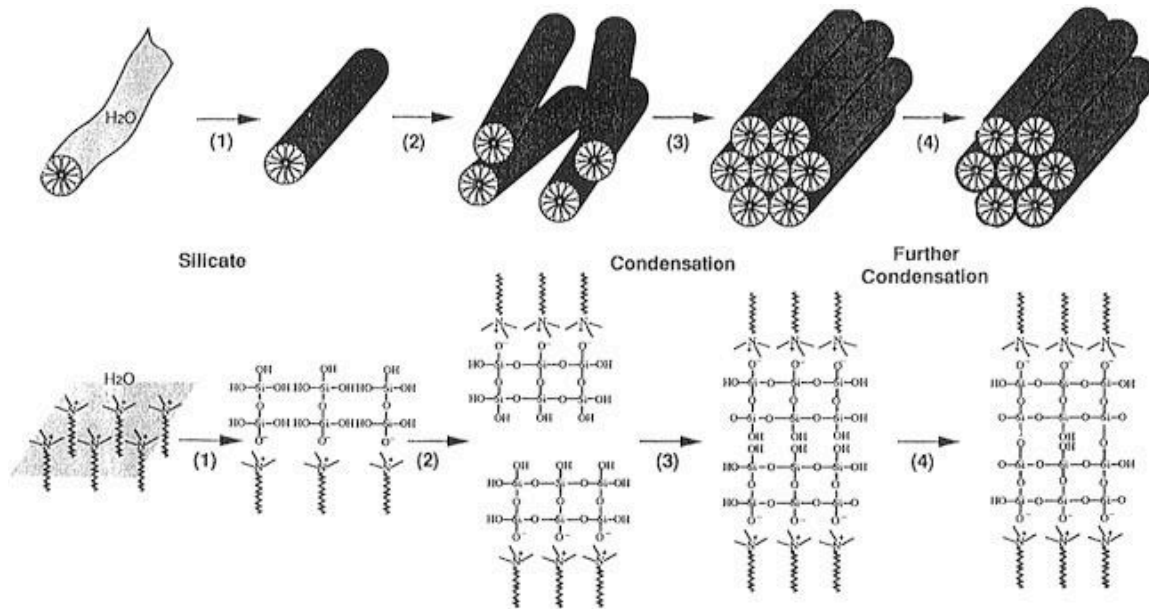
Figure 1-6.   **Concerted condensation mechanism of the surfactant templating**[48]

Although the interaction between the negatively charged silicate (I^-) and the positively charged ammonium surfactant (S^+) is the driving force to form meso-structured hybrid components (S^+I^-) in basic media, it is possible to prepare quite similar mesoporous silicas under acidic and even neutral conditions (Table 1-1).

Table 1-1. Representative combinations of effective charge matching systems and mesoporous silica materials synthesized[47]

combination pattern	surfactant	condition	representative products
S^+I^-	cationic	basic	MCM-41[23], MCM-48[23], MCM-50[23], SBA-6[49], SBA-2[41], SBA-8[50]
$S^+X^-I^+$	cationic	acidic	SBA-1[51], 2[52], 3[41]
$S^-N^+-I^-$	anionic	basic, CSDA	AMS[53]
S^0I^0	non ionic	neutral	HMS[54], MSU[55]
$S^0H^+X^-I^+$	non ionic	acidic	SBA-11, 12, 15, 16[24]

Under acidic conditions(pH < 2), anions derived from the acid (X^-) take part in ion pairing with positively charged silicas to form the $S^+X^-I^+$ combination as described by Stucky and co-workers.[56] Not only cationic surfactants but also neutral supramolecular surfactants and anionic surfactants can also be employed as templates.[24, 54, 57, 58] Although anionic surfactants (S^-) have typically proved ineffective at producing mesoporous silica, the use of silica sources that are covalently connected to alkylammonium functionalities (N^+-I^-) can be used to maintain the interaction between the micelles and silica sources. Such silica precursors are called *co-structure directing agents* (CSDA).[53]

Table 1-1 shows combinations of charge matching systems that have been shown to lead to well ordered mesoporous materials. One of the most important mesoporous materials, SBA-15, prepared under acidic conditions, will be described below.

1.2.3 SBA-15: mesoporous silica with large pore diameter

Mesoporous silica materials with much larger pore diameters (~8 nm) than MCM-41 (~2 nm) were reported by Stucky and co-workers in 1998.[24, 59] These materials were named SBA-15, and were prepared using the neutral triblock polymer P123 (Pluronic 123®) under acidic conditions. According to the seminal study by Jaroniec and co-workers,[60] SBA-15 has a hexagonally ordered mesoporous structure with micropores present within the walls, caused by the penetration of hydrophilic poly-ethyleneoxide (PEO) moieties of P123 into the silica walls (Figure 1-7, Figure 1-8).[61]
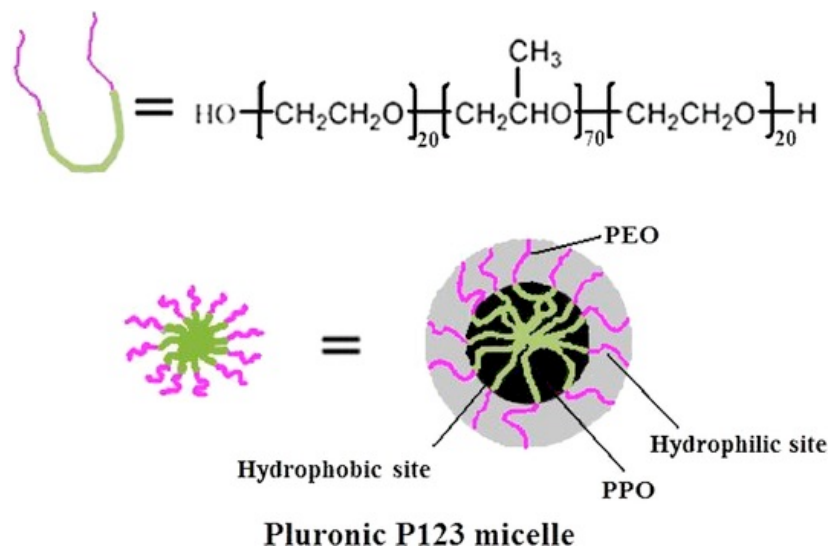
Figure 1-7. **Triblock polymer P123 as a micelle.**
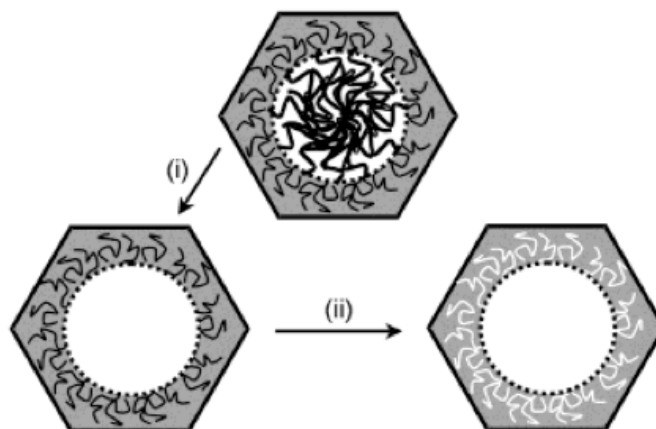
Figure 1-8. **Micropore formation in mesoporous SBA-15 where steps (i) and (ii) correspond to treatment with sulfuric acid and calcination, respectively .[62]**

The large mesopores that characterize SBA-15 are even more favorable in terms of increased accessibility and diffusion of any guest molecules inside the pores,. For this reason, in addition to the ease of synthesis, there are many publications describing applications of SBA-15 in heterogeneous catalysis, heavy metal scavenging, or in drug

delivery systems.[63-72] Selected examples of these applications are introduced in upcoming sections of this chapter.

1.2.4 Packing Factor

Despite the considerable attention paid to interactions between the surfactant, silica sources, and additive species in terms of charge matching, the balance of the charges is not the critical factor for determination of the mesostructure. The key parameter which dominates the structure of the supramolecular species is the packing factor: $g = V/aL$, where V is the excluded volume of the surfactant, a is the effective area of the surfactant head moiety, and L is the kinetic length of the alkyl chain of the surfactant.[73, 74] (Figure 1-9)
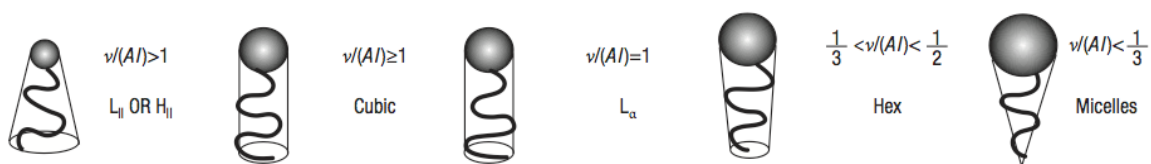
Figure 1-9.   Relationship between the packing factor (g) and the resulting micelle[74]

As the packing factor g becomes smaller, the interface in between the surfactant and the aqueous medium takes on a larger curvature, resulting in different micelle structures as shown in Scheme 1-1. This phenomenon is due to the energy optimization at the interface of the micelle consisting of the surfactant head and inorganic condensable

species. Thus the changes of the mesostructure shape as described above, correspond to the most stable structure at each temperature, concentration, pH, and charge for the selected surfactant and also the inorganic species.
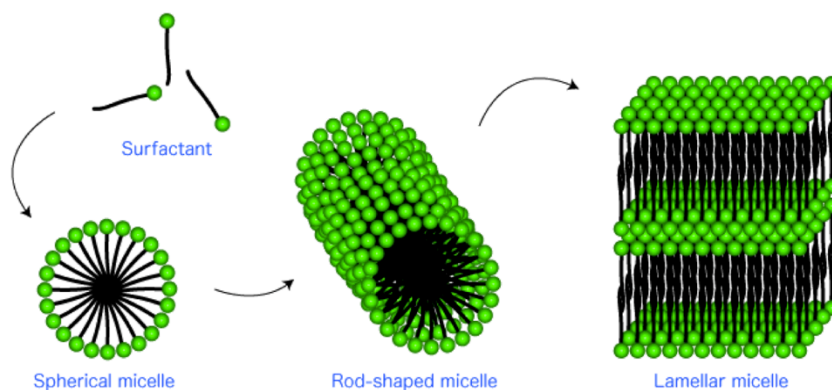
Scheme 1-1. Self-assembly of surfactants

1.3   Functionalization of Mesoporous Silicas

One of the main differences between the typical mesoporous materials that are the focus of this thesis and commonly employed zeolites is wall structure. In the case of mesoporous silica, the walls are amorphous whereas zeolites have crystalline walls which impart much greater hydrothermal stability to the latter.[75, 76] Another significant difference between zeolites and mesoporous materials is the considerably stronger Brønsted acidity of silanols in the former, which results from the presence of framework aluminum acting as a bridge as shown in Scheme 1-2.[77] In the case of mesoporous silicas,

silanols are less acidic, but more abundant, and more applicable as anchors for grafting

functional groups by a variety of approaches (Figure 1-10).
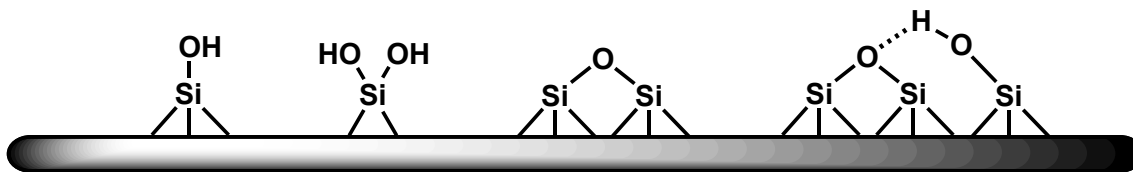
Figure 1-10. Surface silanols/siloxanes on mesoporous silicas
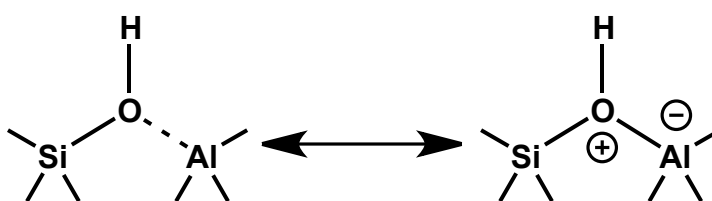
Scheme 1-2.   Resonance structure of the bridging silanol in common aluminosilica

zeolites
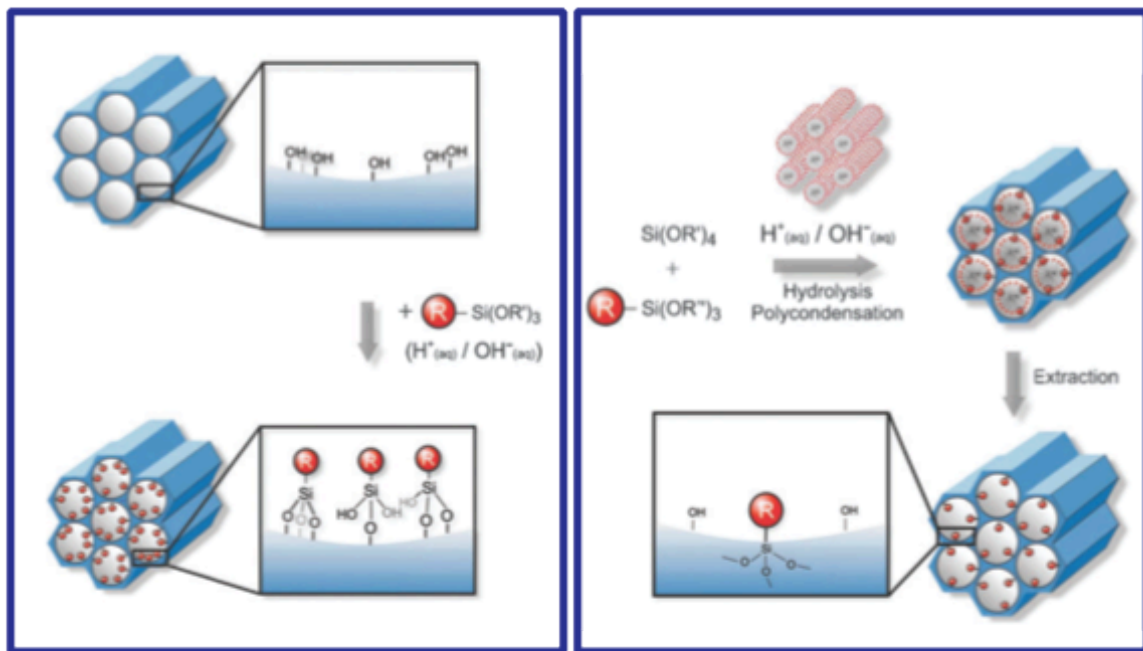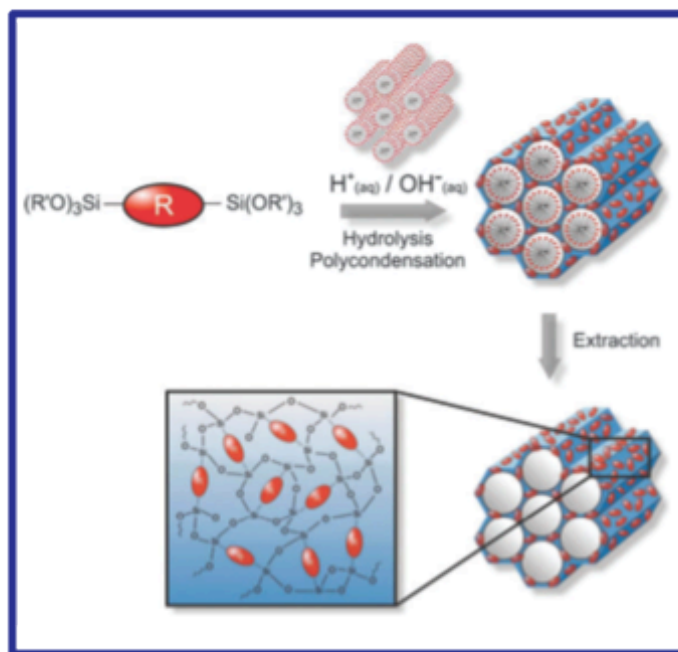
Scheme 1-3. Three methods to synthesize functionalized mesoporous silicas [78]

1.3.1 Post-synthesis grafting and co-condensation

There are three basic methods to install functionalities in or on mesoporous silicas as illustrated in Scheme 1-3.[78] The most versatile method is called post-synthesis grafting, in which a variety of functional groups containing trichloro- or trialkoxysilane groups are grafted onto the surface silanols of the mesoporous silica by reaction of these groups with surface silanols. Another method is co-condensation, in which the functionalized silyl monomers as described above are added to the micelle template solution at the same time as the silica monomers (TMOS or TEOS), yielding co-condensed materials, in which the functional monomer is incorporated into the backbone of the material. Yokoi *et al.* studied the effect of the different functionalization methods by comparing amine (*N*), ethylenediamine (*NN*), and diethylenetriamine (*NNN*) functionalized MCM-41 materials that were synthesized by both of these methods (Figure 1-11).[79]
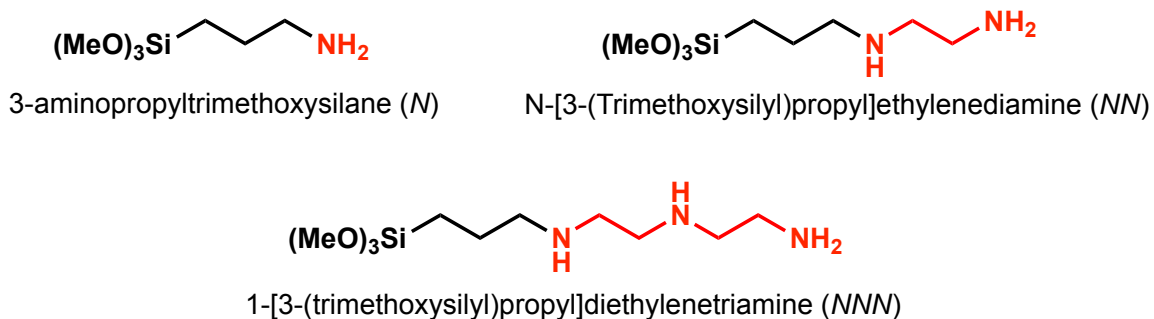
Figure 1-11. Amino functional monomers employed by Yokoi et al.[79]

Analysis of the materials by solid state ^{29}Si NMR showed that the maximum proportion of *N*, *NN*, and *NNN* monomers incorporated in the materials were 20.6, 19.2, and 17.9 mol% when post-synthesis grafting methods were employed, while 26.0, 17.0, and 6.8 mol% were incorporated by co-condensation methods. Thus the size or nature of the functional group is almost irrelevant in grafting methods, but clearly significant decreases in the amount incorporated are observed for co-condensation approaches. This implies that the hydrophilic amino moieties are strongly interacting with the surfactant micelles at the early stages of the synthesis. Which is to say, the bulky head amino groups prevent each *NN* or *NNN* monomers aligning on the micelle's polar surface closer resulting less incorporation, whereas the steric bulkiness of the head group doesn't effect too much in post-synthesis grafting as long as the surface silanols can be accessible to trimethoxysilyl group due to the flexible propyl linker.

Also Co^{2+} and Fe^{2+} adsorption tests were carried out to investigate where the functionalities were located. The results were clearly different for the two materials, such that the post-synthesis grafted material had most functionalities near the aperture of the pores and on the external surface of the particle. On the other hand, the functionalities were homogeneously dispersed on the co-condensed material. It should be also mentioned that some parts of the functional groups were not exposed to the surface but buried in the wall structure on the co-condensed material, however results from our lab have shown that very high levels of accessibility can be observed in some systems prepared by co-condensation.[80, 81] Other work from our lab has also demonstrated the protective effect that can be observed in grafting methods vs. co-condensation approaches, since reactive surface silanols still remain in the latter case.[82]

There are many applications of the functionalized mesoporous silicas of these types were reported, by installing carboxylic acid-,[29, 83] sulfonic acid-,[29, 84] phosphoric acid-,[85] phosphine-,[86] thiol-,[29, 63, 67, 71, 87-89] and amine-functionalized silyl monomers.[29, 83, 90, 91] The common applications of these functionalized materials are as catalysts, catalyst supports, metal scavengers and even heavy metal scensors. Some examples of such applications are described in the following section of this chapter.

1.3.2 Periodically ordered Mesoporous Organosilicas (PMOs)

The third method for the preparation of functionalized mesoporous silicas employs functionalized silica sources that contain bistrialkoxysilanes bridged through organic groups (Figure 1-12).[92] This is similar to co-condensing strategies, however a more robust incorporation of the functional monomer can be expected since it can be truly used as a monomer in the polymerization process due to the presence of two siloxanes (Scheme 1-3). Functionalized mesoporous silicas prepared by sole-condensation or co-condensation of such organic-bridged bissiloxy precursors are called PMOs, which stands for periodically ordered mesoporous organosilicas.[78, 93, 94] One of the advantages of PMOs is that organic functionality can be introduced with high density but without simultaneously introducing blockages in the pore cavities. The disadvantage of PMOs is that, as shown in Figure 1-12, thus far, only relatively simple groups have been introduced, such that very limited functionality is actually available, especially compared with the wide variety of functional groups that have been introduced by grafting techniques.[95] This is partly due to the more challenging synthesis of functionalized bissiloxane monomers.

21
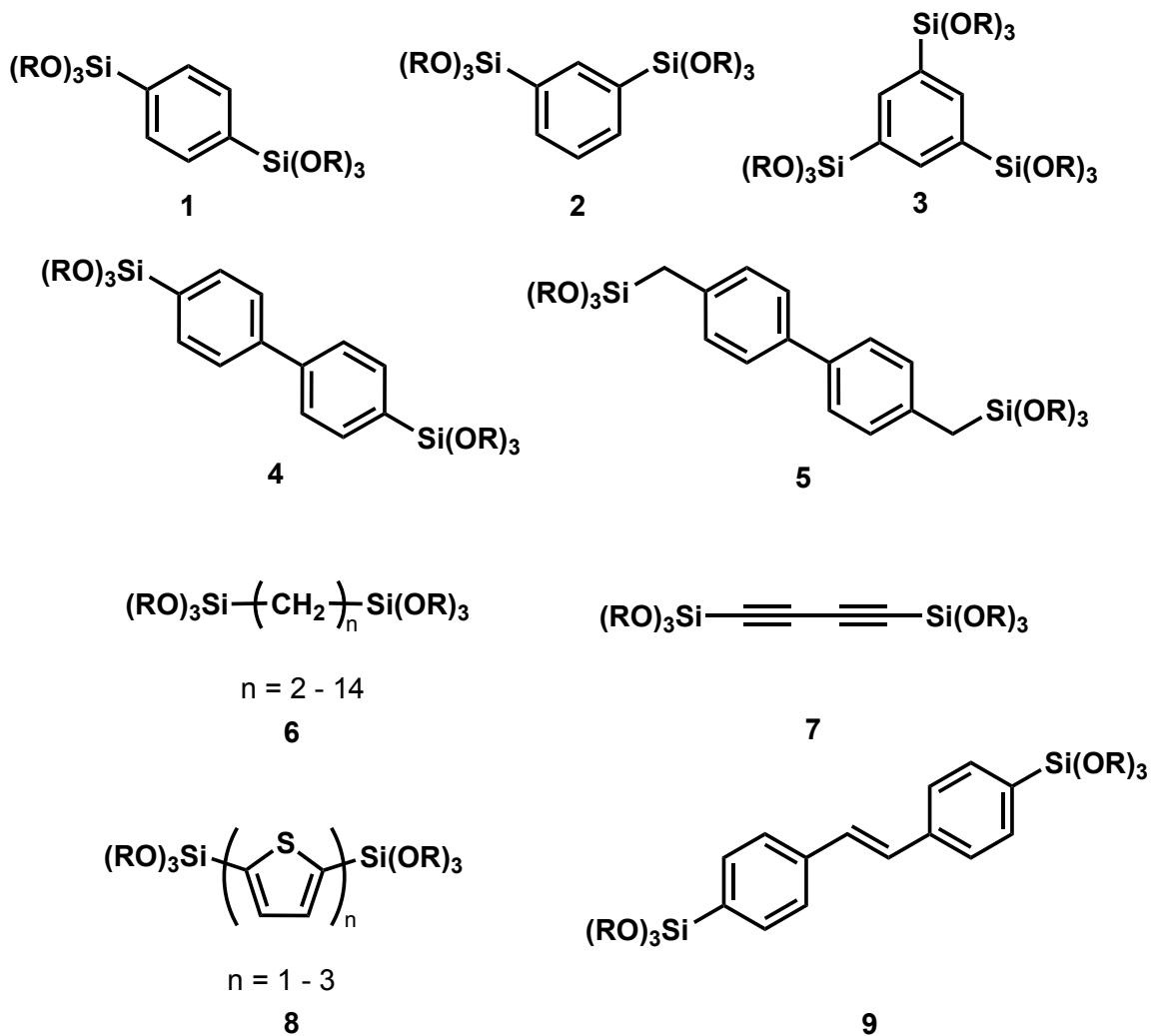
Figure 1-12.   Organic-bridged bissiloxy precursors[92]

Another interesting feature of some PMOs is that they can be prepared such that

the organic groups in the walls are stacked in crystal-like fashion.[96, 97] This is typically

observed for organic-bridged bissiloxy precursors in which the bridging groups are rigid

aromatic species such as phenylene and biphenylene (Figure 1-13)[92] (Figure 1-14).[93]
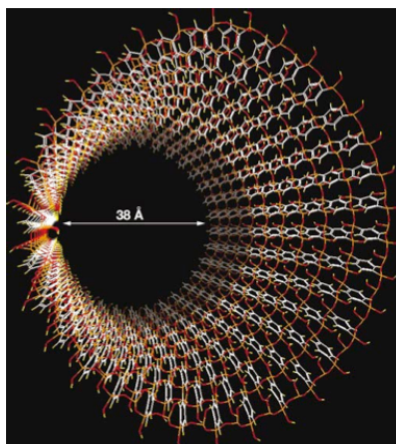
Figure 1-13. CG image of crystal-like framework of phenylene-bridged PMO[92]
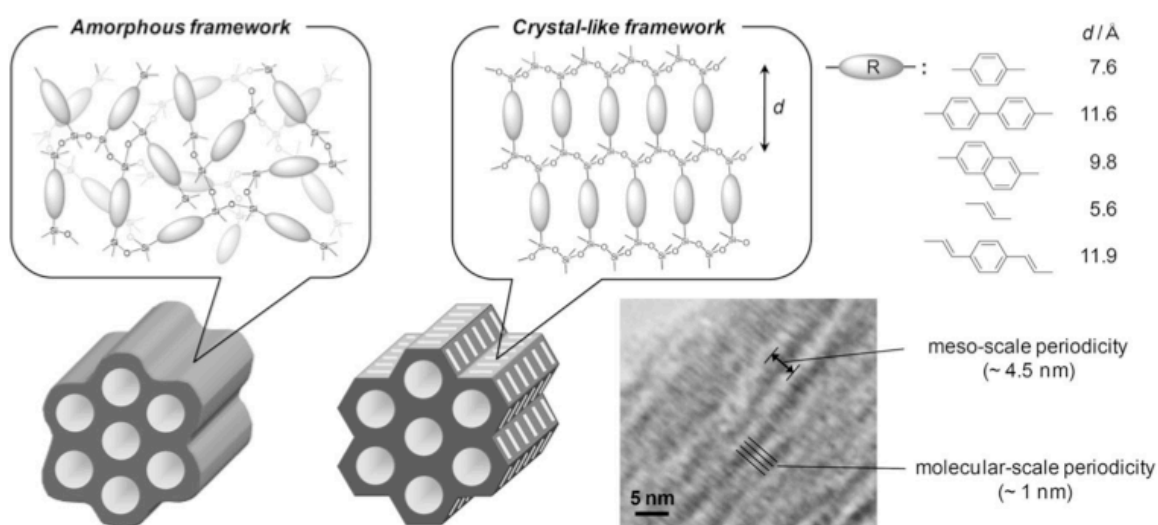
Figure 1-14. Amorphous and Crystal-like frameworks of PMOs, a TEM image of naphthylene-bridged PMO[93]

The stacked π system in the walls of such PMO materials have been shown to exert light harvesting antenna effects by resonance energy transfer.[9, 11-13] Inagaki and co-workers reported a CO_2 reduction to generate CO by introducing a rhenium catalyst in the

pore of biphenylene-bridged PMO (BPh-PMO) synthesized from **4**.[9] The light energy

captured by the BPh-PMO wall was transferred to the Re catalyst which reduced CO_2 to

CO in the presence of triethanolamine as a sacrificial reagent[98-100] (Figure 1-15). The

Re/BPh-PMO catalyst was irradiated with 280 nm wavelength light and showed a low

rate decomposition of the catalyst compared with solutions of the molecular Re catalyst

without the BPh-PMO support, which decomposed quickly under the same conditions.

Even though the Re catalyst in the solution was successfully excited under 365 nm light

without decomposition, it was less effective due to the longer wave length required to

minimize decomposition, and the resulting lower light energy.
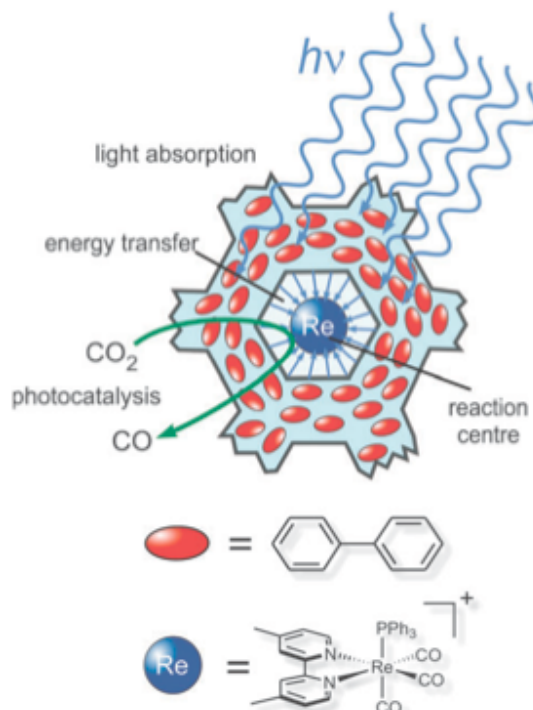
Figure 1-15.   Enhanced photo catalysis by biphenylene-bridged PMO[78]

1.4   Chiral PMOs

PMOs that have chiral organic bridging groups in the wall structure have also been reported (Figure 1-16).[101-106] Under optimized condensation conditions in the presence of surfactant templates, the resulting PMOs show optical activity when examined by circular dichroism (CD) or optical rotation.[102, 103, 106] With many precursors having chiral centers at chemically vulnerable positions, optimization of the condensation conditions must be done with care. For example, PMOs synthesized from **10** and **11** yielded chiral PMOs under acidic conditions for condensation whereas basic conditions

resulted in racemized PMOs.[101, 102] With regard to this point, precursors **12** and **13** are considerably more stable.[106, 107]
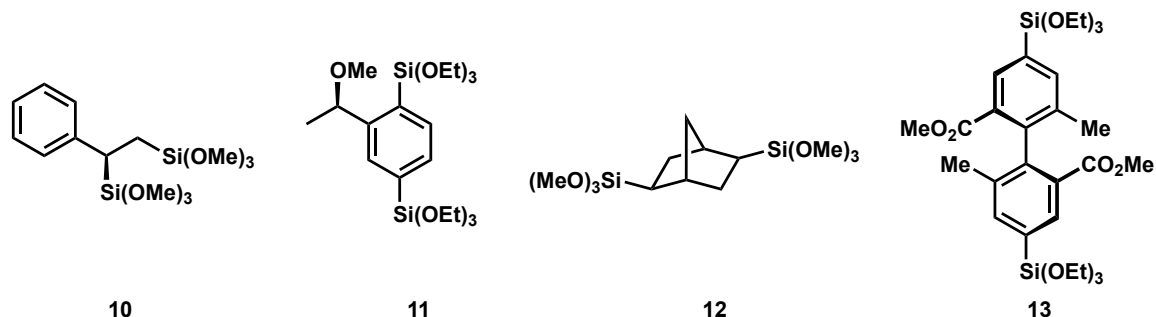
Figure 1-16. Representative chiral organic-bridged PMO precursors

Previous work in our lab included the report of a chiral PMO prepared by co-condensation of achiral biphenylene-bridged precursor **4** and chiral monomer **13** as a chiral dopant. Interestingly, the CD signal of the resulting PMO shows a red shifted signal compared with the CD signal of the chiral dopant **13** (Figure 1-17). This signal is not observed in materials prepared with pure silica rather than the bulk organic monomer **4**. This phenomenon implies that the chirality of the chiral dopant is transferred to the bulk biphenylene constituent through π-π stacking at certain local areas (Scheme 1-4).[106] DFT calculations are in agreement with this interpretation.
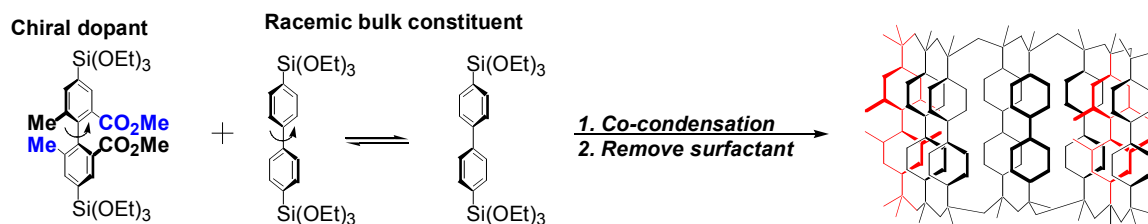
Scheme 1-4. **Chirality transfer on co-condensed biphenylene-bridged PMO**
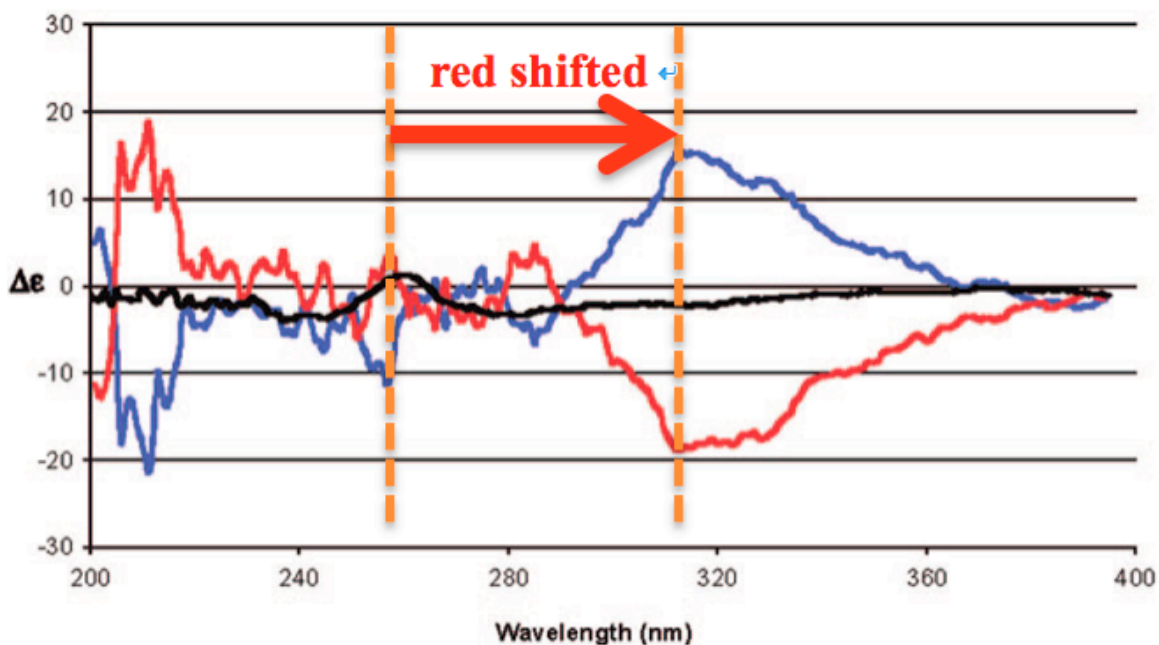
Figure 1-17. **CD spectra of co-condensed chiral materials (blue and red) and chiral dopant monomer 13 (black)[106]**

In order to assess how the chiral PMO can transfer chirality to the guest species, in collaboration with the Lemieux group, our group examined the interaction of chiral PMO materials with liquid crystals when the liquid crystal was introduced to the mesopores of a chiral PMO material.[108] The material chosen was that synthesized from

cocondensation of **4** and **14** was prepared as the chiral dopant material, and achiral liquid

crystals **5CB** and **9OO4** were employed (Figure 1-18).

14

5CB

9OO4
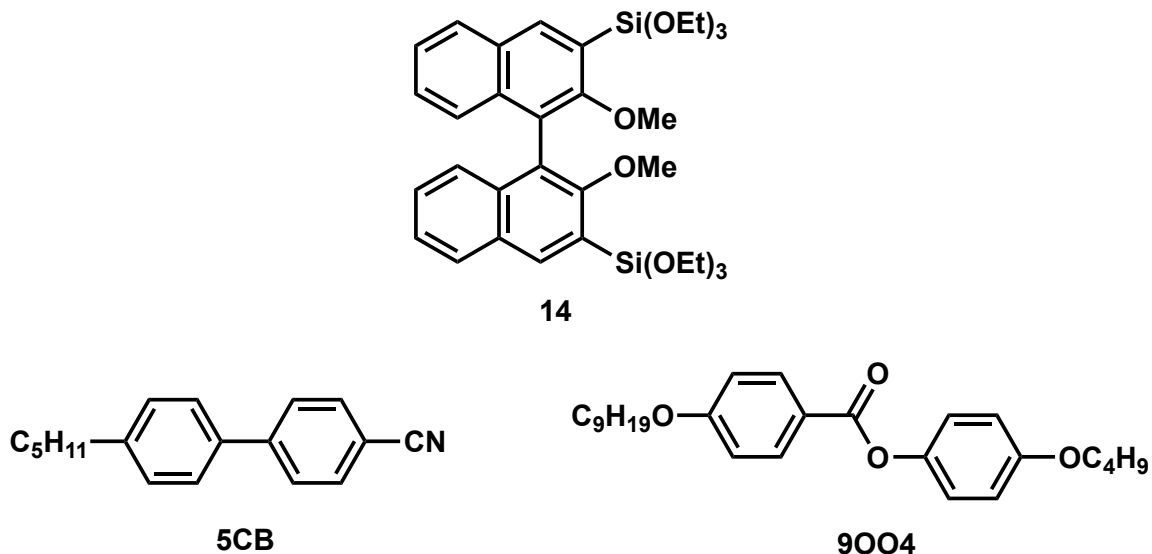
Figure 1-18.   Achiral liquid crystal guest species

Interestingly, chiral PMO materials whose mesopores were free of the templating

surfactant induced a measurable helical pitch in **5CB** and an electroclinic effect in **9OO4**,

whereas the same chiral PMO whose mesopores were blocked by the templating

surfactant showed no chirality transfer to the liquid crystal. These results are consistent

with the chirality transfer taking place inside the pores and propagating to the liquid

crystal phase outside the pores, thus the inner structure of the chiral PMO of this type is

indeed chiral.

1.5   Applications of the functionalized mesoporous silicas and PMOs

1.5.1 Transition metal scavenger and heterogeneous catalyst
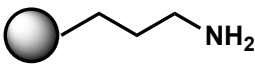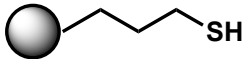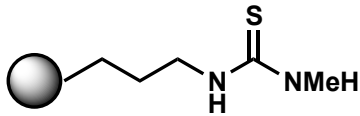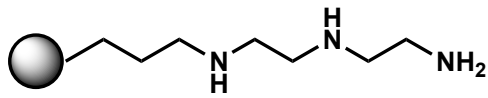
Even with heterogeneous catalysts, solubilization and leaching of the metal species from the support or ligand site often occurs.[109-111] Scavenging these released metals is especially important when pharmaceutical molecules containing heteroatoms are prepared, since standards for metal contamination are high (Table 1-2), and coordination of the heteroatoms in the product to the metals can impede purification. Therefore the invention of effective and cheap metal scavengers[68, 87, 112-116] that directly and selectively absorb precious and/or toxic metal species when the reaction is completed, or from the waste solvent is still an important issue. There are many metal scavengers commercially available (Table 1-3). Most are amorphous silica- or polymer-supported amines, thiols, or their analogues.

Table 1-2.   **Recommended oral and parenteral Permitted Daily Exposures (PDEs)**

for 14 elements in pharmaceutical substances by European Medicines Agency [117]

Element	Oral PDE (μg/kg^a/day)	Parenteral PDE (μg/kg^a/day)
Pt, Pd, Ir, Rh, Ru, Os	2.6 (group)	0.25 (group)
Mo	5	2.5
V	10	0.5
Cu	50	10
Ni	20	2
Cr	25	2.5
Mn	100	5
Zn	300	30
Fe	250	25

^{a} Body weight of the patient.

Table 1-3.   **Examples of commercially available metal scavengers on silica**

support

structure	functionality	price and loading^a
	amino propyl	100 g 323.00 CAD 1.5 - 2.0 mmol/g
	mercapto propyl	100 g 428.00 CAD 1.0 - 1.5 mmol/g
	methyl thiourea	100 g 546.00 CAD 1.0 - 1.5 mmol/g
	triamine	100 g 294.00 CAD 0.5 - 1.5 mmol/g

^{a} Sigma-Aldrich online catalog, December 2012

Taking advantage of the greater surface area and faster diffusion of the guest molecules in mesoporous silicas compared to amorphous silicas or organic polymers, our group has studied a variety of functionalized SBA-15 materials at metal scavengers.[63, 65, 68, 82, 116, 118-121] In particular, materials prepared in which mercaptopropyl trimethoxysilane (MPTMS) was cocondensed or grafted on the SBA-15 (denoted as SBA-15-SH, Scheme 1-5) were studied in detail as scavengers for Pd.[68]
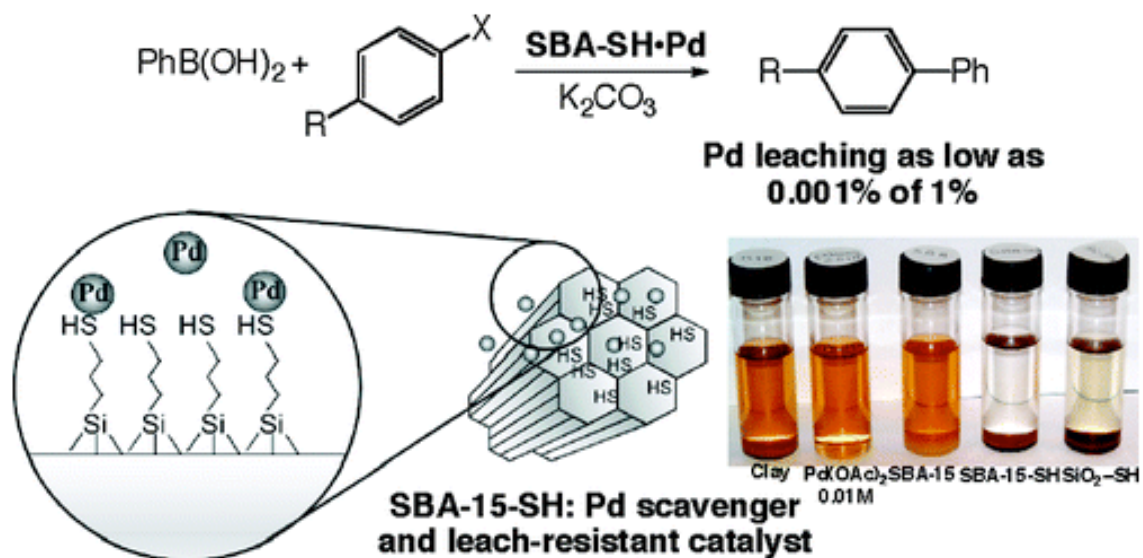
Scheme 1-5. Palladium on SBA-15-SH, a heterogeneous recyclable catalyst for cross coupling reactions[68] A series of attempted Pd(II) scavenging are shown in the photograph. Clay and SBA-15 showed almost no scavenging, whereas SBA-15-SH effectively worked to show the disappearance of the orange color due to Pd(II) scavenging. Thiol modified silica gel (SiO₂-SH) also scavenged Pd(II) but not as effectively as SBA-15-SH.

This work was initially inspired by the thiol-functionalized mesoporous silica mercury scavengers that were reported by Fryxell *et al.*[122] and Pinnavaia *et al.*[123] Also Kang *et al.*[71, 124] had reported that SBA-15-SH has a higher affinity for palladium and platinum than other metals. Remarkably, the resulting material after scavenging palladium by SBA-15-SH was itself catalytically active in cross coupling reactions. The catalyst material, Pd/SBA-15-SH, was prepared from a fresh palladium solution of palladium acetate in THF by addition of SBA-15-SH as Pd / SH = 1 / 2 molar ratio. After

one hour stirring of the suspension at room temperature, the pale orange powder was isolated by simple filtration. ICPMS analysis of the filtrate revealed that most of palladium was successfully "scavenged". This palladium catalyst can be easily handled under open air, and showed high catalytic activity in Suzuki-Miyaura,[65, 68, 82, 116, 118, 120] Sonogashira,[120] and Mizoroki-Heck[68, 116] reactions. Recycling over five uses was demonstrated.[82] Addition to the palladium scavenging, amine-functionalized SBA-15 was effective for ruthenium scavenging[121] thus the choice of the scavenger depended on the target metal species is important.

1.5.2 Portable heavy metal sensor with tetrasulfide PMO film

Addition to the synthetic organic chemistry, metal scavenging is crucial in mining industry and heavy industry in terms of to avoid pollution of the environment.[125-132] Moreover, contaminant monitoring is important as well before planning any environmental cleanups. Our group, in collaboration with Dr. Hans-Peter Loock at Queen's University, reported PMO films as the key component for fiber optic-based heavy metal sensors (Scheme 1-6).[133, 134] This device is small and light weight and thus can be used in remote sites for instant monitoring, whereas typical analytical methods

require sending samples away for ICPMS, which is costly in terms of dollars and time

(Figure 1-19).[134]
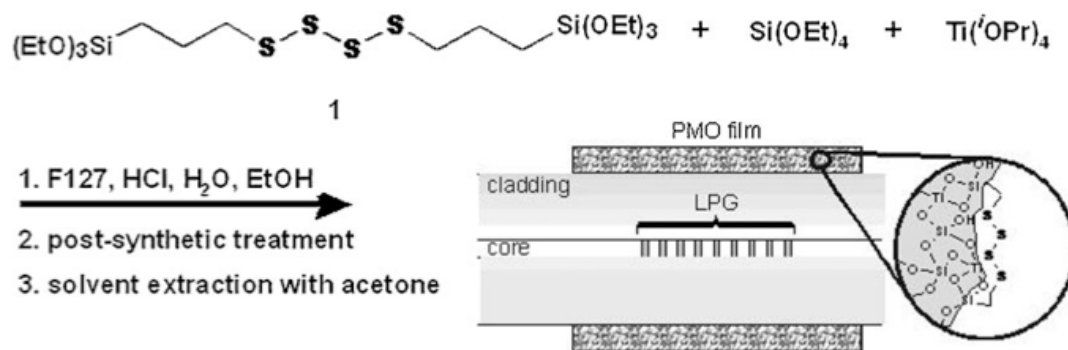
Scheme 1-6.   Tetrasulfide-bridged PMO film, coated on optic fiber[133]
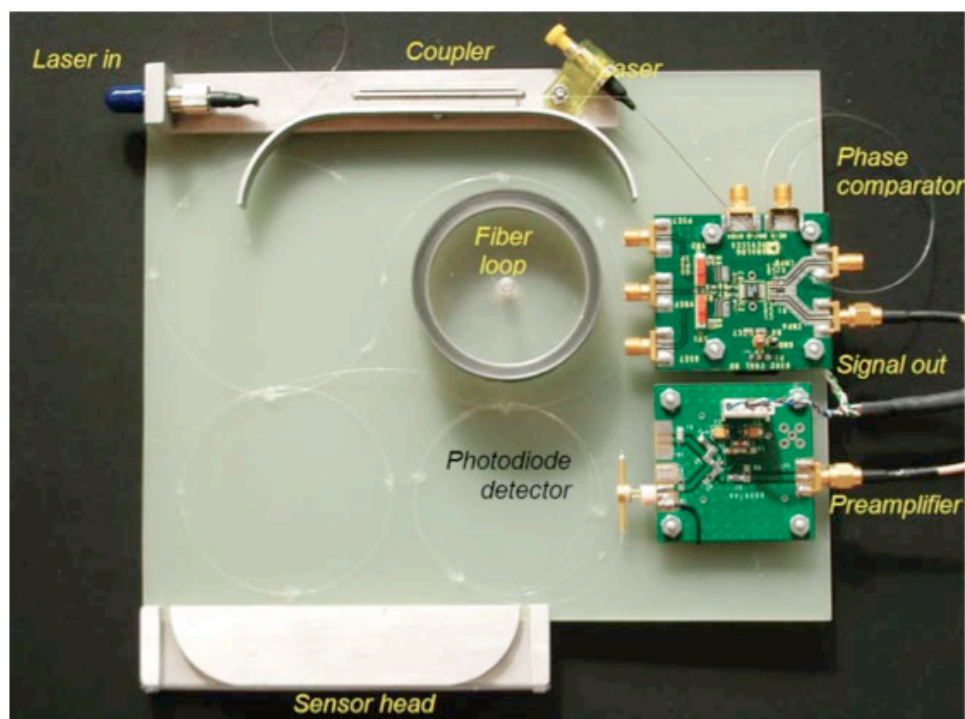
Figure 1-19.   Picture of the compact metal sensor including the component of Scheme 1-6 [134]

1.6 Nitrogen Adsorption Analysis for Mesoporous Materials

Nitrogen adsorption analysis is the most common method employed to study physical characteristics of mesoporous materials. The details of this methodology are summarized in IUPAC's 1985 report.[135] Practically, a known mass of the porous material is introduced into a chamber, evacuated, then cooled to liquid nitrogen (for example) temperatures, and nitrogen gas is slowly introduced. The volume, temperature and pressure of the sample chamber are then measured simultaneously to determine what volume of nitrogen gas is adsorbed on the cold sample material at every step as relative pressure is increased. Since the mass of the sample is known, one is able to estimate the actual surface area, pore diameter distribution, volume of the porous space, and hydrophilicity of the surface of the sample. In general, the results of nitrogen adsorption analyses are depicted by isotherm plots, in which the X-axis shows the relative pressure of nitrogen gas, and the Y-axis corresponds to the volume of the nitrogen gas adsorbed (Figure 1-20). When the sample is mesoporous, an isotherm plot as shown in Figure 1-20 results. The steeper area of the plot at low pressure corresponds to the initial step of nitrogen adsorption, which is formation of a nitrogen monolayer on the reactive bare surface. Once the monolayer has completely formed, successive multilayer formation

steps appear as flat domains on the plot. At certain relative pressures, which are related to

the size of the mesopores, a capillary effect comes into play resulting in the absorption of

significant amounts of nitrogen over small changes in relative pressure.
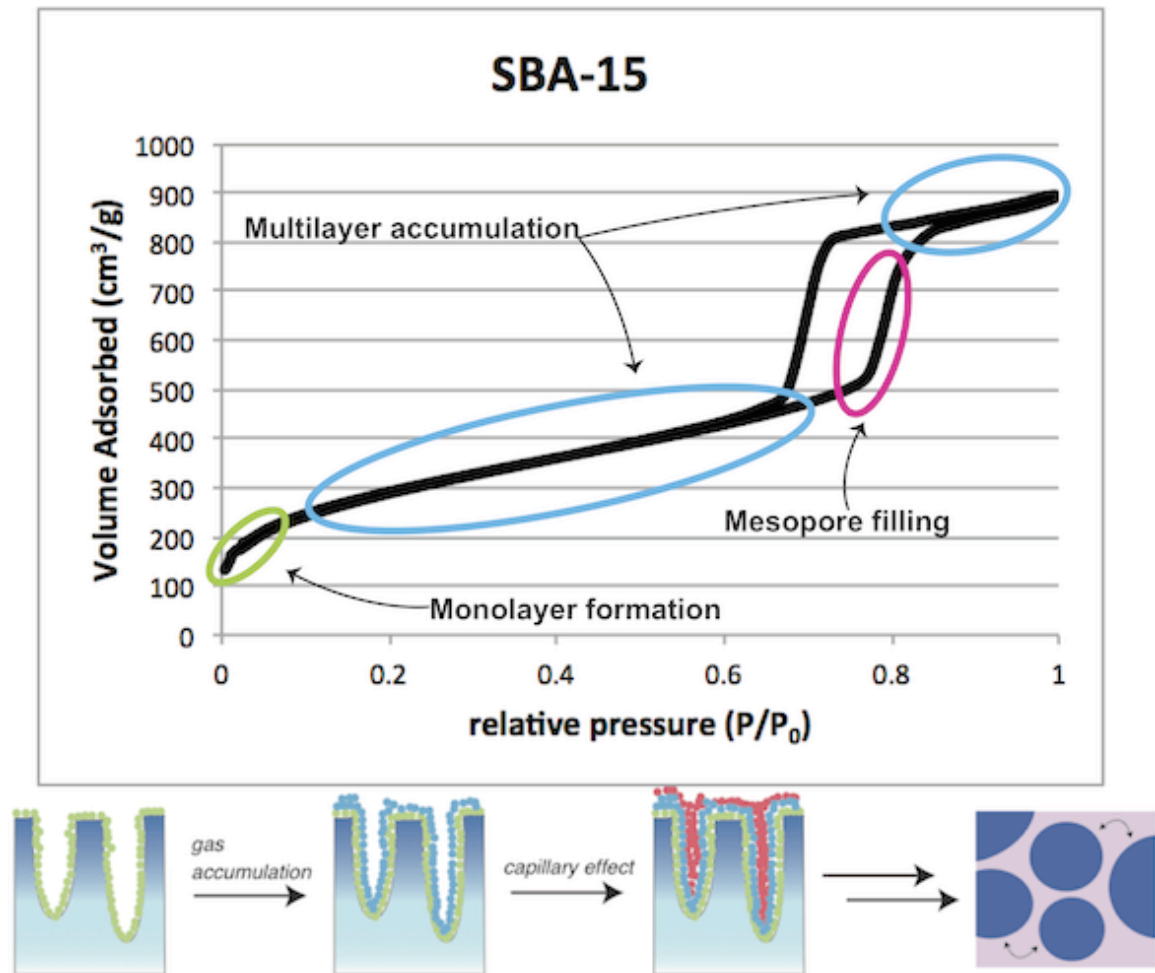
Figure 1-20. Schematic sketch of nitrogen adsorption isotherm plot of SBA-15

1.6.1 BET plot and BJH method

Mathematically, there are two standard calculation methods often employed to

estimate surface area, pore diameter distribution, pore volume, surface hydrophilicity of

the sample materials; BET (Brunauer, Emmet and Teller) plot, and BJH (Barrett, Joyner

and Holenda) methods. In a BET plot, the parameters are calculated by following

equation (equation 1-1). Increasingly, DFT methods are also employed to estimate

surface parameters from data obtained by porosimetry. [136-138]

$$\frac{x}{V_a(1-x)} = \frac{1}{V_mC} + \frac{(C-1)}{V_mC}x \qquad (x = P/P_0)$$

(Equation 1-1)

x is relative pressure P/P_0, volume absorbed at each relative pressure is V_a,

volume absorbed to form monolayer is V_m, and BET constant is C. The BET constant,

$C \propto exp\left(\frac{Q_1-Q_L}{RT}\right)$ representing a qualitative indicator of the hydrophobicity of a surface

within a series of closely related materials in which Q_1 is heat of adsorption to form the

first monolayer, Q_L is heat of adsorption for following multilayers, R is gas constant, and

T is temperature. V_a and x are observed from the actual measurement, and placing the

relative pressure x on X-axis and $\frac{x}{V_a(1-x)}$ on Y-axis gives a plot of linear line whose

slope is $\frac{(C-1)}{V_mC}$ and Y-intercept is $\frac{1}{V_mC}$, this plot is called BET plot. And then V_m and C

are calculated by substituting the X and Y values from the plot. According to the cross-

sectional area of nitrogen gas, 0.162 nm^2, and V_m obtained from BET plot, the surface

area is simply calculated.

BJH method is based on Kelvin model of pore filling (equation 1-2), and approximating the shape of pores as cylindrical.[58]

$$\ln \frac{p}{p_0} = \frac{2\gamma V_m}{rRT}$$
(equation 1-2)

p is the each equilibrium vapor pressure, p_0 is the saturated pressure, γ is the surface tension of the liquid condensate generated from nitrogen gas, V_m is the molar volume of the liquid condensate generated from nitrogen gas, R is the gas constant, r is the radius of capillary in cm unit and T is the temperature.
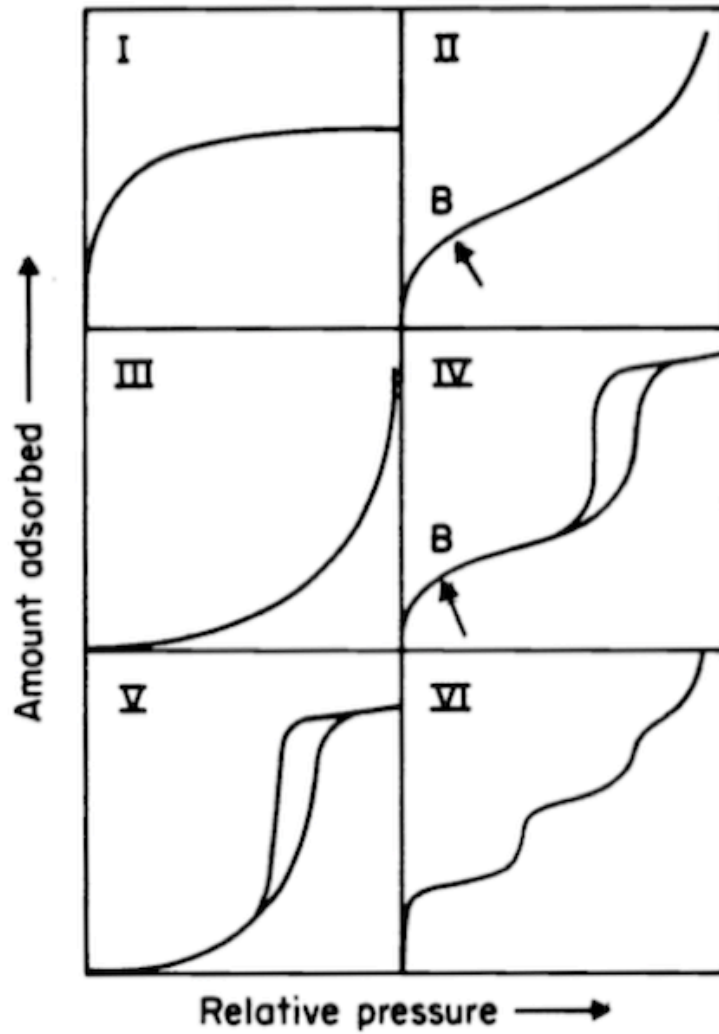
Figure 1-21. Typical isotherm curve shapes[135]

Even though some calculations are needed to estimate the physical characteristics of the sample materials, the isotherm plot obtained by nitrogen adsorption measurement gives quick idea of the sample information simply by the shape of the curves (Figure 1-21).[135] Type I is microporous absorbent, type II is non-porous or marcroporous absorbent, type III is non-porous absorbent with weak adsorbate-absorbent interactions,

type IV is mesoporous absorbent, type V is porous absorbent with weak adsorbate-adsorbent interactions, and type VI is molecularly flat adsorbent.

Among the materials of type IV and V, the adsorption and desorption curve may not perfectly match in the mesopore region. This phenomenon is called *hysteresis*, which is related to the capillary effect in porous materials (Figure 1-22).[135] There are multiple types of pore shape models that can lead to this effect, such as cylindrical, slits (spaces in between parallel sheets), inkbottle, and interparticle spaces in aggregates of spherical particles since each has a special irreversible process of condensation and vaporization of the adsorbate gas.[139] Thus, the shape of the isotherm curve provides critical information with respect to the shape of the mesopore. In general, both adsorption and desorption curves follow one another in the lower relative pressure domain, then the hysteresis is observed at the mesopore filling step.

The general classification of hysteresis is given in Figure 1-22. Type H1 shows a vertically parallel hysteresis loop, this type of isotherm curve corresponds to the aggregates of uniform sized spherical particles. Type H4 shows horizontally parallel loop, which implies the slits type mesopores. Type H3 connotes the slit type mesopores as well, but the isotherm curve is a mixture of H1 and H4 types. Type H2 is the typical shape for

silica gels, and it is difficult to determine the pore shape from the isotherm curve for

these materials.
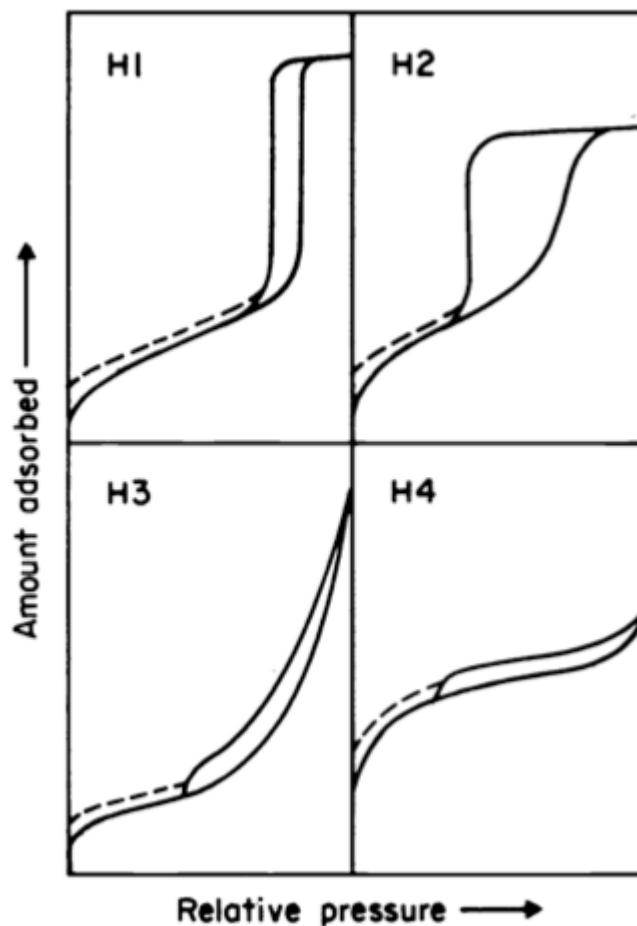
Figure 1-22. Hysteresis classification[135]

1.7 Summary

As mentioned above, mesoporous silica materials have applications in a variety of

areas such as catalysis, absorbents and ion exchangers. Because of the chemically flexible

character of the surface silanols and silica framework, there are three functionalization

techniques available, and selection of the method from these three depends on the final usage. Thus, post-synthesis grafting is the easiest pathway to give functionalized materials from versatile mesoporous silicas and a wide range of functionalized alkylsiloxy reagents are available in most cases. Using the same functionalized precursor with TEOS or TMOS by co-condensation method is also a simple method but optimization of condensation conditions is often needed. PMO synthesis from organic-bridged bissiloxy precursors can result in fundamentally new materials with new properties such as observed in light harvesting materials, however the synthesis of the functional precursors still needs improvements especially for the installation of alkoxysilyl groups on the target functional organic molecules. To study the mechanism and take advantage of mesoporous catalysts, finely controlled immobilization of the catalysts on the pore surface is needed, however there are no established methods to control the grafting domain on the large pore materials such as SBA-15. Also, similar to the synthesis of chiral PMO materials from bissiloxy organic precursors, chiral polymer gels can be synthesized from divinyl monomers. Star shaped polymers are one such polymer gel comprised of linear polymer arms growing on the exterior of a particle, which lends solubility in certain solvents. Attempts to synthesize star polymers that contain similar chiral components to the chiral PMOs in the core structure will be

42

discussed in this thesis. In the following chapters of this thesis, the synthesis and use in

catalysis of a chiral phosphine ligand PMO, surface–selective passivation of SBA-15, and

star shaped polymers with chiral core-gel are discussed. The goal of this thesis is to

suggest a method and a tactics for preparing heterogeneous catalysts in which the

catalytic species are immobilized by effectively taking advantage of the characteristics of

the porous support. This will continue to new inventions of powerful heterogeneous

catalysts that can be employed even in the synthesis of complicated fine molecules by

showing improved activity relative to the homogeneous catalysts, not only in terms of the

recyclability or easiness of separation due to heterogeneity but also using the porosity or

finely controlled nano-space.

1.8　References

1.　　　Wang, Z. P.; Yu, J. H. and Xu, R. R., *Chem. Soc. Rev.* **2012,** *41*, 1729.

2.　　　Taguchi, A. and Schuth, F., *Microporous Mesoporous Mater.* **2005,** *77*, 1.

3.　　　Stein, A., *Adv. Mater.* **2003,** *15*, 763.

4.　　　Davis, M. E., *Nature* **2002,** *417*, 813.

5.　　　Corma, A., *Chem. Rev.* **1995,** *95*, 559.

6.　　　Kerker, M. and Kratohvil, J. P., *Pure Appl. Chem.* **1983,** *55*, 931.

7.   Baerlocher, C.; Meier, W. M.; Olson, D. and Meier, W. M., *Atlas of zeolite framework types*. 5th rev. ed.; Elsevier: Amsterdam ; New York, 2001; p vi.

8.   International_Zeolite_Association Database of Zeolite Structures. http://www.iza-structure.org/databases/.

9.   Takeda, H.; Ohashi, M.; Tani, T.; Ishitani, O. and Inagaki, S., *Inorg Chem* **2010,** *49*, 4554.

10.   Tani, T.; Mizoshita, N. and Inagaki, S., *J. Mater. Chem.* **2009,** *19*, 4451.

11.   Takeda, H.; Goto, Y.; Maegawa, Y.; Ohsuna, T.; Tani, T.; Matsumoto, K.; Shimada, T. and Inagaki, S., *Chem. Commun.* **2009**, 6032.

12.   Ohashi, M.; Aoki, M.; Yamanaka, K.; Nakajima, K.; Ohsuna, T.; Tani, T. and Inagaki, S., *Chem. Eur. J.* **2009,** *15*, 13041.

13.   Inagaki, S.; Ohtani, O.; Goto, Y.; Okamoto, K.; Ikai, M.; Yamanaka, K.; Tani, T. and Okada, T., *Angew Chem Int Ed Engl* **2009,** *48*, 4042.

14.   Kapoor, M. P. and Inagaki, S., *Bull. Chem. Soc. Jpn.* **2006,** *79*, 1463.

15.   Miyazawa, K. and Inagaki, S., *Chem. Commun.* **2000**, 2121.

16.   Han, Y.; Zhao, L. and Ying, J. Y., *Advanced Materials (Weinheim, Germany)* **2007,** *19*, 2454.

17.   Stein, A., *Advanced Materials (Weinheim, Germany)* **2003,** *15*, 763.

18.   Raman, N. K.; Anderson, M. T. and Brinker, C. J., *Chem. Mater.* **1996,** *8*, 1682.

19.   Chiola, V.; Ritsko, J. E. and Vanderpool, C. D., *US Patent* **1971**, 3.

20.   Yanagisawa, T.; Shimizu, T.; Kuroda, K. and Kato, C., *Bull. Chem. Soc. Jpn.* **1990,** *63*, 988.

21.   Kresge, C. T.; Leonowicz, M. E.; Roth, W. J.; Vartuli, J. C. and Beck, J. S., *Nature* **1992,** *359*, 710.

22.   Inagaki, S.; Fukushima, Y. and Kuroda, K., *Journal of the Chemical Society-Chemical Communications* **1993**, 680.

23.   Beck, J. S.; Vartuli, J. C.; Roth, W. J.; Leonowicz, M. E.; Kresge, C. T.; Schmitt, K. D.; Chu, C. T. W.; Olson, D. H. and Sheppard, E. W., *J. Am. Chem. Soc.* **1992,** *114*, 10834.

24.   Zhao, D. Y.; Feng, J. L.; Huo, Q. S.; Melosh, N.; Fredrickson, G. H.; Chmelka, B. F. and Stucky, G. D., *Science* **1998,** *279*, 548.

25.   Sakamoto, Y.; Inagaki, S.; Ohsuna, T.; Ohnishi, N.; Fukushima, Y.; Nozue, Y. and Terasaki, O., *Microporous Mesoporous Mater.* **1998,** *21*, 589.

26.   Kimura, T.; Kamata, T.; Fuziwara, M.; Takano, Y.; Kaneda, M.; Sakamoto, Y.; Terasaki, O.; Sugahara, Y. and Kuroda, K., *Angew. Chem., In. Ed.* **2000,** *39*, 3855.

27.   Chen, C. Y.; Xiao, S. Q. and Davis, M. E., *Microporous Mater.* **1995,** *4*, 1.

28.   Hara, K.; Akahane, S.; Wiench, J. W.; Burgin, B. R.; Ishito, N.; Lin, V. S. Y.;

Fukuoka, A. and Pruski, M., *J. Phys. Chem. C* **2012,** *116*, 7083.

29.   Mondal, J.; Nandi, M.; Modak, A. and Bhaumik, A., *J. Mol. Catal. A-Chem.* **2012,**

363, 254.

30.   Osei-Prempeh, G.; Lehmler, H. J.; Rankin, S. E. and Knutson, B. L., *Industrial &*

Engineering Chemistry Research **2008,** *47*, 530.

31.   Bleloch, A.; Johnson, B. F. G.; Ley, S. V.; Price, A. J.; Shephard, D. S. and

Thomas, A. W., *Chem. Commun.* **1999**, 1907.

32.   Ciesla, U.; Froba, M.; Stucky, G. and Schuth, F., *Chem. Mater.* **1999,** *11*, 227.

33.   Sayari, A., *Chem. Mater.* **1996,** *8*, 1840.

34.   Corma, A., *Chem. Rev.* **1997,** *97*, 2373.

35.   Moller, K. and Bein, T., *Chem. Mater.* **1998,** *10*, 2950.

36.   Ciesla, U. and Schuth, F., *Microporous Mesoporous Mater.* **1999,** *27*, 131.

37.   Ying, J. Y.; Mehnert, C. P. and Wong, M. S., *Angew. Chem., In. Ed.* **1999,** *38*, 56.

38.   Sayari, A. and Hamoudi, S., *Chem. Mater.* **2001,** *13*, 3151.

39.   Vallet-Regi, M.; Balas, F. and Arcos, D., *Angew. Chem., In. Ed.* **2007,** *46*, 7548.

40.   Corma, A.; Kan, Q. B.; Navarro, M. T.; PerezPariente, J. and Rey, F., *Chem.*

Mater. **1997,** *9*, 2123.

41.   Huo, Q. S.; Margolese, D. I. and Stucky, G. D., *Chem. Mater.* **1996,** *8*, 1147.

42.   Wan, Y. and Zhao, D. Y., *Chem. Rev.* **2007,** *107*, 2821.

43.   Attard, G. S.; Glyde, J. C. and Goltner, C. G., *Nature* **1995,** *378*, 366.

44.   Shopsowitz, K. E.; Qi, H.; Hamad, W. Y. and MacLachlan, M. J., *Nature* **2010,** *468*, 422.

45.   Dujardin, E.; Blaseby, M. and Mann, S., *J. Mater. Chem.* **2003,** *13*, 696.

46.   Cai, Q.; Lin, W. Y.; Xiao, F. S.; Pang, W. Q.; Chen, X. H. and Zou, B. S., *Microporous Mesoporous Mater.* **1999,** *32*, 1.

47.   Wan, Y. and Zhao, D., *Chem Rev* **2007,** *107*, 2821.

48.   Chen, C.-Y.; Burkett, S. L.; Li, H.-X. and Davis, M. E., *Microporous Mater.* **1993,** *2*, 27.

49.   Sakamoto, Y.; Kaneda, M.; Terasaki, O.; Zhao, D. Y.; Kim, J. M.; Stucky, G.; Shim, H. J. and Ryoo, R., *Nature* **2000,** *408*, 449.

50.   Zhao, D. Y.; Huo, Q. S.; Feng, J. L.; Kim, J. M.; Han, Y. J. and Stucky, G. D., *Chem. Mater.* **1999,** *11*, 2668.

51.   Huo, Q. S.; Margolese, D. I.; Ciesla, U.; Feng, P. Y.; Gier, T. E.; Sieger, P.; Leon, R.; Petroff, P. M.; Schuth, F. and Stucky, G. D., *Nature* **1994,** *368*, 317.

52.   Huo, Q. S.; Leon, R.; Petroff, P. M. and Stucky, G. D., *Science* **1995,** *268*, 1324.

53. Che, S.; Garcia-Bennett, A. E.; Yokoi, T.; Sakamoto, K.; Kunieda, H.; Terasaki, O. and Tatsumi, T., *Nature Materials* **2003,** *2*, 801.

54. Tanev, P. T. and Pinnavaia, T. J., *Science* **1995,** *267*, 865.

55. Bagshaw, S. A.; Prouzet, E. and Pinnavaia, T. J., *Science* **1995,** *269*, 1242.

56. Huo, Q. S.; Margolese, D. I.; Ciesla, U.; Demuth, D. G.; Feng, P. Y.; Gier, T. E.; Sieger, P.; Firouzi, A.; Chmelka, B. F.; Schuth, F. and Stucky, G. D., *Chem. Mater.* **1994,** *6*, 1176.

57. Tanev, P. T.; Chibwe, M. and Pinnavaia, T. J., *Nature* **1994,** *368*, 321.

58. Bagshaw, S. A.; Prouzet, E. and Pinnavaia, T. J., *Science* **1995,** *269*, 1242.

59. Zhao, D. Y.; Huo, Q. S.; Feng, J. L.; Chmelka, B. F. and Stucky, G. D., *J. Am. Chem. Soc.* **1998,** *120*, 6024.

60. Kruk, M.; Jaroniec, M.; Ko, C. H. and Ryoo, R., *Chem. Mater.* **2000,** *12*, 1961.

61. Suwanchawalit, C. and Wongnawa, S., *J. Nanopart. Res.* **2010,** *12*, 2895.

62. Yang, C.-M.; Zibrowius, B.; Schmidt, W. and Schüth, F., *Chem. Mater.* **2003,** *15*, 3739.

63. El Hankari, S.; El Kadib, A.; Finiels, A.; Bouhaouss, A.; Moreau, J. J. E.; Crudden, C. M.; Brunel, D. and Hesemann, P., *Chem. Eur. J.* **2011,** *17*, 8984.

64. Bui, T. X.; Kang, S. Y.; Lee, S. H. and Choi, H., *J. Hazard. Mater.* **2011,** *193*, 156.

65. Glasspoole, B. W.; Webb, J. D. and Crudden, C. M., *J. Catal.* **2009,** *265*, 148.

66. Katiyar, A.; Yadav, S.; Smirniotis, P. G. and Pinto, N. G., *J. Chromatogr. A* **2006,** *1122*, 13.

67. Jiang, Y. J. and Gao, Q. M., *J. Am. Chem. Soc.* **2006,** *128*, 716.

68. Crudden, C. M.; Sateesh, M. and Lewis, R., *J. Am. Chem. Soc.* **2005,** *127*, 10045.

69. Asefa, T. and Lennox, R. B., *Chem. Mater.* **2005,** *17*, 2481.

70. Lu, A. H.; Li, W. C.; Schmidt, W.; Kiefer, W. and Schuth, F., *Carbon* **2004,** *42*, 2939.

71. Kang, T.; Park, Y. and Yi, J., *Industrial & Engineering Chemistry Research* **2004,** *43*, 1478.

72. Chiu, J. J.; Pine, D. J.; Bishop, S. T. and Chmelka, B. F., *J. Catal.* **2004,** *221*, 400.

73. Israelachvili, J. N.; Mitchell, D. J. and Ninham, B. W., *Journal of the Chemical Society-Faraday Transactions Ii* **1976,** *72*, 1525.

74. Mezzenga, R.; Schurtenberger, P.; Burbidge, A. and Michel, M., *Nature Materials* **2005,** *4*, 729.

75.   Choi, M.; Cho, H. S.; Srivastava, R.; Venkatesan, C.; Choi, D.-H. and Ryoo, R., *Nature Materials* **2006,** *5*, 718.

76.   Tosheva, L. and Valtchev, V. P., *Chem. Mater.* **2005,** *17*, 2494.

77.   Corma, A., *Curr. Opin. Solid State Mater. Sci.* **1997,** *2*, 63.

78.   Hoffmann, F. and Froba, M., *Chem. Soc. Rev.* **2011,** *40*, 608.

79.   Yokoi, T.; Yoshitake, H. and Tatsumi, T., *J. Mater. Chem.* **2004,** *14*, 951.

80.   Seki, T.; McEleney, K. and Crudden, C. M., *Chem. Commun.* **2012,** *48*, 6369.

81.   Dickson, S. E. and Crudden, C. M., *Chem. Commun.* **2010,** *46*, 2100.

82.   Webb, J. D.; MacQuarrie, S.; McEleney, K. and Crudden, C. M., *J. Catal.* **2007,** *252*, 97.

83.   Brunelli, N. A.; Venkatasubbaiah, K. and Jones, C. W., *Chem. Mater.* **2012,** *24*, 2433.

84.   Melero, J. A.; van Grieken, R. and Morales, G., *Chem. Rev.* **2006,** *106*, 3790.

85.   Sheng, X. L.; Zhou, Y. M.; Zhang, Y. W.; Duan, Y. Z.; Zhang, Z. W. and Yang, Y. L., *Microporous Mesoporous Mater.* **2012,** *161*, 25.

86.   Hu, Q.; Hampsey, J. E.; Jiang, N.; Li, C. and Lu, Y., *Chem. Mater.* **2005,** *17*, 1561.

87.   Richardson, J. M. and Jones, C. W., *J. Catal.* **2007,** *251*, 80.

88.   Huang, X.; Yang, M.; Wang, G. and Zhang, X., *Microporous Mesoporous Mater.* **2011,** *144*, 171.

89.   Sun, J. M.; Ma, D.; Zhang, H.; Liu, X. M.; Han, X. W.; Bao, X. H.; Weinberg, G.; Pfander, N. and Su, D. S., *J. Am. Chem. Soc.* **2006,** *128*, 15756.

90.   Mondal, J.; Modak, A.; Dutta, A.; Basu, S.; Jha, S. N.; Bhattacharyya, D. and Bhaumik, A., *Chem. Commun.* **2012,** *48*, 8000.

91.   Rosenholm, J. M. and Linden, M., *Chem. Mater.* **2007,** *19*, 5023.

92.   Fujita, S. and Inagaki, S., *Chem. Mater.* **2008,** *20*, 891.

93.   Mizoshita, N.; Tani, T. and Inagaki, S., *Chem. Soc. Rev.* **2011,** *40*, 789.

94.   Hoffmann, F.; Cornelius, M.; Morell, J. and Froba, M., *Angew Chem Int Ed Engl* **2006,** *45*, 3216.

95.   Stein, A.; Melde, B. J. and Schroden, R. C., *Advanced Materials (Weinheim, Germany)* **2000,** *12*, 1403.

96.   Kapoor, M. P.; Yang, Q. and Inagaki, S., *J Am Chem Soc* **2002,** *124*, 15176.

97.   Yang, Y. and Sayari, A., *Chem. Mater.* **2007,** *19*, 4117.

98.   Prasad, D. R. and Hoffman, M. Z., *J. Phys. Chem.* **1984,** *88*, 5660.

99.   Hoffman, M. Z.; Prasad, D. R.; Jones, G. and Malba, V., *J. Am. Chem. Soc.* **1983,** *105*, 6360.

100.   Georgopoulos, M. and Hoffman, M. Z., *J. Phys. Chem.* **1991,** *95,* 7717.

101.   Inagaki, S.; Guan, S. Y.; Yang, Q.; Kapoor, M. P. and Shimada, T., *Chem. Commun.* **2008**, 202.

102.   Morell, J.; Chatterjee, S.; Klar, P. J.; Mauder, D.; Shenderovich, I.; Hoffmann, F. and Froba, M., *Chem. Eur. J.* **2008,** *14*, 5935.

103.   Polarz, S. and Kuschel, A., *Chem. Eur. J.* **2008,** *14*, 9816.

104.   Zhuang, T. Y.; Shi, J. Y.; Ma, C. and Wang, W., *J. Mater. Chem.* **2010,** *20*, 6026.

105.   Ide, A.; Voss, R.; Scholz, G.; Ozin, G. A.; Antonietti, M. and Thomas, A., *Chem. Mater.* **2007,** *19*, 2649.

106.   MacQuarrie, S.; Thompson, M. P.; Blanc, A.; Mosey, N. J.; Lemieux, R. P. and Crudden, C. M., *J. Am. Chem. Soc.* **2008,** *130*, 14099.

107.   Zhuang, T. Y.; Shi, J. Y.; Ma, B. C. and Wang, W., *J. Mater. Chem.* **2010,** *20*, 6026.

108.   Jayalakshmi, V.; Wood, T.; Basu, R.; Du, J. N.; Blackburn, T.; Rosenblatt, C.; Crudden, C. M. and Lemieux, R. P., *J. Mater. Chem.* **2012,** *22*, 15255.

109.   Pachon, L. D. and Rothenberg, G., *Appl. Organomet. Chem.* **2008,** *22*, 288.

110.   Blaser, H. U.; Indolese, A.; Schnyder, A.; Steiner, H. and Studer, M., *J. Mol. Catal. A-Chem.* **2001,** *173*, 3.

111.   Arends, I. and Sheldon, R. A., *Applied Catalysis a-General* **2001,** *212*, 175.

112.   Galaffu, N.; Man, S. P.; Wilkes, R. D. and Wilson, J. R. H., *Organic Process Research & Development* **2007,** *11*, 406.

113.   Patra, M. and Sharma, A., *Botanical Review* **2000,** *66*, 379.

114.   Frankham, J. and Kauppinen, P., *Platinum Met. Rev.* **2010,** *54*, 200.

115.   Jimenez-Jimenez, J.; Algarra, M.; Rodriguez-Castellon, E.; Jimenez-Lopez, A. and da Silva, J., *J. Hazard. Mater.* **2011,** *190*, 694.

116.   Crudden, C. M.; McEleney, K.; MacQuarrie, S. L.; Blanc, A.; Sateesh, M. and Webb, J. D., *Pure Appl. Chem.* **2007,** *79*, 247.

117.   EuropeanMedicinesAgency Note for guidance on Specification Limits for Residues of Metal Catalysts. http://www.ema.europa.eu/docs/en_GB/document_library/Scientific_guideline/2009/09/WC500003588.pdf.

118.   Nohair, B.; MacQuarrie, S.; Crudden, C. M. and Kaliaguine, S., *J. Phys. Chem. C* **2008,** *112*, 6065.

119.   MacQuarrie, S.; Nohair, B.; Horton, J. H.; Kaliaguine, S. and Crudden, C. M., *J. Phys. Chem. C* **2010,** *114*, 57.

120.   El Kadib, A.; McEleney, K.; Seki, T.; Wood, T. K. and Crudden, C. M., *Chemcatchem* **2011,** *3*, 1281.

121.   McEleney, K.; Allen, D. P.; Holliday, A. E. and Crudden, C. M., *Org. Lett.* **2006,** *8*, 2663.

122.   Feng, X.; Fryxell, G. E.; Wang, L.-Q.; Kim, A. Y.; Liu, J. and Kemner, K. M., *Science* **1997,** *276*, 923.

123.   Mercier, L. and Pinnavaia, T. J., *Adv. Mater.* **1997,** *9*, 500.

124.   Kang, T.; Park, Y.; Park, J. C.; Cho, Y. S. and Yi, J., Functionalized mesoporous adsorbents for Pt(II) and Pd(II) adsorption from dilute aqueous solution. In *Stud. Surf. Sci. Catal.*, Sang-Eon Park, R. R. W.-S. A. C. W. L.; Jong-San, C., Eds. Elsevier: 2003; Vol. Volume 146, pp 527.

125.   Ribey, S. C.; Munkittrick, K. R.; McMaster, M. E.; Courtenay, S.; Langlois, C.; Munger, S.; Rosaasen, A. and Whitley, G., *Water Quality Research Journal of Canada* **2002,** *37*, 229.

126.   Hylander, L. D. and Goodsite, M. E., *Sci. Total Environ.* **2006,** *368*, 352.

127.   da Silva, E. F.; Zhang, C. S.; Pinto, L. S.; Patinha, C. and Reis, P., *Appl. Geochem.* **2004,** *19*, 887.

128.   Blais, J. F.; Dufresne, S. and Mercier, G., *Revue des Sciences de l'Eau* **1999,** *12*, 687.

129.   Herr, C. and Gray, N. F., *Environ. Geochem. Health* **1997,** *19*, 73.

130.   Haggarty, D. R.; McCorquodale, B.; Johannessen, D. I.; Levings, C. D. and Ross, P. S., *Canadian Technical Report of Fisheries and Aquatic Sciences* **2003,** *2507*, 1.

131.   Cidu, R., *Environmental Earth Sciences* **2011,** *64*, 503.

132.   Blasco, J.; Arias, A. M. and Saenz, V., *Environment International* **2002,** *28*, 111.

133.   Du, J.; Cipot-Wechsler, J.; Lobez, J. M.; Loock, H.-P. and Crudden, C. M., *Small* **2010,** *6*, 1168.

134.   Barnes, J.; Dreher, M.; Plett, K.; Brown, R. S.; Crudden, C. M. and Loock, H.-P., *Analyst* **2008,** *133*, 1541.

135.   Sing, K. S. W.; Everett, D. H.; Haul, R. A. W.; Moscou, L.; Pierotti, R. A.; Rouquerol, J. and Siemieniewska, T., *Pure Appl. Chem.* **1985,** *57*, 603.

136.   Yu, J.; Xiang, Q. and Zhou, M., *Applied Catalysis B-Environmental* **2009,** *90*, 595.

137.   Song, H.; Rioux, R. M.; Hoefelmeyer, J. D.; Komor, R.; Niesz, K.; Grass, M.; Yang, P. D. and Somorjai, G. A., *J. Am. Chem. Soc.* **2006,** *128*, 3027.

138.   Barolo, C.; Nazeeruddin, M. K.; Fantacci, S.; Di Censo, D.; Comte, P.; Liska, P.;

Viscardi, G.; Quagliotto, P.; De Angelis, F.; Ito, S. and Graetzel, M., *Inorg. Chem.* **2006,**

45, 4642.

139.   Gregg, S. J. and Sing, K. S. W., *Adsorption, surface area, and porosity*. 2nd ed.;

Academic Press: London ; New York, 1982; p xi.

Chapter 2

Enantioselective Catalysis on a Chiral PMO Material

2.1   Introduction

Catalysis by means of transition metal complexes is a valuable technology to achieve chemo-, regio-, diastereo- and enantioselective processes, which are often necessary for the production of pharmaceuticals, fragrant materials, organic ELs, and variety of industrial materials.[1, 2] In particular, carbon-carbon bond formation by homo-[3-5] and cross-coupling reactions[6-8], direct amination, etherification, and thioetherification of halogenated aromatic substrates[9-13], or catalytic functionalization of carbon-hydrogen bonds[14, 15] are good examples where no alternative method is available. However, most of the transition metals employed as catalysts are rare and expensive, and also cause problems for purification of products and waste water treatment because of high toxicity[16, 17].

2.1.1   General Advantage of Heterogeneous Catalysis

Heterogeneous catalysis in which active species are supported on polymer substrates to immobilize them has been studied extensively[18]. This is a fascinating approach especially for industrially relevant processes because of the ease of catalyst separation, the reusability of recovered catalysts, and the workup which requires much less organic solvent (Figure 2-1). It is also reported that air, moisture and even temperature tolerance of the catalytic species, which may not be stable in homogeneous systems, can be reinforced by installing these on a support.[19-22] The other notable advantage in heterogeneous catalysis is the ease of handling. For example, the low loadings of most catalysts by comparison to the corresponding substrates can make the accurate determination of weights and ratios difficult. However, catalysts supported on materials are already diluted and thus are more easily handled. Furthermore, such high dispersion and separation among each catalytic molecule by the solid support wall suppress the deactivation by dimerization or aggregation of catalytic metal species, consequently the catalysts show longer life time and durability toward recycles.[23]
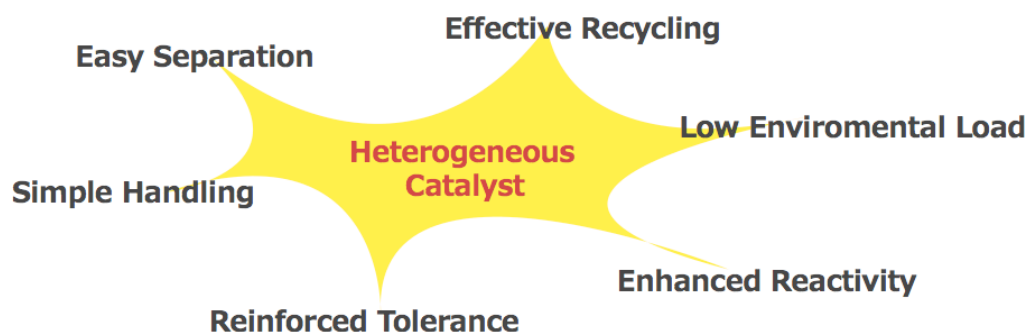
Figure 2-1.   Typical advantages of heterogeneous catalysts

2.1.2 Mesoporous silica materials in heterogeneous catalysis

Heterogeneous catalysts of this type are prepared, in most cases, by immobilizing ligands and transition metals on commercially available organic polymers such as polystyrene.[24-26] However, swelling organic polymers in organic solvents can result in catalytic active sites buried inside of materials and then not accessible, leading to decreased catalytic activity[27].   An alternative would be to use highly cross-linked organic polymers, which have higher accessibility.
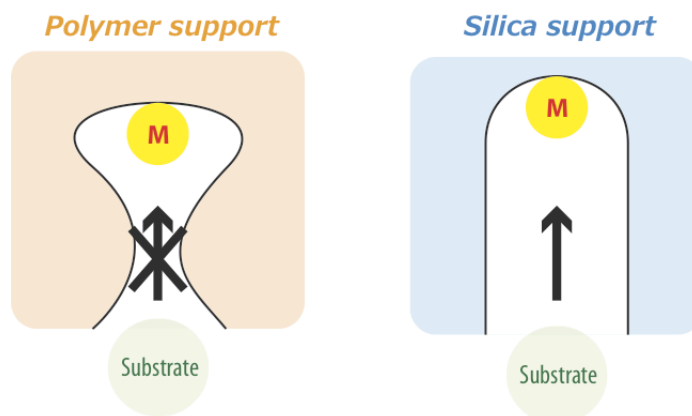
Figure 2-2. **Image of accessibility to the catalysts on polymer and silica supports**

In contrast, silica does not swell in organic solvents and because of its rigid structure, can be employed in any solvent (Figure 2-2). Therefore if prepared with mesoporosity, introduced, for example, by a surfactant templating method, materials such as periodic mesoporous organosilicas can be highly effective supports.[28, 29] The huge surface area ($\sim$1000 m^2/g) that these materials have will likely contribute to accessibility and high reactivity.[30] In fact, to take advantage in terms of surface area and porosity, mesoporous polymers such as p-DVB-EGDMA (copolymer of divinylbenzene and ethyleneglycol dimethacrylate) can be prepared by using silica particles as hard structural templates.[31] But introducing functional groups by a post-grafting method, which is to say, modifying the surface of materials after polymerization of monomers, decreases the surface area and pore size, and occasionally results in a loss of mesoporosity.[32] With the

invention of organic/inorganic hybrid monomer-based PMOs[33-36] prepared by a co-condensation method, it became possible to introduce organic functional groups into materials with less damage to surface and pore properties (Scheme 2-1).[37] In the other words, condensable bistrialkoxysilyl groups are employed as the monomer in the polymerization/condensation reaction in the presence of structure directing agent, or surfactant micelle templates. These monomers can be simple aliphatic or aromatic functionalities, or they can contain groups that can act as ligands for metals. One key difference between these materials and simple silica-based mesoporous materials is that the conditions for removal of the surfactant needs to be optimized to ensure the functional groups are not decomposed. Because of the method of synthesis, the resulting material has the functional groups directly attached to the mesoporous framework, therefore the pore space remains unhindered.
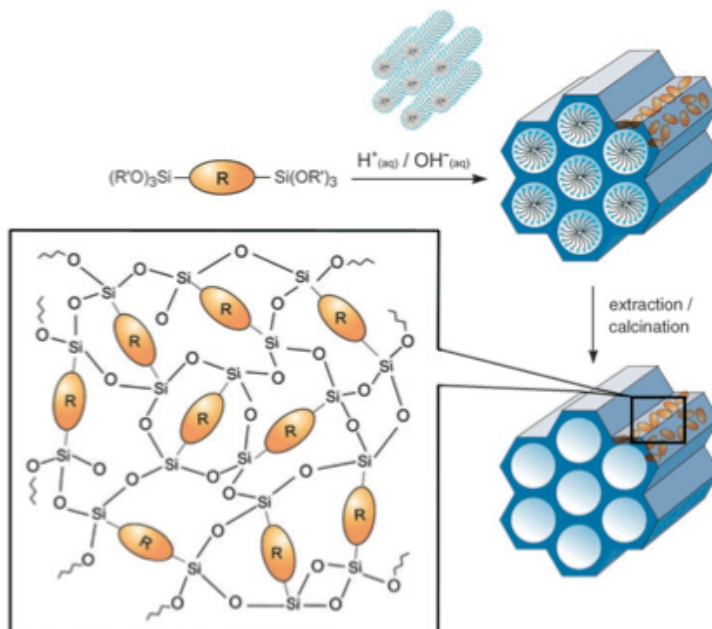
Scheme 2-1. General scheme of PMO preparation by surfactant templating method[38]

2.1.3 Further enhancement effect of the mesoporous support in catalysis

As mentioned above, immobilizing transition metal catalysts inside mesopores results in improved durability of the catalysts because of high dispersion and separation effects.[39] In some cases, unique phenomena can be attributed to the presence of the support material.[22, 28, 29, 39-45] One example is the achievement of unique regioselectivity in allylic aminations (Scheme 2-2).[45] In this Tsuji-Trost[46] type allylic amination[47], the linear product is exclusively obtained in homogeneous systems and in non-porous heterogeneous systems. However, a significant change in regioselectivity in favor of the branched product is observed when Pd catalysts are supported on mesoporous materials

such as MCM-41. Yudin and co-workers reported that the addition of a base improves

branched selectivity in homogeneous systems,[48] however MCM-41 supported-catalysts

result in changes in linear/branched selectivity without the addition of base, and are thus

operating under a completely different mechanism. The most plausible mechanism to

explain this regioselectivity is a steric effect that the catalytic site (Pd-bound

diphenylphosphinoferrocene (DPPF)) experiences as it is pushed against the concave wall

of the material by the alkyl linker attached on the opposite side of the wall in the

mesopore, although there is no clear evidence to prove this hypothesis (Figure 2-3).[49]

	Linear (%) / Branched (%)
Homogeneous	99 / -
Heterogeneous	
- Non porous	98 / 2
- Mesoporous	50 / 50
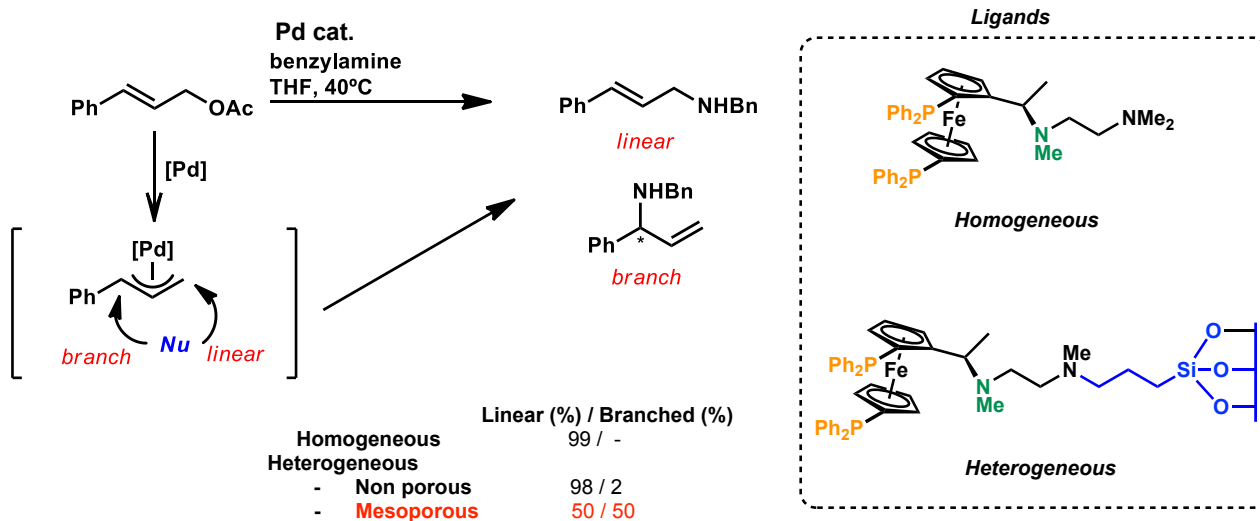
Scheme 2-2. Effect of mesoporous grafted catalyst with regard to the regioselectivity of the allylic amination reaction
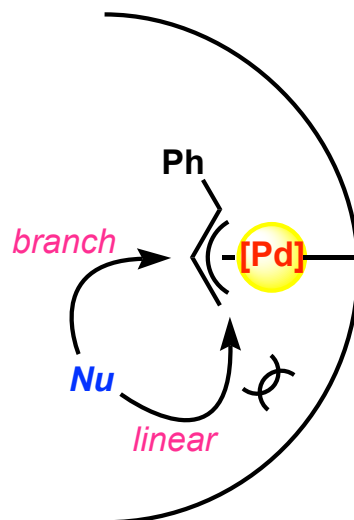
Figure 2-3.   **Plausible concave wall effect providing unique regioselectivity**

Another unique effect observed on supported catalysts is enhanced enantioselectivity (Scheme 2-3).[29] A cationic rhodium complex shows moderate yield and no enantioselectivity in the asymmetric hydrogenation of alpha-keto esters, whereas the same rhodium catalyst gives over 90% yield and significant enantioselectivity when it is anchored on mesoporous silica by electrostatic interaction with counter anionic as shown in Scheme 2-3. It should be also noted that the non-covalently immobilized transition metal catalyst was readily retained on the mesoporous silica in the absence of highly polar solvents, and was recyclable.[29]
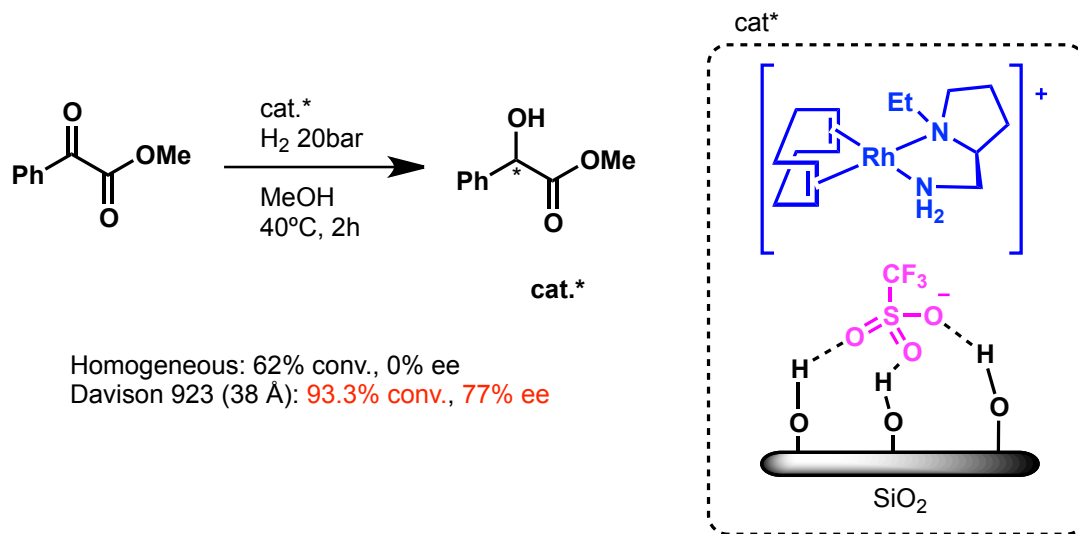
Scheme 2-3.   Enhanced enantioselectivity using a catalyst grafted on mesoporous silica
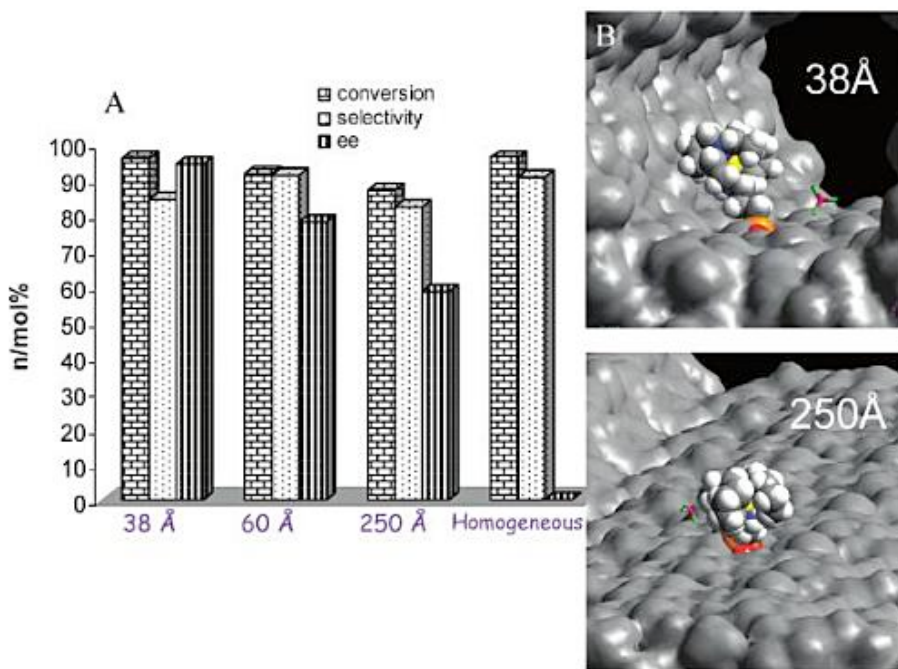
Figure 2-4.   Relationship between pore diameters and induction of enantioselectivity (A), and CG images of diamine ligands on concave surface (B)[40]

A series of mesoporous silicas with different pore diameters were applied to this reaction to investigate the detailed mechanism (Figure 2-4). It is obvious that the larger pore diameter is, the lower the enantioselectivity is, such that no enantioselectivity was observed in non porous, or homogeneous systems. This trend implies that steric constraints induced from the concave sidewall affect the interaction between the substrate and the catalyst. Such a confinement effect has been suggested and demonstrated by multiple groups independently.[40, 41, 49-51]

2.1.4 BINAP-PMO as a novel heterogeneous chiral ligand

Previous work in our group showed that PMOs can be prepare in which functional chiral organic monomers can be introduced directly into the backbone by the co-condensation approach.[52] A study of the chiroptical properties of a material prepared by admixing the chiral dopant shown below with a racemic bulk constituent showed that chirality was induced throughout the material via π-π stacking between aromatic systems, thus by employing an axially chiral monomer as a dopant in 15-30%, and a racemic biphenyl bulk constituent, chirality can be propagated throughout the material (Scheme 2-4).
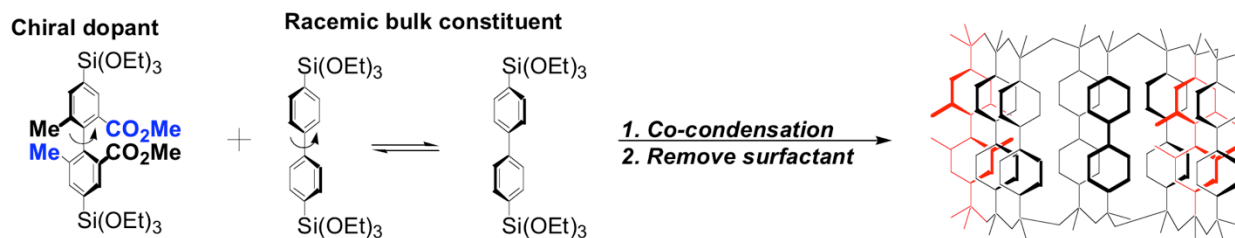
Scheme 2-4. PMO with Induced Chirality

Although this study provided useful information about the transmission of chirality in the solid state, the dopant did not contain a good ligand for transition metal complexes that would be active in catalysis. Among numerous atropisomeric ligands, 2,2'-bis(diphenylphosphino)-1,1'-binaphthyl (BINAP) is one of the most practical and widely used bidentate phosphine ligands.[53-55] Enantiomerically pure BINAP has been often used for asymmetric hydrogenations with either Rh or Ru as the active metal, and the impact of this work was recognized in the awarding of the 2001 Nobel Prize in Chemistry to Ryoji Noyori.[56] Thus we planned to employ 4,4'-bis(siloxane) substituted BINAP monomers in addition to biphenyl monomers to prepare a PMO that could act as a heterogeneous catalyst ligand. Considering its importance in organic synthesis, it is not surprising that there have been various supported versions of BINAP reported.[49, 57-59] For example, van Koten and co-workers reported the immobilization of BINAP on amorphous silica using di-ureyl functionalized BINAP monomer **4** (Figure 2-5),[57] and

Yang and co-workers co-condensed the same functionalized BINAP monomer **4** with tetramethylorthosilicate (TMOS) under acidic conditions employing the tri-block copolymer P123 as a surfactant template to obtain BINAP-supported in all silica porous materials.[60] However, the introduction of condensable siloxane groups directly on the backbone of BINAP, the introduction of the resulting monomer into the backbone of a PMO, and the synthesis of the dual hybrid PMO employing such a functionalized chiral ligand was not realized prior to this work. Furthermore, it was hoped that the introduction of chirality into the material as well as the ligand by the mechanism shown above, would enhance the chirality transfer.

In this chapter, the synthesis of BINAP-PMO materials in which an immobilization of BINAP was successfully achieved via the co-condensation of **1** along with **2** under acidic conditions employing Brij76 surfactant resulting in pore diameters of about 25 Å is described. In addition, the application of the resulting functional material to heterogeneous asymmetric hydrogenation both under high pressure hydrogenation conditions and atmospheric hydrogen transfer were demonstrated.[61]
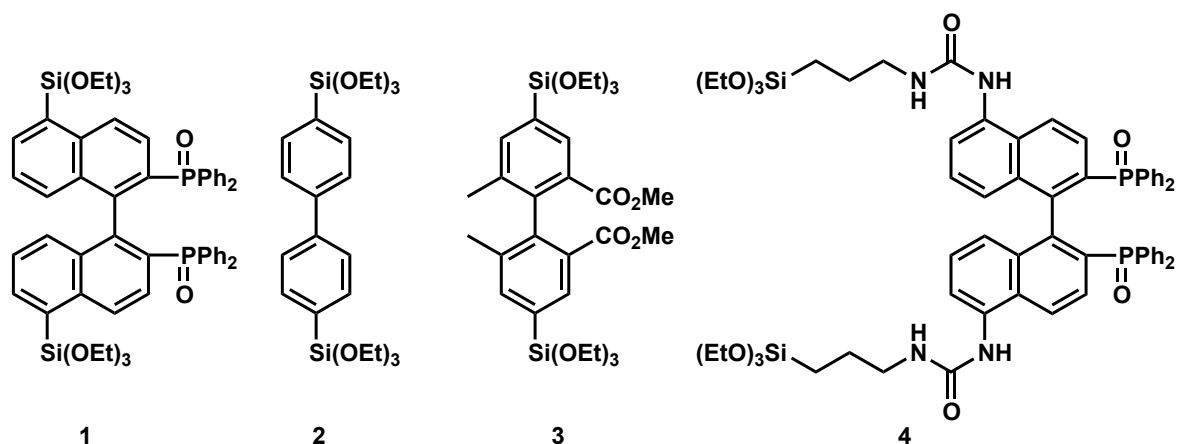
Figure 2-5. Organic-bridged siloxane precursors with biphenyl and binaphthyl structures

2.2 Synthesis of BINAP-bridged PMOs

In our initial studies, we found that 4,4'-dibromo-BINAPO (**5**) could not be converted into the desired bistriethoxysilylated product by lithiation or Grignard reaction (Scheme 2-5). As an alternative, we attempted the synthesis of the corresponding 4,4'-diiodo-BINAPO (**6**), which was successful, but only low yields of the desired compound were obtained. Furthermore, this diiodo substrate was inactive under the conditions of rhodium catalyzed coupling with triethoxysilane, the so-called Masuda-Murata coupling, which is one of the best methods for the synthesis of bistrialkoxysilyl-substituted monomers (Scheme 2-5).[62] Although the 4,4'-functionalized BINAP was the target chiral dopant which can connect to the silica framework on the chiral axis of the BINAP, we

decided to continue the installation of the BINAP unit by preparing the 5,5'-functionalized precursor.
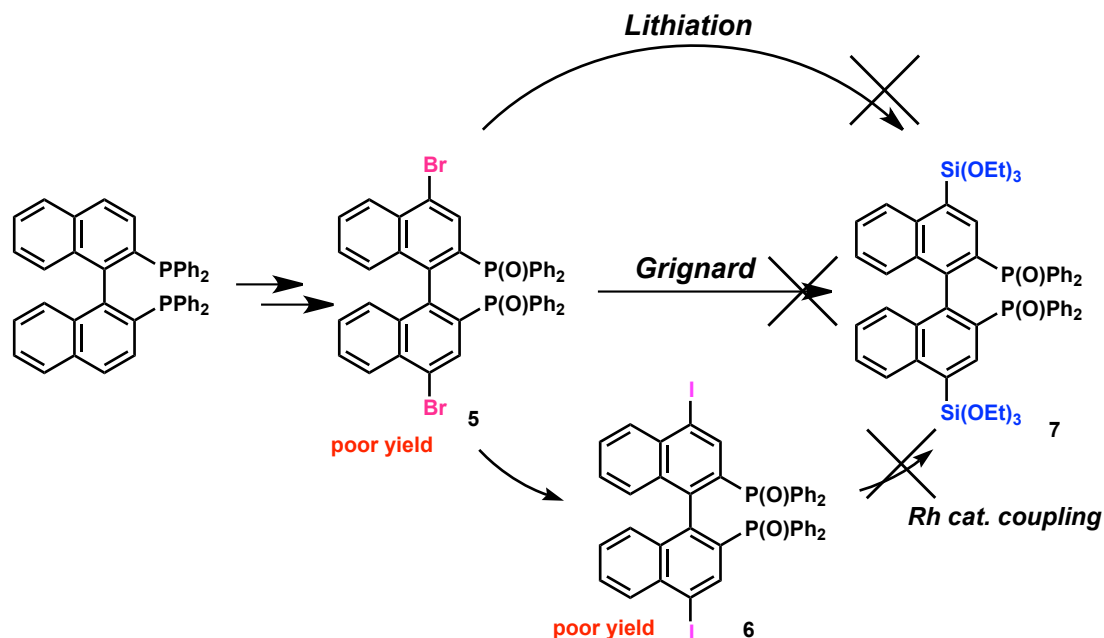
Scheme 2-5. Initial attempts at the synthesis of 4,4'-bistriethoxysilyl BINAPO

The related 5,5'-diiodo BINAPO compound (**9**) was able to be isolated in bulk through in three steps from commercially available BINAP both racemic and chiral pure form (Scheme 2-6). Thus, protection of the phosphines of BINAP was quantitatively accomplished by oxidation with hydrogen peroxide to yield BINAPO **6**, followed by diiodination at the 5- and 5'-positions to give diiodo BINAPO **7**. Direct installation of the trialkoxysilyl moieties (Si(OEt)$_3$) on the binaphthyl structure was performed by a rhodium-catalyzed Masuda reaction. This last step proved to be a significant challenge

since the Masuda reaction resulted in bissilylation along with monosilylation/monoreduction. The desired bissilylated precursor **1** was then only obtained cleanly after chromatographic separation of the monosilylated byproduct. Thus the low yield resulted from a combination of the poor selectivity in the Masuda coupling, and losses during the chromatography of the pH and moisture sensitive bistriethoxysilyl product. Regardless, since all other steps are high yielding (>90%), and the lowest yielding step was the final step, this route provided sufficient material to prepare and test PMO materials containing **1** as an additive (Scheme 2-6).
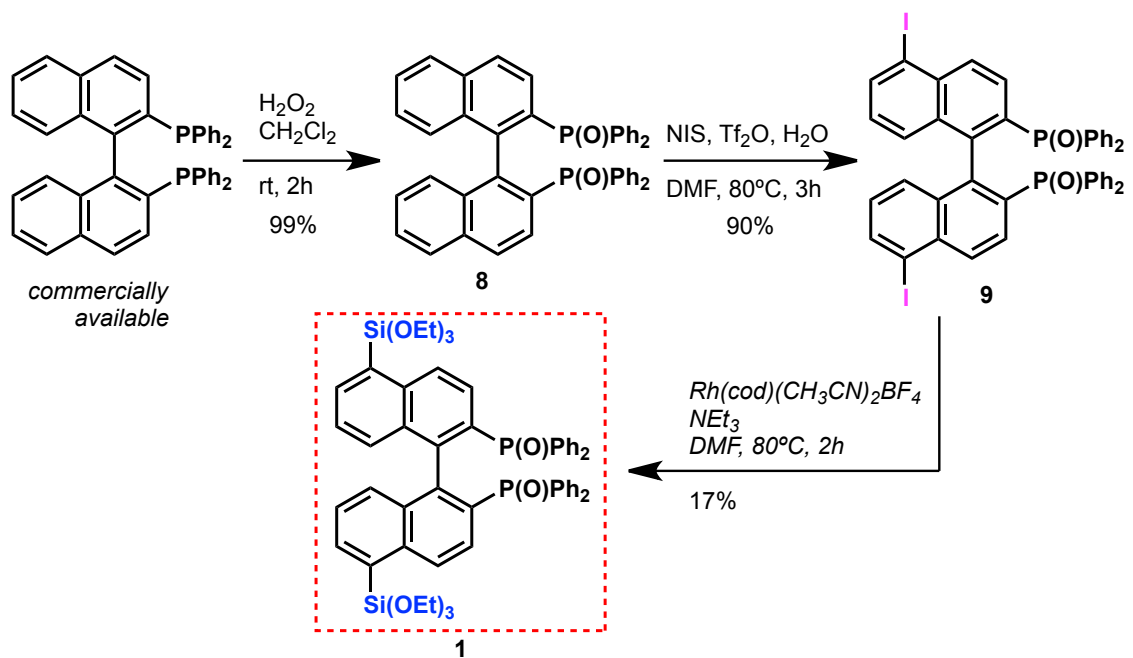
Scheme 2-6. **Synthetic scheme of the bistrialkoxysilyl-BINAP precursor.**

2.2.1 Phosphineoxide formation as a protection of phosphines

Phosphines are one of the most attractive functional groups to install on a solid support because of its versatile ligand functionality. However, immobilization of phosphines on silica leads to a formation of byproduct predominantly, or almost quantitatively (Figure 2-6).[63, 64]
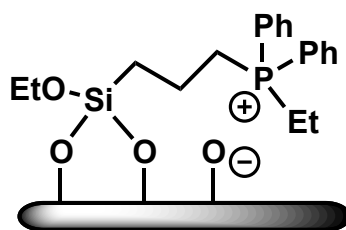
Figure 2-6.   Typical phosphonium product on silica

Such a byproduct cannot coordinate to the transition metal therefore it must be avoided by protecting phosphines prior to immobilization. It was reported that none of the phosphonium byproduct was observed when ethoxy-modified silica was treated with triphenylphosphine in refluxing toluene, therefore the phosphines should be stable to such an alkylation on silica surface once the alkoxy groups are fixed on the solid surface.[65]

Furthermore, the bidentate ligand functionality of BINAP may completely inhibit the rhodium catalyzed silylation reaction by binding the Rh catalyst, thus protection of phosphines on BINAP was carried out in the first step by hydrogen peroxide oxidation.

The desired product (**8**) was obtained quantitatively[66], and was used in the next step without purification.

2.2.2 Iodination of electron deficient binaphthyls by NIS/TfOH system

As mentioned above, both bromination and iodination at the 4- and 4'-position of BINAPO gave poor yield. The iodination was especially poor, such that it was necessary to generate the dibromo compound first and then convert this to the diiodo product via Finkelstein reaction.[67, 68] Consequently the yields were very poor. Instead, a direct iodination was applied to access to 5,5'-diiodoBINAPO (**9**) from BINAPO (**8**) by employing a mixture of N-iodosuccinimide (NIS) and trifluoromethanesulfonic, or triflic, acid (Scheme 2-7).[69] The mixture of triflic acid and NIS generates an extremely electron deficient iodonium species which can behave as an electrophile even toward electron deficient BINAPO (Scheme 2-8). This procedure yielded the 5,5'-diiodo product exclusively. It should be noted that the racemic product does not dissolve in THF but the chiral pure product does, therefore the racemic one is much easier to isolate simply by washing with THF on a filter paper however the enantiomerically pure version must be isolated by silica gel column chromatography.
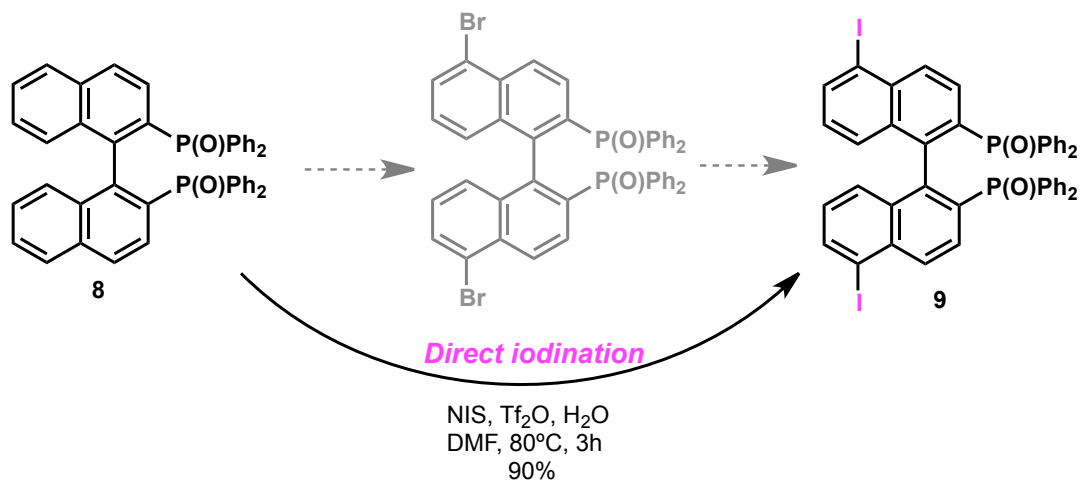
Scheme 2-7.   Direct iodination of BINAPO at the 5- and 5'-position

electron defficient iodonium specie
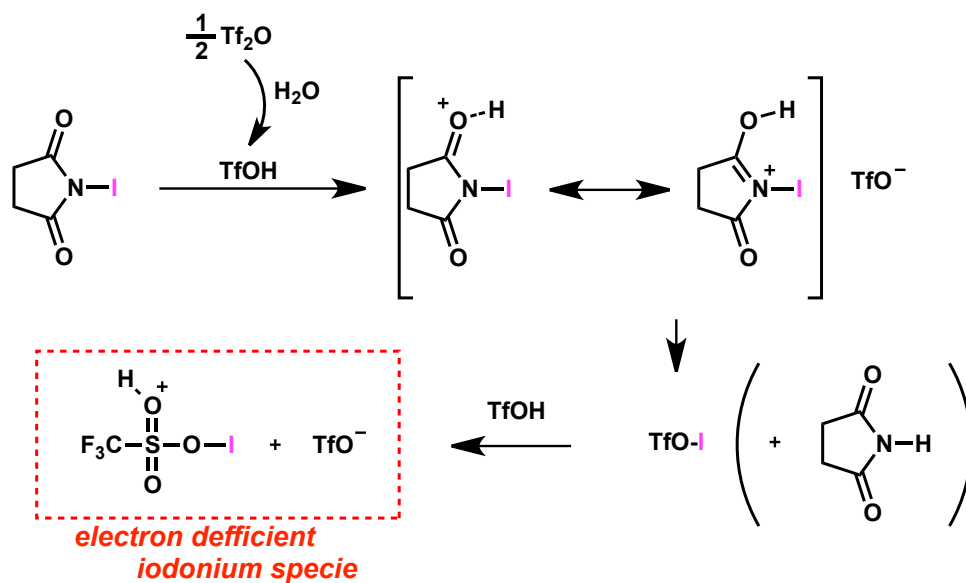
Scheme 2-8.   Iodonium formation in NIS/TfOH

2.2.3 Rhodium catalyzed trialkoxysilylation of aromatic halides

With the diiodo substrate **9** in hand, a cross coupling reaction invented by Masuda and Murata[62] was carried out, which yields mono- and bis-silylated BINAPO with mono- and di-reduced byproducts (Scheme 2-9). According to independent reports by Murata *et al.*[70], Yamanoi *et al.*[71], Kondo *et al.*[72], Komuro *et al.*[73] and DeShong *et al.*[74], reactions of this type both catalyzed by palladium and rhodium give silyl coupled products in low yield along with reduced products dominantly when substrates that have electron-withdrawing groups are employed. In fact, the reduction of aromatic halides with hydrosilanes catalyzed by transition metals can be accomplished by this route.[75-77] Optimization of this cross coupling was attempted especially for the substrate we required, however no remarkable improvement was observed even with latest conditions for electron deficient substrates reported in the literatures above. Overviewing literature reports in this area led to the conclusion that the substrates which give good yield are less electron deficient, and also substrates having ortho-substituents result in low yields. Our BINAPO substrate experiences 1,3-allyllic strain between the 4,4'- and 5,5'-positions of binaphthyl, which hinders coupling. Furthermore, there have been no report of this reaction with substrates that contain phosphineoxides.

Nakajima *et al.* reported chiral Lewis base, including BINAPO, catalyzed asymmetric aldol reactions, allylations, and phosphonylations where the chelating Lewis base interacts with silyl species to make intermediates.[78] The in situ generation of similar BINAPO-silane adducts may also contribute to slow coupling and fast reduction in our system. Even employing *t*-BuLi followed by triethoxysilyl chloride with the diiodo-BINAPO substrate did not give the desired product but instead reduced product. However, without other viable options, we were forced to use this low-yielding procedure.
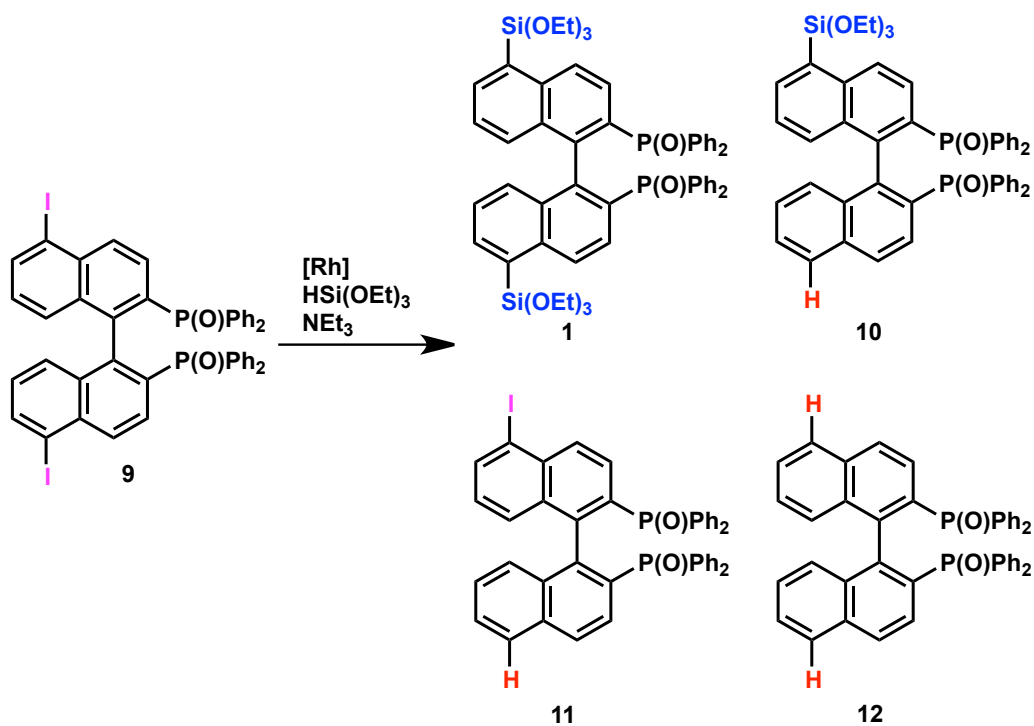
Scheme 2-9. Masuda-Murata reaction and products from 5,5'-diiodo BINAPO

2.2.4 Preparing BINAPO-bridged PMOs and their characterizations

PMOs were prepared using both enantiopure and racemic 5,5'-bissilylated

monomer **1** along with 4,4'-bis(triethoxysilyl) biphenyl **2** or tetraethyl orthosilicate

(TEOS) as the bulk constituents employing Brij 76, Pluronic P123 and $C_{18}TMABr$ as

structure directing agents, SDA (Figure 2-7) (Scheme 2-10).
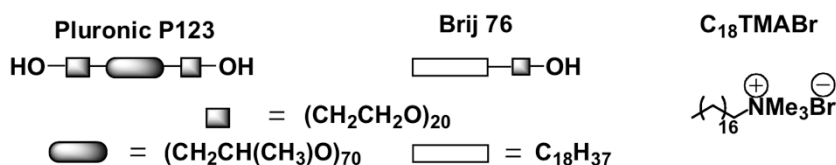
Figure 2-7. Surfactants used as structure directing agents
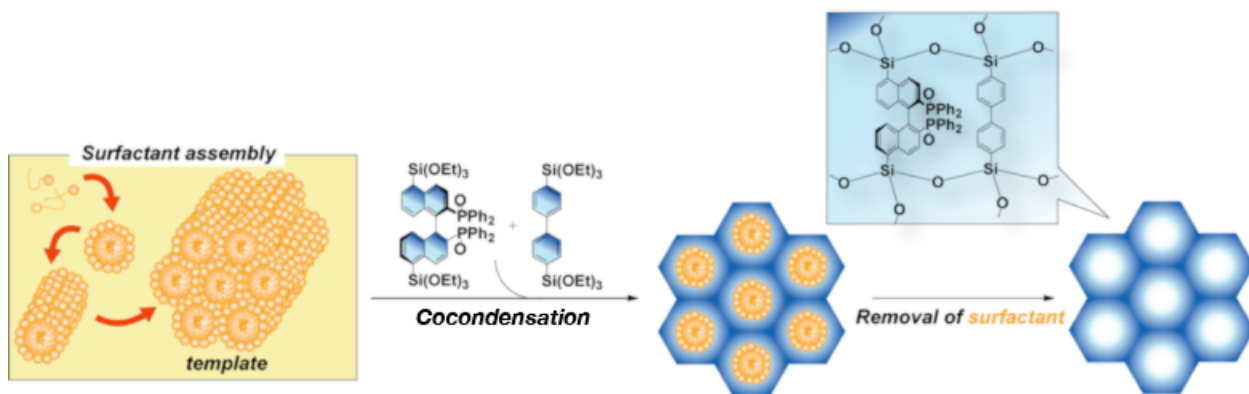
Scheme 2-10. Sol-gel process of BINAPO-PMO

> In typical examples, compounds **1** and **2** (15/85 ~ 5/95 molar ratios)
> were mixed along with surfactant **Brij-76** as an SDA under acidic
> conditions (Molar ratio: Si / water / HCl / NaCl / EtOH / Brij-76 =
> 1.00 / 600 / 8.40 / 19.0 / 18.4 / 0.533).

After extraction of the surfactant, nitrogen adsorption analysis of this material

showed that it was highly ordered with a pore diameter of ca. 26 Å (Table 2-1, entry 1-4).

These values are reproduced by a PMO synthesized from 100% **2**, BPh-PMO, therefore

addition of **1** followed by cocondensation with **2** does not prevent the sol-gel process

from taking place to give the expected mesoporous ordered structure. Similar materials

were prepared employing TEOS ($Si(OEt)_4$) as the bulk constituent (**1**/TEOS = 7.5/92.5

molar ratio) (entries 6 and 7). These primarily silica materials had less ordered and

smaller pores making them micro- rather than mesoporous, but they were characterized

by high surface areas and good pore volumes. Also employing other surfactants as SDAs

yielded PMOs with variable pore diameters (entry 8 and 9). These results clearly showed

that installing the functionality in the wall structure by condensation of rigidly bridged

precursors gives finely functionalized PMOs with larger surface areas, compared with the

PMO which was functionalized via monomer **4**, which bears a long flexible tether (entry

10)[60].

Table 2-1. Physical Characteristics of BINAPO-bridged PMOs

Entry	Surfactant	Molar ratio of **1/2**	Surface area /m^{2}g^{-1} [a]	Pore size /Å [b]	Pore Volume /cm^{3}g^{-1}
1		*rac*-15/85	785	25.1	0.549
2		(*S*)-15/85	626	26.4	0.461
3		(*R*)-15/85	703	24.2	0.626
4	Brij76	(*R*)-5/95	708	26.9	0.574
5		0/100	668	27	0.54
6[c]		(*S*)-7.5/92.5	701	18.1	0.345
7[c]		(*R*)-7.5/92.5	786	16.5	0.347
8	C17TAB	rac-5/95	729	33.7	0.756
9	P123	rac-5/95	788	50.6	1.12
10[d]	P123	(*R*)-11/89	331	77	0.61

[a]Calculated from BET plot. [b]BJH adsorption average pore size. [c] TEOS (Si(OEt)$_4$) was employed instead of **2**. [d]Compound **4** and TMOS (Si(OMe)$_4$) were co-condensed, reported by Wang et al.[48]
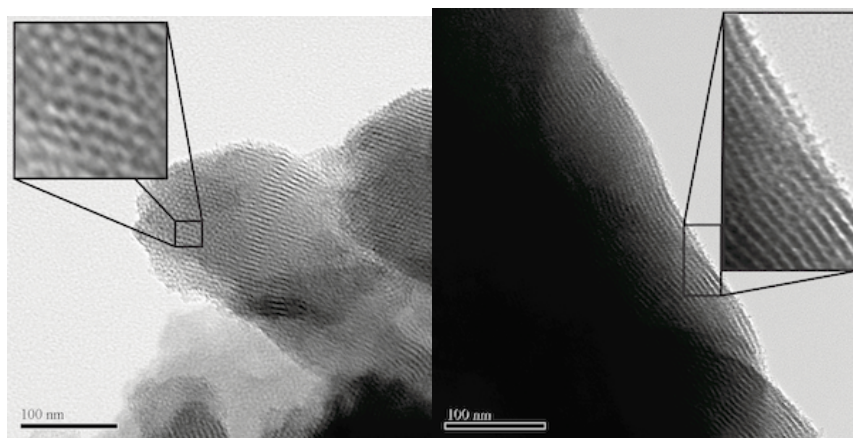
Figure 2-8. **TEM image of BINAP-PMO synthesized in the presence of Brij76**

2.3 Post-condensation modification

To generate an effective heterogeneous catalyst from this material, three post-condensation steps were required: silanol residues on the silica surface were protected as trimethysilyl ethers (TMS), initially oxidized phosphines were regenerated by reducing phosphineoxides, and finally complexation of ruthenium was carried out. In the following discussion, BINAPO-PMO corresponds to a PMO synthesized from 5% of (R)-BINAPO-bridged precursor **1** and 95% of biphenylene-bridged precursor **2** in the presence of Brij76 surfactant as SDA unless otherwise noted.

2.3.1 TMS capping of free silanols on the material

Trimethylsilyl (TMS) capping to protect silanol residues on the surface of the PMOs was carried out by employing hexamethyldisilazane (HMDS) prior to attempting the reduction of phosphineoxide to prevent unexpected side reactions (Scheme 2-11).[63] The treated material was analyzed by ^{29}Si solid state CP-MAS NMR (**Figure 2-9**). A new peak at 10 ppm was observed that corresponds to the introduced TMS groups. The increase in intensity for T^2- and T^3-sites, and decreased peak intensity for the T^1-sites clearly shows that silanols were successfully protected. Furthermore, there is no Q-site peak even after the HMDS treatment, thus no carbon-silicon bond cleavage was observed.

The porous parameter taken by nitrogen adsorption analysis showed no critical loss of porosity (Table 2-2, entry 1).
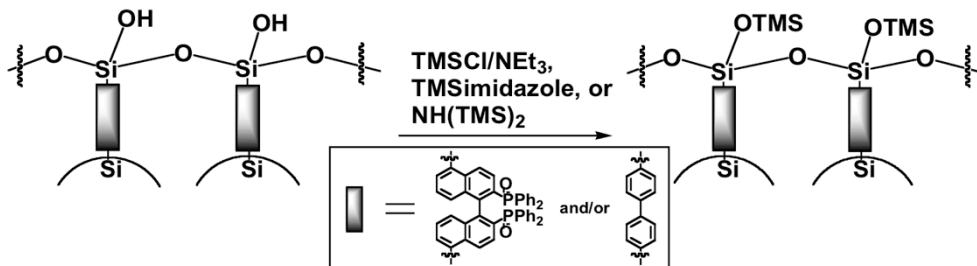
Scheme 2-11. TMS Protection of silanol residue on PMO
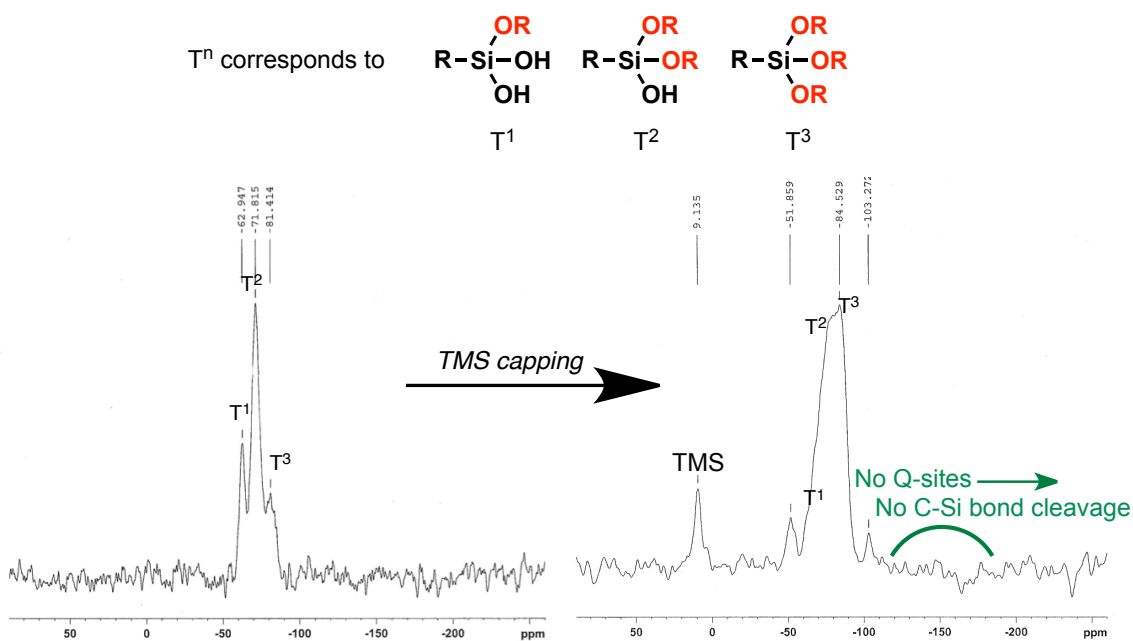
Figure 2-9. ^{29}**Si CP-MAS NMR before and after TMS capping of BINAPO-PMO**

2.3.2   Reduction of phosphine oxides in the solid state

Reduction of phosphineoxides of BINAPO-PMO was attempted by several methods. Scheme 2-12 shows the conditions for phosphineoxide reduction attempted. It

was difficult to reduce the phosphine oxides on silica-based materials with high conversion even after prolonged reaction times, with excesses of reagents. In the majority of cases, the mesoporosity of the PMO material was destroyed under conditions **a**, **b**, and **c** (Scheme 2-12). Finally, method **d** was shown to yield a significant amount of reduced phosphines by ^{31}P solid state CP-MAS NMR, but removal of triethyl phosphate, employed as an oxygen scavenger, was problematic. Pre-activation of PMO under high vacuum at 120ºC for 3h gave improved results to some extent, but this was far from perfect.

a. HSiCl$_3$/PhSiH$_3$ (reflux, 3d)
b. SmI$_2$/HMPA/THF (rt, 5 min)
c. HSiCl$_3$/NBu$_3$/m-xylene (140ºC, 24h)
or
d. P(OEt)$_3$/HSiCl$_3$/toluene/THF (80ºC. 3h)
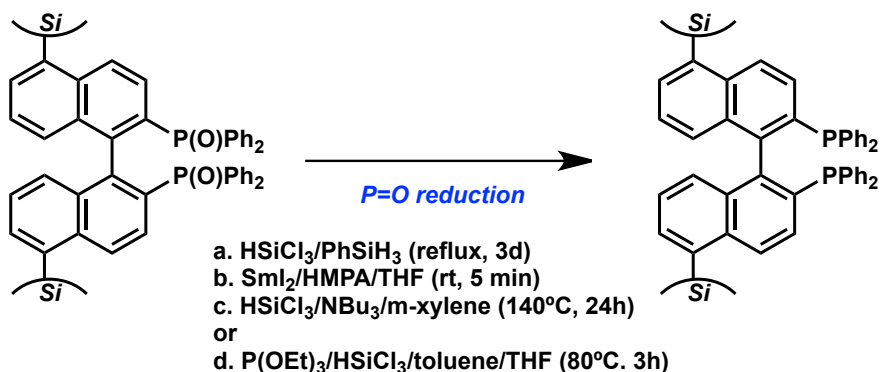
Scheme 2-12. Attempted conditions for phosphineoxide reduction

The reduction of phosphine oxides to phosphines is typically carried out with excess trichlorosilane at elevated temperatures, conditions that can result in dramatic losses of surface area and porosity in mesoporous materials by cleavage of carbon-silicon bonds, also possibly by agglomeration of the silane on the surface of the materials. Trichlorosilane is an extremely moisture sensitive compound, which generates

hydrochloric acid immediately, then this *in-situ* generated acid can also damage the silica

scaffolds, and catalyze the formation of siloxane aggregates. To avoid the damage of the

material through such a phenomenon, after considerable experimentation by myself and

other group members, I determined that ultra high purity trichlorosilane is needed. The

method **d** reaction was carried out with a new trichlorosilane purchased in an ampule,

which was carefully transferred to a Schlenk flask under argon then preserved with

activated basic alumina. ^{31}P solid state CP-MAS NMR was used to probe the success of

the reduction as the signal at 30 ppm for BINAPO shifted to -15 ppm for the trivalent

phosphine of BINAP (Figure 2-10).
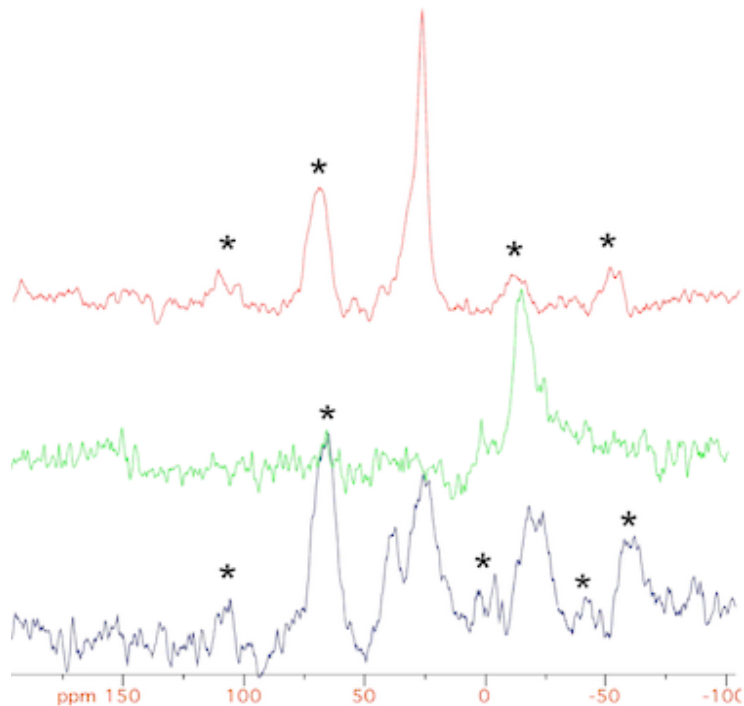
Figure 2-10.   Solid state CP MAS ^{31}P NMR spectra of a series of BINAP-PMOs.
Spinning side bands are shown with a star, and are confirmed by running two

83

separate MAS NMR spectra of each sample at different spinning rates. (Top) Before

reduction of phosphine oxides, the peak at 30 ppm corresponds to phosphine oxides

of BINAPO. (Middle) After reduction, the peak at -15 ppm is from the trivalent

phosphine of BINAP, and no phosphine oxide remains. (Bottom) After complexation

of ruthenium. The peaks at 28 and 40 ppm correspond to two phosphines

coordinating to ruthenium as forming [Ru(binap)(C_6H_6)Cl]Cl. The signal at -15

ppm is due to residual phosphine since a sub-stoichiometric amount of Ru (relative

to phosphine) was added.

Only under these conditions was the reaction completed without loss of

mesoporosity or order, Table 2-2 (entry 2). It is notable that clean conversion of the

phosphine oxide to the phosphine, at least as observed by ^{31}P solid state CP-MAS NMR,

implies perfect accessibility of BINAP functionalities on the surface of this material.

Considering that the phosphine oxide was added during the co-condensation step, this is a

remarkable result.

2.3.3   Complexation of ruthenium on BINAP-PMO

With the reduction successfully completed, complexation of ruthenium on the

BINAP unit was carried out by following reported conditions[79] but we found that the

PMO had to be activated under high vacuum at 80 ºC in an oil bath for over night prior to

use. Successive filtration and washing with copious amount of THF followed by acetone gave a pale red powder (Table 2-2, entry 3). This powder was stored in a vial filled with argon, but still could be handled in open air when it was dry. ^{31}P CP MAS NMR of this material (Ru/5%(R)-BINAP-PMO) showed successful complexation (Figure 2-10) and powder XRD revealed locally aligned lamellar structure (Figure 2-11) Thus, two distinctive phosphorous atoms coordinating to the cationic ruthenium (II) were observed, one trans to the chlorine atom at 40 ppm, another one at 28 ppm, which match with the reported data for BINAP-Ru complexes (Scheme 2-13).[79] The BINAP unit is fixed in the wall structure covalently at the 5- and 5'-position of the binaphthyl unit but the chiral axis is the carbon-carbon bond between the 1- and 1'-positions, therefore some strain of the twist angle should exist (Scheme 2-13), which may result in an alteration of the optimal bite angle. However, the successful complexation of the ruthenium revealed by ^{31}P NMR proved that the distortion of this twist angle or bite angle of the ligand was not so severe as to prevent complexation. Also, the amount of ruthenium doped on the material was determined by ICP-MS analysis to be 0.084 mmol/g Considering that the estimated amount of BINAP included in the material was 0.160 mmol/g, about 50% of BINAP was bound to the Ru(II) catalyst. The amount of the Ru(II) doped on the material

and also the colorless filtrate after the complexation implies quantitative trapping of the

Ru(II) specie on the material, but was not analyzed by ICPMS.
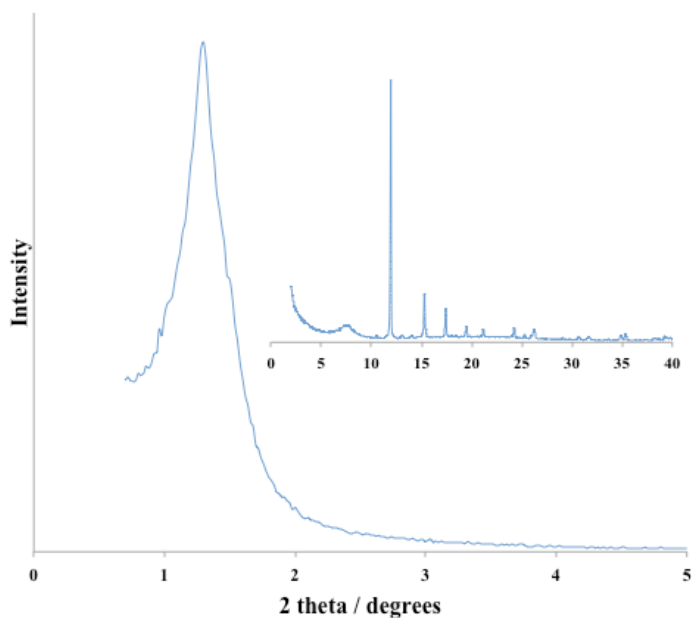
Figure 2-11.   Powder X-ray diffraction pattern of Ru/5%(R)-BINAP-BPh-PMO. The peak at 7.5 degree 2theta (inset) corresponds to $d = 11.7$ Å.
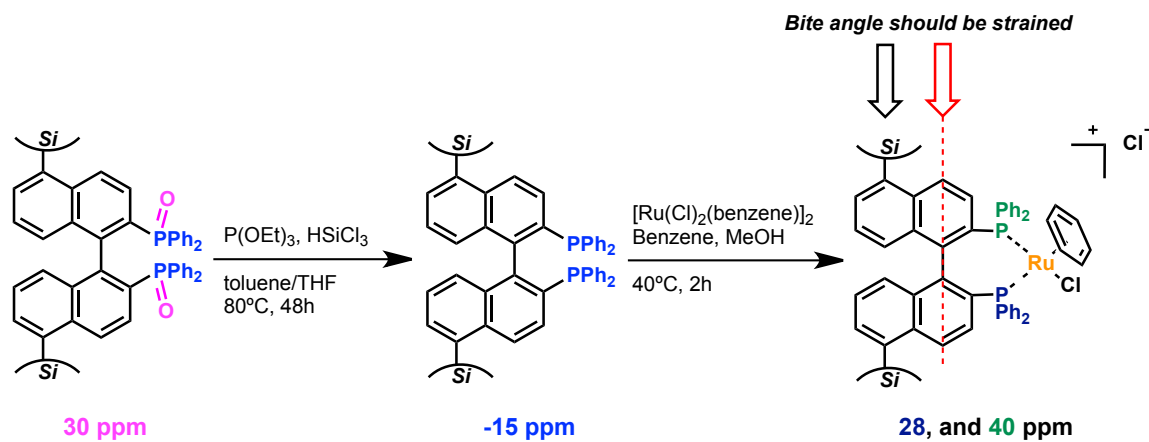
Scheme 2-13. ^{31}P solid state CP-MAS NMR results over post-condensation steps

Table 2-2.   **Physical characteristics of (R)-BINAP-PMOs after post-grafting modifications and catalysis use.**

Entry	Surface area /m^{2}g^{-1} [a]	Pore size /Å [b]	Pore Volume /cm^{3}g^{-1}	Modification/Catalysis use
1	750	28.2	0.669	TMS capping
2	812	26	0.717	Reduction of phosphine oxide
3	613	26.4	0.548	Complexation of ruthenium
4	694	28.2	0.607	High pressure hydrogenation
5	459	26.7	0.432	Hydrogen transfer in basic isopropanol

*Brij76 surfactant was used as a template. Molar ratio of **1/2** = 5/95.

2.4   BINAP-PMO in catalysis

2.4.1   Asymmetric hydrogenation of beta-keto esters under high-pressure hydrogen gas

Having prepared a well ordered mesoporous material containing a BINAP-modified Ru catalyst in the walls, we then set out to test the catalytic activity of this material in the ruthenium-catalyzed asymmetric hydrogenation of β-ketoesters (Scheme 2-14). As mentioned above, since the condensation points for the bis-triethoxysilyl BINAP monomer are the 5- and 5'-positions that are not in the line with the atropisomeric axis, and since there are no spacer units between the BINAP but rather the

polymerization points are rigidly held through carbon-silicon bond, it is conceivable that the twist angle will be distorted upon inclusion of the ligand in the material. Since the twist angle controls the bite angle of the two phosphine units and affects the transmission of chirality,[80, 81] it is possible that the BINAP-PMO will give different results compared to the solution catalyst, which is free to adopt the most favorable conformation around the central atropisomeric axis. Despite these concerns, the BINAP-PMO catalyst was exceptionally reactive, giving the expected products in excellent yields and stereoselectivities, consistent with solution results (Table 2-3). Since this is not often the case for supported catalysts,[59] these results are exceptionally important to validate our approach to the design of novel catalytically active PMOs.

Additionally, no differences in reactivity were observed relative to the size of the substrates employed, at least for typical substrates, indicating that the mesoporosity permits access to the active sites (Table 2-3, entry 1-6). Furthermore, since the catalyst is completely heterogeneous, recycling of the catalyst was easily carried out by a quick centrifugation followed by taking the supernatant out then the addition of fresh substrate solution (entry 2).

The physical characteristics of the recovered PMOs were analysed, and showed that the mesoporosity was maintained even after treatment under high-pressures of hydrogen (Table 2-2, entry 4).
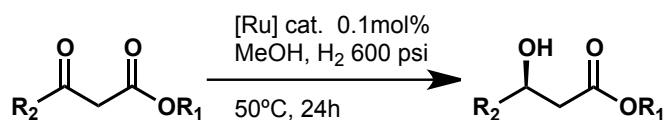
Scheme 2-14. Asymmetric hydrogenation of beta-ketoesters

Table 2-3.   Asymmetric catalytic hydrogenation under high pressure hydrogen gas

Entry	R1, R2	yield (%)[a]	e.e. (%)[b]
1	Me, Me	99	>99
2		99	>99
3	Me, Et	99	>99
4	Et, Me	99	>99
5	Me, iPr	99	>99
6	Me, 4-MeOPh	99	>99
7[c]	Me, Me	0	-

Ru/5%-(R)-BINAP-PMO was employed. [a]Isolated yield. [b]Determined by supercritical fluid chromatography(SFC). The onother enantiomer was below detection. [c]Control reaction employing 5%(R)-BINAP-PMO without Ru(II).

Another notable advantage of the use of a heterogeneous catalyst is that simple filtration is sufficient to purify the organic products. Thus, after the hydrogenation reaction, the PMO in the reaction mixture was separated by filtration and concentrating the filtrate by removal of the solvent in vacuo gives colorless oil. Both ^{1}H and ^{13}C NMR showed a pure product without any further purification by simple filtration (Figure 2-12).

Tiny peaks at aromatic region observed in the proton NMR likely result from residual

PMO powder which passed through the filter paper, and thus the use of a smaller pore

filter would likely provide even cleaner spectra.
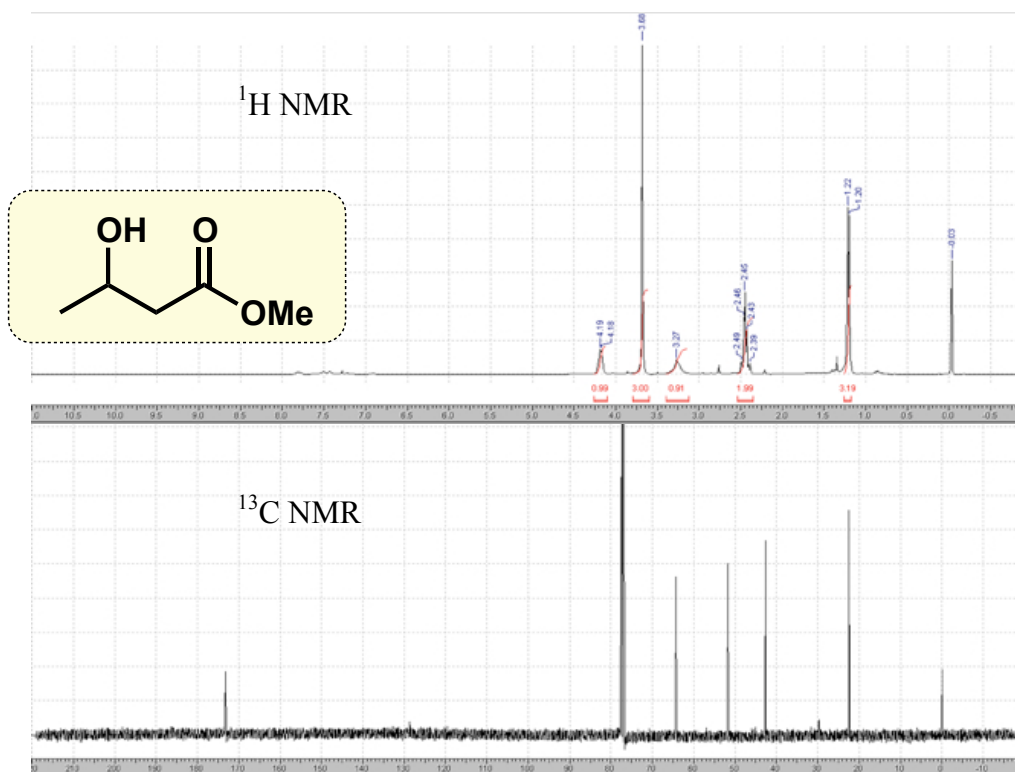
Figure 2-12. **^{1}H and ^{13}C NMRs of hydrogenation reaction product**

2.4.2 Hydrogen transfer reduction of acetophenone

Finally, we also employed the PMO catalyst in a ruthenium-catalyzed transfer

hydrogenation (Scheme 2-15). Although it is still necessary to add a chiral diamine ligand

to run the reaction stereoselectively, the hydrogenated product was obtained in good yield,

and importantly, the mesostructure was maintained even after reaction, despite being

subjected to a solution of basic isopropanol (Table 2-2, entry 5).
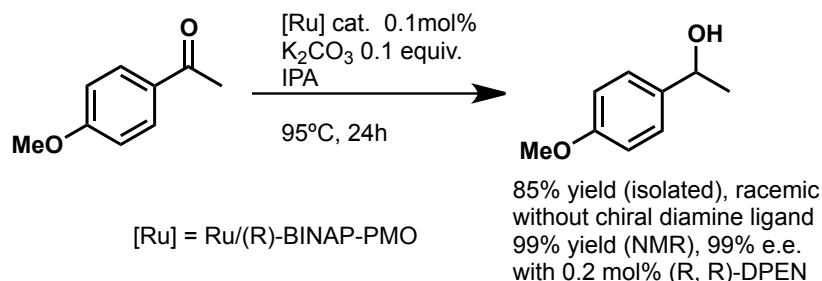
Scheme 2-15. Transfer hydrogenation of 4-methoxyacetophenone

2.5   Conclusions

In conclusion, BINAP and biphenylene-bridged hybrid periodic mesoporous

organosilicas (PMOs) were synthesized by co-condensation of the newly synthesized

5,5'-bistriethoxysilyl BINAP monomer **1** and 4,4'-bistriethoxysilylbiphenyl **2** in the

presence of surfactant templates. We have demonstrated the use of this PMO as a

heterogeneous asymmetric catalyst in two enantioselective hydrogenation methods, and

the preparation of PMOs with finely controlled structure including a crystal-like local

alignment of the aromatic monomers by co-condensation of two types of organic-bridged

precursors where both precursors have nearly the same distance between two siloxane

moieties of both ends. It is also noteworthy that the twist angle of the binaphthyl

atropisomeric axis of BINAP was fixed by installing the unit via rigid linkers at the 5 and

5'-positions, inhibiting rotation of this axially chiral moiety, but no negative effects for

binding transition metals or chirality transfer were observed. Fixing the axis of BINAP

should stabilize the axial chirality under harsh conditions, implying, for example, a

tolerance for asymmetric catalysis at high temperature which often results in decreases in

stereoselectivity. Further studies to apply this material for other new catalysis and

hybridization of our other organic-bridged precursors, and control of the morphology are

in progress.

2.6   References

1.   Crabtree, R. H., *Organometallic Chemistry of the Transition Metals, 4th Edition*.
2005; p 1.

2.   Hegedus, L. S. and Soderberg, B. C. G., *Transition Metals in the Synthesis of
Complex Organic Molecules, 3rd Ed.* 2009.

3.   Ullmann, F. and Bielecki, J., *Ber. Dtsch. Chem. Ges.* **1901,** *34*, 2174.

4.   Kornblum, N. and Kendall, D. L., *J. Am. Chem. Soc.* **1952,** *74*, 5782.

5.   Pitsinos, E. N.; Vidali, V. P. and Couladouros, E. A., *Eur. J. Org. Chem.* **2011**,
1207.

6.   Miyaura, N. and Suzuki, A., *Chem. Rev.* **1995,** *95*, 2457.

7.   Monnier, F. and Taillefer, M., *Angew. Chem., In. Ed.* **2009,** *48*, 6954.

8.   Crudden, C. M.; Glasspoole, B. W. and Lata, C. J., *Chem. Commun.* **2009**, 6704.

9.   Sadig, J. E. R. and Willis, M. C., *Synthesis-Stuttgart* **2011**, 1.

10.   Hartwig, J. F., *Acc. Chem. Res.* **2008,** *41*, 1534.

11.   Surry, D. S. and Buchwald, S. L., *Angew. Chem., In. Ed.* **2008,** *47*, 6338.

12.   Muci, A. R. and Buchwald, S. L., *Cross-Coupling Reactions* **2002,** *219*, 131.

13.   Hicks, J. D.; Hyde, A. M.; Cuezva, A. M. and Buchwald, S. L., *J. Am. Chem. Soc.* **2009,** *131*, 16720.

14.   Murai, S.; Kakiuchi, F.; Sekine, S.; Tanaka, Y.; Kamatani, A.; Sonoda, M. and Chatani, N., *Nature* **1993,** *366*, 529.

15.   Neufeldt, S. R. and Sanford, M. S., *Acc. Chem. Res.* **2012,** *45*, 936.

16.   Bryan, G. W. and Langston, W. J., *Environ. Pollut.* **1992,** *76*, 89.

17.   Giller, K. E.; Witter, E. and McGrath, S. P., *Soil Biology & Biochemistry* **1998,** *30*, 1389.

18.   Canali, L. and Sherrington, D. C., *Chem. Soc. Rev.* **1999,** *28*, 85.

19.   Buchmeiser, M. R. and Wurst, K., *J. Am. Chem. Soc.* **1999,** *121*, 11101.

20.   Terashima, T.; Nomura, A.; Ouchi, M. and Sawamoto, M., *Macromol. Rapid Commun.* **2012,** *33*, 833.

21.   Terashima, T.; Kamigaito, M.; Baek, K. Y.; Ando, T. and Sawamoto, M., *J. Am. Chem. Soc.* **2003,** *125*, 5288.

22.   Rouzaud, J.; Jones, M. D.; Raja, R.; Johnson, B. F. G.; Thomas, J. M. and Duer, M. J., *Helv. Chim. Acta* **2003,** *86*, 1753.

23.   Glasspoole, B. W.; Webb, J. D. and Crudden, C. M., *J. Catal.* **2009,** *265*, 148.

24.   Bianchini, C.; Frediani, M. and Vizza, F., *Chem. Commun.* **2001**, 479.

25.   Byun, J. W. and Lee, Y. S., *Tetrahedron Lett.* **2004,** *45*, 1837.

26.   Kim, J. H.; Jun, B. H.; Byun, J. W. and Lee, Y. S., *Tetrahedron Lett.* **2004,** *45*, 5827.

27.   Takizawa, S.; Arai, T. and Sasai, H., *J. Synth. Org. Chem. Jpn.* **2009,** *67*, 194.

28.   Bleloch, A.; Johnson, B. F. G.; Ley, S. V.; Price, A. J.; Shephard, D. S. and Thomas, A. W., *Chem. Commun.* **1999**, 1907.

29.   Raja, R.; Thomas, J. M.; Jones, M. D.; Johnson, B. F. G. and Vaughan, D. E. W., *J Am Chem Soc* **2003,** *125*, 14982.

30.   Kresge, C. T.; Leonowicz, M. E.; Roth, W. J.; Vartuli, J. C. and Beck, J. S., *Nature* **1992,** *359*, 710.

31.   Johnson, S. A., *Science* **1999,** *283*, 963.

32.   Stein, A.; Melde, B. J. and Schroden, R. C., *Advanced Materials (Weinheim, Germany)* **2000,** *12*, 1403.

33.   Inagaki, S.; Guan, S.; Fukushima, Y.; Ohsuna, T. and Terasaki, O., *J. Am. Chem. Soc.* **1999,** *121*, 9611.

34.   Melde, B. J.; Holland, B. T.; Blanford, C. F. and Stein, A., *Chem. Mater.* **1999,** *11*, 3302.

35.   Asefa, T.; MacLachlan, M. J.; Coombs, N. and Ozin, G. A., *Nature* **1999,** *402*, 867.

36.   Yoshina-Ishii, C.; Asefa, T.; Coombs, N.; J. MacLachlan, M. and A. Ozin, G., *Chem. Commun.* **1999,** *0*, 2539.

37.   Kapoor, M. P.; Yang, Q. and Inagaki, S., *J Am Chem Soc* **2002,** *124*, 15176.

38.   Hoffmann, F.; Cornelius, M.; Morell, J. and Froba, M., *Angew Chem Int Ed Engl* **2006,** *45*, 3216.

39.   Zhou, W. Z.; Thomas, J. M.; Shephard, D. S.; Johnson, B. F. G.; Ozkaya, D.; Maschmeyer, T.; Bell, R. G. and Ge, Q. F., *Science* **1998,** *280*, 705.

40.   Thomas, J. M.; Harris, K. D. M.; Edwards, P. P. and RSC, *Turning Points in Solid-State, Materials and Surface Science: A Book in Celebration of the Life and Work of Sir John Meurig Thomas*. RSC Pub.: 2008.

41.   Jones, M. D.; Raja, R.; Thomas, J. M.; Johnson, B. F. G.; Lewis, D. W.; Rouzaud, J. and Harris, K. D. M., *Angew. Chem. Int. Ed.* **2003,** *42*, 4326.

42.   Bianchini, C.; Burnaby, D. G.; Evans, J.; Frediani, P.; Meli, A.; Oberhauser, W.; Psaro, R.; Sordelli, L. and Vizza, F., *J. Am. Chem. Soc.* **1999,** *121*, 5961.

43.   de Rege, F. M.; Morita, D. K.; Ott, K. C.; Tumas, W. and Broene, R. D., *Chem. Commun.* **2000**, 1797.

44.   Shephard, D. S.; Maschmeyer, T.; Johnson, B. F. G.; Thomas, J. M.; Sankar, G.; Ozkaya, D.; Zhou, W. Z.; Oldroyd, R. D. and Bell, R. G., *Angew. Chem., In. Ed.* **1997,** *36*, 2242.

45.   Johnson, B. F. G.; Raynor, S. A.; Shephard, D. S.; Mashmeyer, T.; Thomas, J. M.; Sankar, G.; Bromley, S.; Oldroyd, R.; Gladden, L. and Mantle, M. D., *Chem. Commun.* **1999**, 1167.

46.   Tsuji, J.; Takahash.H and Morikawa, M., *Tetrahedron Lett.* **1965**, 4387.

47.   Johannsen, M. and Jorgensen, K. A., *Chem. Rev.* **1998,** *98*, 1689.

48.   Dubovyk, I.; Watson, I. D. G. and Yudin, A. K., *J. Am. Chem. Soc.* **2007,** *129,* 14172.

49.   Song, C. E. and Lee, S. G., *Chem. Rev.* **2002,** *102,* 3495.

50.   Yang, H.; Li, J.; Yang, J.; Liu, Z.; Yang, Q. and Li, C., *Chem. Commun.* **2007**, 1086.

51.   Heitbaum, M.; Glorius, F. and Escher, I., *Angew. Chem. Int. Ed.* **2006,** *45,* 4732.

52.   MacQuarrie, S.; Thompson, M. P.; Blanc, A.; Mosey, N. J.; Lemieux, R. P. and Crudden, C. M., *J. Am. Chem. Soc.* **2008,** *130,* 14099.

53.   Miyashita, A.; Takaya, H.; Souchi, T. and Noyori, R., *Tetrahedron* **1984,** *40,* 1245.

54.   Takaya, H.; Akutagawa, S. and Noyori, R., *Organic Syntheses* **1989,** *67,* 20.

55.   Noyori, R., *Adv. Synth. Catal.* **2003,** *345,* 15.

56.   Noyori, R., *Angew. Chem., In. Ed.* **2002,** *41,* 2008.

57.   McDonald, A. R.; Müller, C.; Vogt, D.; van Klink, G. P. M. and van Koten, G., *Green Chemistry* **2008,** *10,* 424.

58.   Hu, A.; Ngo, H. L. and Lin, W., *Angew Chem Int Ed Engl* **2004,** *43,* 2501.

59.   Framery, E.; Andrioletti, B. and Lemaire, M., *Tetrahedron-Asymmetry* **2010,** *21,* 1110.

60.   Wang, P. Y.; Liu, X.; Yang, J.; Yang, Y.; Zhang, L.; Yang, Q. H. and Li, C., *J. Mater. Chem.* **2009,** *19*, 8009.

61.   Seki, T.; McEleney, K. and Crudden, C. M., *Chem. Commun.* **2012,** *48*, 6369.

62.   Murata, M.; Ishikura, M.; Nagata, M.; Watanabe, S. and Masuda, Y., *Org. Lett.* **2002,** *4*, 1843.

63.   Sommer, J.; Yang, Y.; Rambow, D. and Blumel, J., *Inorg. Chem.* **2004,** *43*, 7561.

64.   Blumel, J., *Inorg. Chem.* **1994,** *33*, 5050.

65.   Blumel, J., *J. Am. Chem. Soc.* **1995,** *117*, 2112.

66.   Berthod, M.; Saluzzo, C.; Mignani, G. and Lemaire, M., *Tetrahedron-Asymmetry* **2004,** *15*, 639.

67.   Finkelstein, H., *Ber. Dtsch. Chem. Ges.* **1910,** *43*, 1528.

68.   Klapars, A. and Buchwald, S. L., *J. Am. Chem. Soc.* **2002,** *124*, 14844.

69.   Olah, G. A.; Wang, Q.; Sandford, G. and Prakash, G. K. S., *J. Org. Chem.* **1993,** *58*, 3194.

70.   Murata, M.; Yamasaki, H.; Ueta, T.; Nagata, M.; Ishikura, M.; Watanabe, S. and Masuda, Y., *Tetrahedron* **2007,** *63*, 4087.

71.   Yamanoi, Y. and Nishihara, H., *J. Org. Chem.* **2008,** *73*, 6671.

72.   Iizuka, M. and Kondo, Y., *Eur. J. Org. Chem.* **2007**, 5180.

73.   Komuro, K.; Ishizaki, K. and Suzuki, H., *Toagosei Annual Res. Report* **2003,** *6*, 24.

74.   Manoso, A. S. and DeShong, P., *J. Org. Chem.* **2001,** *66*, 7449.

75.   Ferreri, C.; Costantino, C.; Chatgilialoglu, C.; Boukherroub, R. and Manuel, G., *J. Organomet. Chem.* **1998,** *554*, 135.

76.   Boukherroub, R.; Chatgilialoglu, C. and Manuel, G., *Organometallics* **1996,** *15*, 1508.

77.   Ferreri, C.; Costantino, C.; Romeo, R. and Chatgilialoglu, C., *Tetrahedron Lett.* **1999,** *40*, 1197.

78.   Kotani, S.; Hashimoto, S. and Nakajima, M., *Tetrahedron* **2007,** *63*, 3122.

79.   Mashima, K.; Kusano, K. H.; Ohta, T.; Noyori, R. and Takaya, H., *Journal of the Chemical Society-Chemical Communications* **1989**, 1208.

80.   van Leeuwen, P. W. N. M.; Kamer, P. C. J.; Reek, J. N. H. and Dierkes, P., *Chem. Rev.* **2000,** *100*, 2741.

81.   Subramanium, S. S. and Slaughter, L. M., *Abstracts of Papers of the American Chemical Society* **2009,** *238*.

Chapter 3

Surface Selective Passivation of SBA-15

by Surfactant Reloading Method

3.1 Introduction

This chapter introduces and discusses a new methodology developed in our labs

to selectively deactivate the external surface of the mesoporous silica SBA-15[1, 2], which

has mesopores with larger diameter (~8 nm) than the more common mesoporous silica,

MCM-41[3] (~2.5 nm). The outcome of the procedure leads to exclusive protection of the

silanols on the exterior surface with trimethylsilyl (TMS) ether groups while maintaining

silanols on the internal surface of the pores. Most of the functionalized mesoporous

silicas used as catalysts[4], templates for nanoparticle synthesis[5], or drug delivery carriers[6]

are prepared by the post-synthesis grafting method as described in Chapter 1. This

method leads to unselective grafting, and even likely preferential grafting on the exterior

surface and at pore openings that are more accessible. However, since the external

surface of these materials is known to be 10% of the total surface area at a maximum[7],

the materials functionalized through such post-synthesis grafting methods have been

assumed to have all the functionalities are located on the interior of the pores even though

they are not perfect. This could be especially important in cases where catalysts are

immobilized since even small amounts of highly active catalyst can be responsible for all

observed activity. If chiral surfaces are employed, understanding the localization of the

catalyst is even more important. Finally, even catalysts that are not strongly immobilized

can benefit from a defined position of grafting since studies from our group have shown

that the shape of the pores can provide important protection against Ostwald ripening and

large nanoparticle formation.[8, 9]

3.1.1 Typical characteristics of mesoporous silica SBA-15

SBA-15 is one of the most popular mesoporous silica materials that are

commonly used in varieties of application as mentioned above and in Chapter 1[10-12].

Compared with MCM-41, the larger pore diameter allows even large molecules access to

the meso channels. The main difference between the synthetic procedures is the use of

non-ionic block copolymer P123 as a structure directing agent (SDA) for SBA-15,

compared with MCM-41, which is synthesized using cationic ammonium surfactants as

the template.[13] In addition to different sizes of the pore walls, SBA-15 is also different

from MCM-41 in that the former has micropores in the pore walls of various sizes

depending on the reaction conditions that interconnect the pores, formed by protrusion of polyethyleneglycol chain ends of P123 into the newly forming walls[14, 15] (Figure 3-1). In addition, the density of silanol groups on the surface is about 3.7 silanols per square nanometer ($SiOH/nm^2$) for SBA-15, while MCM-41 has 3.0 $SiOH/nm^2$.[16, 17]
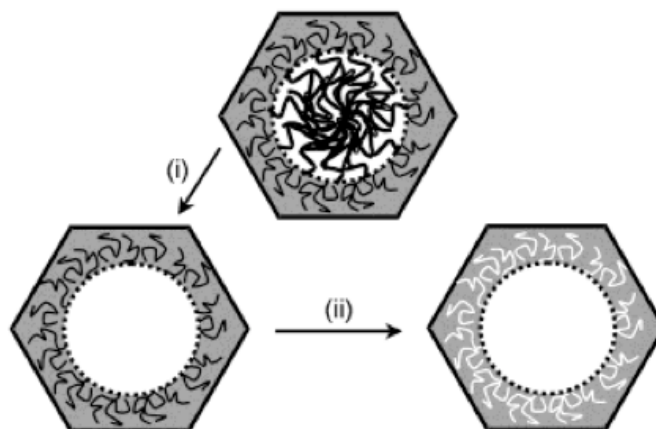
Figure 3-1. **Micropore formation in mesoporous SBA-15.[15]**

(i) Sulfuric acid (ii) calcination

3.1.2 Diffusion control and pore protection

Prior to our work, others have attempted to control the position of grafting in the functionalization of mesoporous materials.[5, 18-22] The methods attempted can be divided into two fundamental ideas, diffusion control and pore protection (Scheme 3-1).[23]
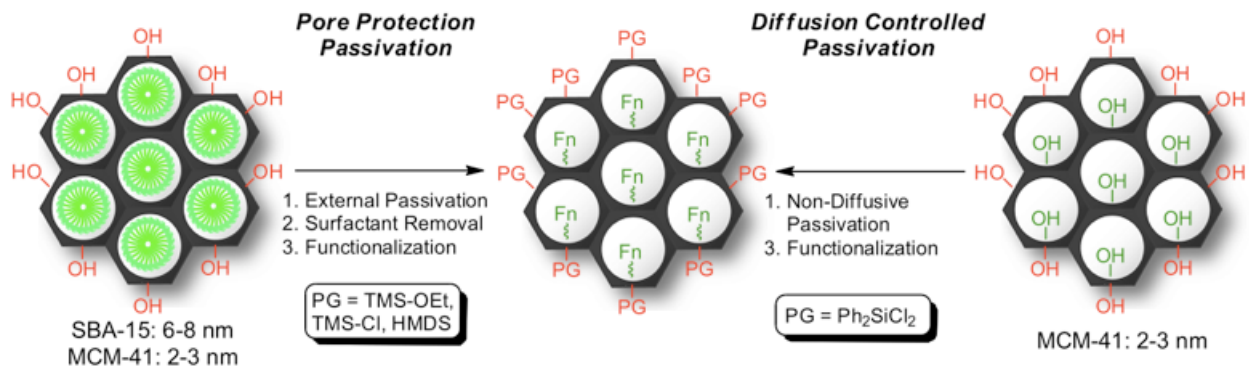
Scheme 3-1. General reagents and steps employed by selective passivation methods[23]

In diffusion control, a bulky protecting reagent, for example diphenyldichlorosilane, is employed to selectively protect silanols on the external surface first, followed by a treatment with smaller functionalizing reagents, which are proposed to then selectively functionalize the internal surface. It is believed that the protecting silyl groups are not installed on the internal pore surface due to size exclusion, therefore the mesopores of the sample materials remain free after the passivation process.[18-20] This method can be effective for MCM-41 type materials, whose pore diameters are relatively smaller, however not for SBA-15 or any other materials with larger pores.

In the pore protection strategy, the structure directing agents (CTAB or P123) or externally introduced polymers (poly-methylmethacrylate) are used to protect the internal surface prior to functionalization of external surface. Then after passivation of the

external surface, the polymer or surfactant is removed to permit selective functionalization of the internal surface.[5, 20-22]

3.1.3 Literature attempts at selective functionalization

In 2004, Schüth and co-workers reported a functionalized SBA-15 with magnetic cobalt nanoparticles deposited on the external surface.[22] They revealed that P123 in as-synthesized SBA-15 was insufficient to block the mesopores from functionalization such that some cobalt nanoparticles entered the pores, thus suggesting that the P123 in as-synthesized material doesn't fill the pores completely. In order to completely block the pores, they polymerized methyl methacrylate (MMA) to fill the mesopores with poly methyl methacrylate (PMMA) and demonstrated that this was successful at blocking the mesopores. The drawback of this method is the requirement for exceptionally harsh conditions to then "reveal" the mesopores for subsequent functionalization.

Brühwiler and co-workers reported trials of both diffusion controlled and pore protection approaches towards selective functionalization with aminopropyltrialkoxysilane groups on the external surface by reacting a series of aminopropyltrialkoxysilane agents with SBA-15 and arrays of silica nano channels (ASNC), or large pore- and small pore-materials (**Figure 3-2**)[20]. After installation,

propylamino groups were further reacted with fluorescein isothiocyanate (FITC) to observe the distribution of functional groups. Confocal Laser Scanning Microscopy (CLSM) images were then used to confirm the location of grafting (**Figure 3-2**a). From these images, it is obvious that the diffusion controlled method was not effective for SBA-15, even with the bulkiest silylating agent, likely due to its large pore diameter. However diffusion-controlled methods were successful for ASNC only when the largest silylating agent was employed. (**Figure 3-2**a).

Figure 3-2. Confocal Laser Scanning Microscopy (CLSM) images of SBA-15 (top, round shape particles) and ASNC (bottom, rectangle shaped particles) treated over diffusion controlled (left) and pore protection (right) selective functionalization by Brühwiler *et al*[2]. The same trial was repeated three times. (a) calcined and (b) as-synthesized materials.[20]

The results with the same materials using the pore-protection method in which as-synthesized materials (those containing the surfactant still in the pores) are treated with silylating agents are shown in (**Figure 3-2**b). In the case of ASNCs, again only the bulkiest silane was effective, but now, with the addition of pore protection, the bulky silane was able to be used only to functionalize the external surface of SBA-15 (**Figure 3-2**b). Smaller, more typically employed silanes continued to be ineffective even with pore protection.

These results imply that pore protection is effective only when employed with specialized silanes and depends highly on the functionalization conditions. The choice of organic solvent is critical since the SDAs employed to fill in the mesopores are also soluble in these solvents. In fact, even ASNC samples treated with APTES and BTESPA resulted in full functionalization, it was only the more exotic APTMEES that was effective, and therefore the applicability of this method is likely to be limited.

The first report of diffusion controlled grafting came from the group of Shephard and co-workers who reported an attempt to selectively passivate the external surface of MCM-41 with a bulky silylating agent (Figure 3-3). Diphenylchlorosilane was employed in THF to deactivate silanols on external surface of calcined MCM-41, and the resulting material was treated with APTES to affect internal functionalization. The critical factor in

this type of selective passivation is mobility of the passivation agent, Ph$_2$SiCl$_2$, thus this

approach presumes that silanols on the external surface are much more accessible than

those on the internal surface, consequently yielding an MCM-41 material in which the

external surface is deactivated by Ph$_2$Si- groups and the internal surface is free and

therefore still reactive with additional functionalizing agents.
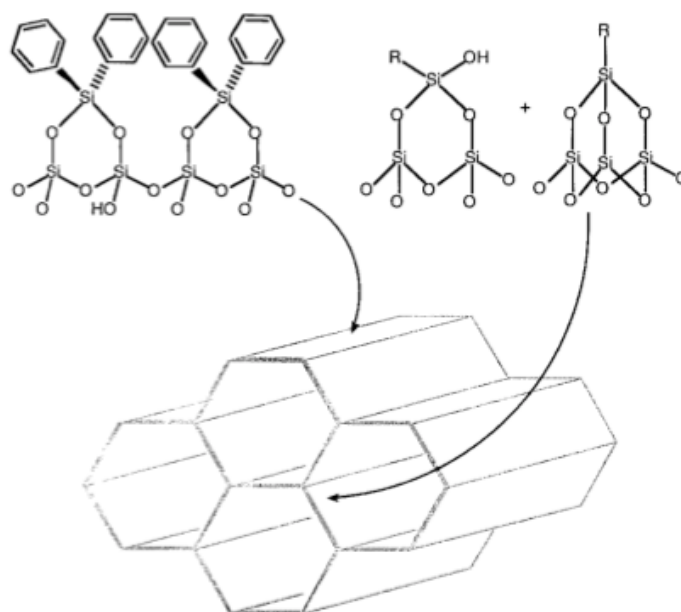
**Figure 3-3.   Schematic representation of selective passivation of external surface
with diphenyldichlorosilane followed by functionalization of internal surface.[19]**

To evaluate the success of this selective functionalization approach, Johnson and

Thomas prepared a material that was fully functionalized with APTES as a control

sample. Thus, the selectively functionalized material contains propylamino groups only

on the internal surface but the fully functionalized material has propylamino groups both

on internal and external surfaces. Both materials were then stained with a ruthenium complex and were observed by high resolution TEM (Figure 3-4). The use of these images, the sole proof of selective grafting, are a very qualitative measure of success, and even in some cases, it has been argued that greater contrast actually denotes less densely functionalized walls.
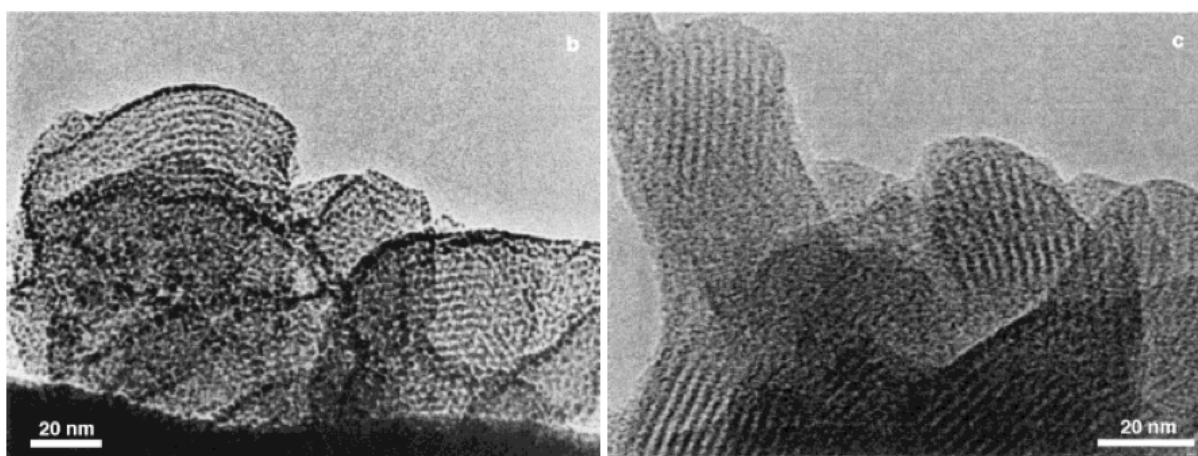
Figure 3-4.   TEM   images   of   (b)   selectively   functionalized   and   (c)   fully functionalized MCM-41 with propylamino groups both stained by ruthenium complex[19]

In spite of this less than clear proof of selective grafting, multiple reports have been published using this Ph_2SiCl_2/THF method on calcined MCM-41 system to prepare materials that are declared to be "selectively passivated MCM-41" for applications in heterogeneous asymmetric hydrogenation[7, 24-28] and allylic amination.[24, 29, 30] Enhanced yields and enantioselectivities, or unique regioselectivities are sometimes observed,

however, in many cases the key controls (in other words non-selectively grafted silica-supported catalysts) are absent.
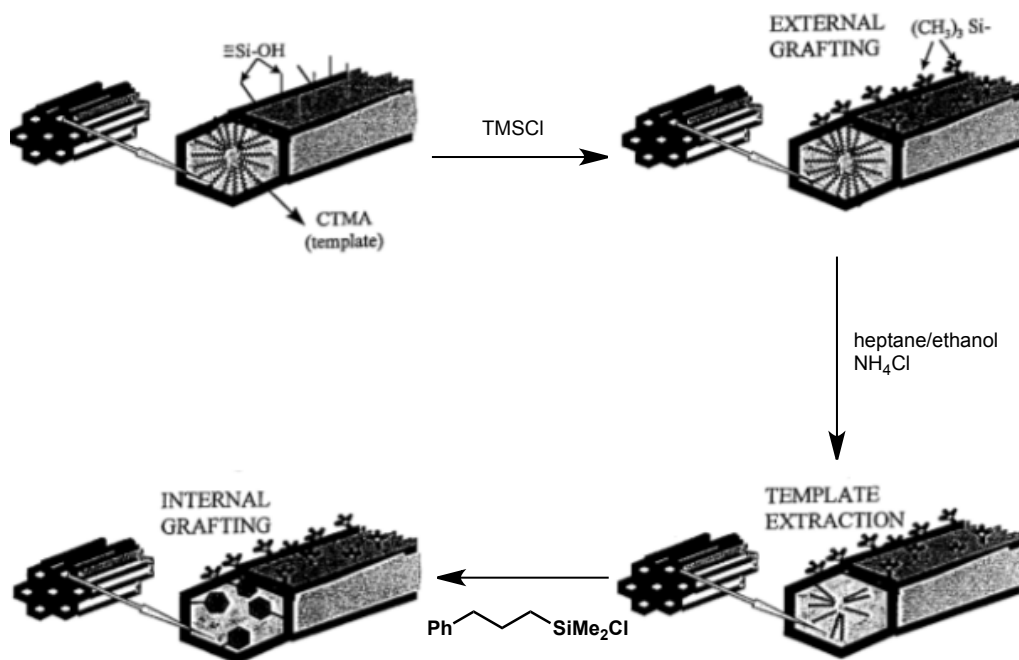
Scheme 3-2. Pore protection passivation (attempted by Ruiz-Hitzky et al.)[21]

Pore-protection methods have also been reported on MCM-41 materials by De Juan and Ruiz-Hitzky using propylphenyldimethyl chlorosilane as the functionalization reagent.[21] Trimethylsilylchloride was employed as the passivation agent in isopropyl alcohol and hydrochloric acid as the solvent. Elemental analysis (EA) of the samples was performed after each step, and the authors concluded that the method was able to selectively protect the exterior and permit subsequent functionalization of the interior. However their passivation conditions are quite harsh and really render it impossible to

maintain the supposedly pore protecting alkylammonium surfactants within the pores. Careful analysis of their published EA results actually indicate that it is likely that a large majority of the surfactant was extracted during the passivation procedure and very little if any propylphenyldimethyl chlorosilane ends up on the interior of the materials.

3.2 Selective passivation of SBA-15 by reloading method

Selective grafting of mesoporous silicas with smaller pore diameters have already been carried out by the diffusion control method[20, 31] or pore protection method with a special passivation agent,[32] however there is no generally effective procedure for the selective grafting of materials with large pores by either method. Thus we began to study selective silylation of the external and internal surfaces both in order to develop an effective, general method, and also to find a method to assess the effectiveness of our approach. Herein we report the first selective passivation of the external surface followed by selective functionalization of the internal surface of SBA-15.

We began with SBA-15, one of the most robust, most often prepared and most valuable mesoporous materials. Examination of the as-synthesized materials, containing the P123 surfactant still in the pores, by nitrogen adsorption revealed that these materials still have significant porosity with a total pore volume of around 150 m^2/g (Figure 3-5).

111

A previous student from our group, Jonathan Webb, found that further loading of appropriate surfactant micelles to as-synthesized materials yielded truly pore-protected materials[23], which showed little or no porosity (Figure 3-5, blue curve, re-SBA-15). The concept of reloading materials with surfactant after the material is synthesized has precedent in the work of Inagaki and co-workers, who employed surfactant micelles to introduce the dye coumarin to biphenylene-bridged PMO to introduce coumarin. The dye was effectively wrapped by micelles to permit its reintroduction to the material and the generation of visible light harvesting PMO materials.[33]
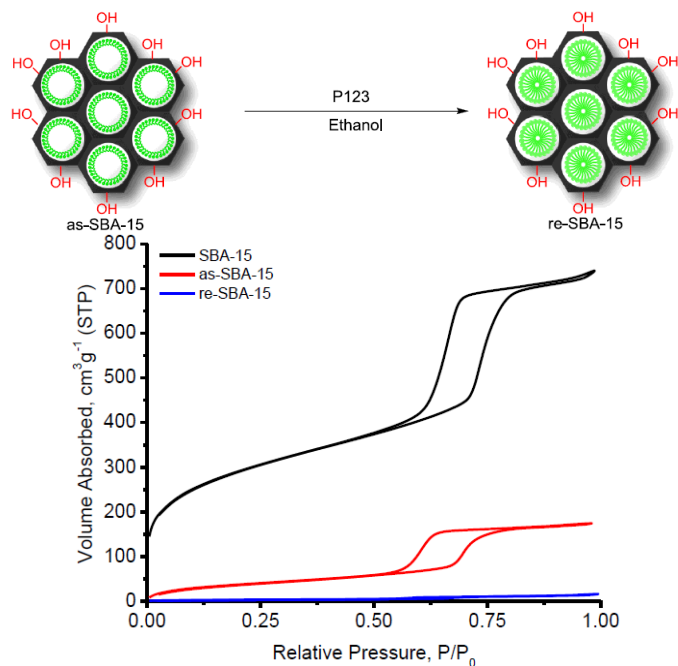
Figure 3-5. **Nitrogen adsorption isotherm plots of extracted SBA-15 (black), as-synthesized SBA-15 (red) and P123-reloaded SBA-15 (blue).**

3.2.1 Nitrogen adsorption evaluation of reloading method

Even though the P123 surfactant was successfully reloaded into as-synthesized SBA-15 (asSBA-15) to give a perfectly pore-protected material termed reSBA-15 as shown above, it must be carefully treated in subsequent passivation conditions otherwise the surfactant, which is also soluble in organic solvents, can be removed, resulting in a complete loss of pore protection. With this in mind, we found that neat hexamethyldisilazane (HMDS) at room temperature for 3 hours could be employed to introduce silyl groups on the exterior while maintain pore protection completely throughout the process as determined by SS NMR and nitrogen physisorption analysis (details are described in experimental section). The material treated with HMDS in this fashion was washed with hexane and then was placed in a Soxhlet extractor with ethanol to remove the P123. The resulting product was denoted sTMS-SBA-15 where "s" stands for selectively grafted. A series of SBA-15 materials treated in this way were analyzed by nitrogen adsorption to compare their porosity and also hydrophobicity, and by elemental analysis to study carbon content (Figure 3-6, Table 3-1)[23].
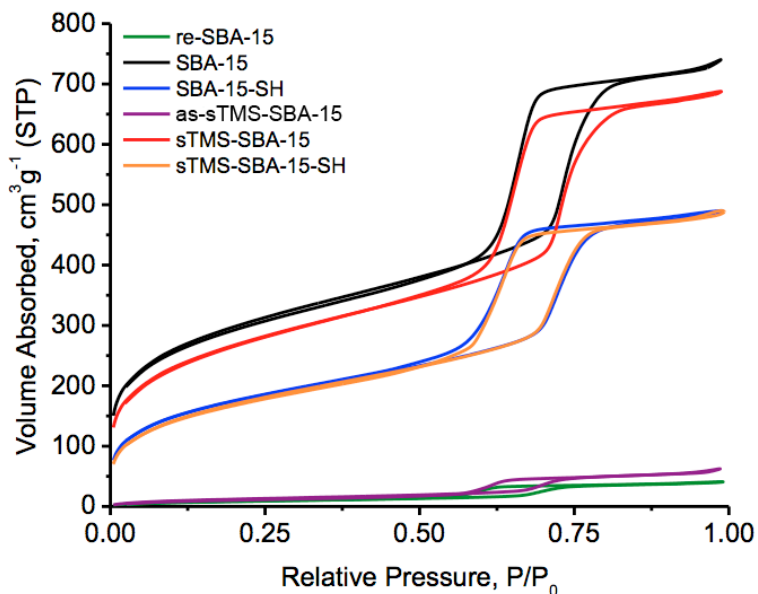
Figure 3-6.   Nitrogen adsorption isotherm plots of SBA-15s[23]

As mentioned above, reSBA-15 (green, Figure 3-6) showed almost no porosity,

and as-sTMS-SBA-15 (purple) exhibited slightly higher porosity, which may be due to

loss of small amount of P123 or may be due to weighing errors. The hydrophobicity

parameter (C value, Table 3-1) revealed that as-sTMS-SBA-15 was more hydrophobic

than reSBA-15, thus it is reasonable to assume that the silanols on the external surface

were successfully capped by TMS groups, although the presence of P123 still inside the

pores complicates the analysis.[7] After extraction of P123 by ethanol, sTMS-SBA-15 (red)

regained the expected high surface area that is within 10% of unfunctionalized SBA-15

(black), and in addition has a much higher hydrophobicity and increased carbon content

(4.6 versus 3.0 wt% carbon) due to TMS and ethoxy groups that were introduced ethanol

extraction process (*vide infra*). This is a huge improvement compared with literature

methods.[5, 21, 34-37]

Subsequently, sTMS-SBA-15 was treated under optimized functionalization

conditions to introduce mercaptopropyl groups exclusively on internal pore surface.

Among many commercially available alkoxysilyl compounds, thiol functionality was

selected because sulfur can be quantitatively analyzed by elemental analysis, also post-

grafting conditions for the introduction of mercaptopropyltrimethoxysilane (MPTMS)

onto SBA-15 materials have been fully established in our lab due to previously reported

palladium catalysis and scavenging projects.[10, 12, 38, 39] The selectively functionalized

material is denoted as sTMS-SBA-15-SH compared to samples which are functionalized

by typical post-synthesis grafting methods using MPTMS, which are called SBA-15-SH.

sTMS-SBA-15-SH (orange) showed an almost perfectly overlapped isotherm curve with

SBA-15-SH (blue). Furthermore, increased hydrophobicity and carbon content from

TMS groups and also the same value of sulfur content were observed (Table 3-1, bottom

two entries). It should be noted that the more functional groups that are installed on the

internal pore surface, the less pore volume and surface area a material has, however

modification of the external surface results in little or no change in the porosity of the

material. The nitrogen adsorption data obtained from a series of selectively functionalized

SBA-15 materials by the reloading method meet these criteria very well.

Table 3-1. **Physical characteristics of a series of SBA-15 materials by nitrogen adsorption and elemental analysis**

Material	$S_{BET}{}^a$, $m^2\,g^{-1}$	C^b	$D_{BJH}{}^c$	$V_p,{}^d\,cm^3\,g^{-1}$	C wt%	S wt%
as-SBA-15	19	26	7.4	0.04	28.7	-
re-SBA-15	6.9	41	6.9	0.01	34.5	-
as-sTMS-SBA-15	19	26	7.4	0.04	25.4	-
SBA-15	973	182	7.5	1.07	3.0	-
sTMS-SBA-15	878	76	7.5	1.04	4.6	-
SBA-15-SH	636	90	7.1	0.77	8.8	3.9
sTMS-SBA-15-SH	627	68	7.1	0.77	9.9	3.9

[a] BET surface area, [b] calculated from BET plot, [c] BJH adsorption pore diameter, [d] BJH adsorption cumulative pore volume.

Even though nitrogen adsorption and elemental analysis results implied successful

selective functionalization of SBA-15, there is still some concern about the stability of

the passivation layer during the P123 removal process and therefore its ability to continue

to block functionalization with the "reactive" reagent, such as MPTMS. Unfortunately,

due to the length scales involved, there is no analytical technique that can directly

determine if this type of functionality is located on the specific domain of the mesoporous material. Due to these remaining questions, multiple analytical techniques were employed together. Among multiple tests, quantitative analysis by high resolution solid state NMR was the most successful, as described below. Prior to turning to this method, we also examined the use of FloDots which, if effective, would have been perfectly able to distinguish between the external and internal surface area.

3.2.2 FloDots test by differential adsorption on hydrophilic surface

Even though the successful installation of TMS groups was observed, in house solid state ^{13}C NMR studies indicated that ethoxy groups were being introduced onto the surface during the extraction of the P123. Since external grafting of small amounts of MPTMS would not change the physisorption parameters significantly, but could affect catalytic performance significantly, we were interested in using a second method to assess the effectiveness of the localization of the MPTMS groups.

Thus we turned to the use of FloDots, which are silica nanoparticles in which a fluorescent dye molecule, dichloro trisbipyridine ruthenate (Ru(bpy)$_3$Cl$_2$), is installed via a reverse phase micelle templating process. Critically, the particle size of these nanoparticles can be finely controlled (Scheme 3-3).[40-42]

117
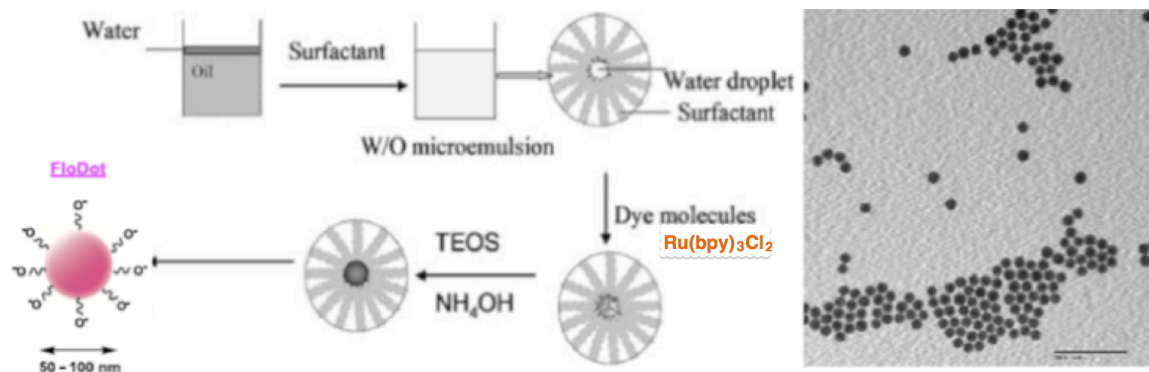
Scheme 3-3. **FloDot synthesis and TEM image of size controlled particle. Modified from a schematic picture in the literature[40]**

The idea of this test employing FloDots is based on the differential adsorption of controlled-size particles. Thus particles whose size is larger than the pore diameter of the mesoporous materials being studies cannot be taken up into the internal surface. Thus if adsorption of the FloDots takes the form of a chemical reaction with an introduced functional group (such as a click reaction) or interaction with surface silanols, the passivation layer on the external surface should prevent the adsorption of FloDots. The FloDots we employed are stabilized and covered by phosphonate species to prevent the particle from over growth or aggregate formation. A second effect of this hydrophilic phosphonate is that it leads to differential adsorption on hydrophilic (SBA-15) or

hydrophobic (sTMS-SBA-15) surfaces, which can provide an estimate of the effectiveness of the passivation layer (Scheme 3-4).[*1]
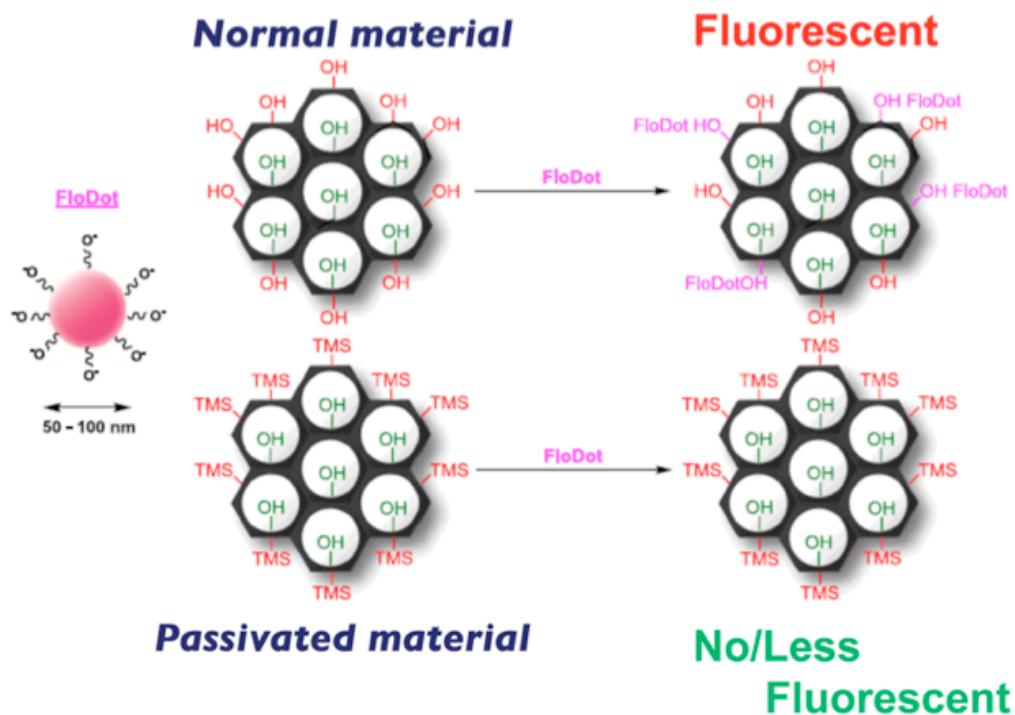
Scheme 3-4. Differential adsorption of FloDots on SBA-15 materials

A series of SBA-15 materials (SBA-15, sTMS-SBA-15 and TMS-SBA-15) were suspended in a suspension of FloDots in tertiary butanol / water as a 1 / 1 mixture. These suspensions were shaken by hand and then left to stand overnight. The powder was

---

[*1] Copper catalyzed azide-alkyne cycloaddition reaction employing azide functionalized SBA-15 and alkyne functionalized FloDots was attempted by Webb, however the test was unsuccessful due to nonspecific adsorption.[23]

recovered by centrifugation then dispersed in CTAB solution to wash out weakly bound

FloDots. This solution was filtered and washed with copious amount of water, ethanol,

and hexane. The recovered materials were dried under in air over night and then placed

under high vacuum at room temperature for 1h prior to fluorescence measurement. The

samples (~5.0 mg) prepared by this procedure were dispersed in 3.5 mL of DMF. The

suspension was stirred with a magnetic stirring bar during the measurement.

The emission scans of three samples are depicted in below (Figure 3-7). Normal

SBA-15 (black), which has silanols on both internal and external surface, showed the

largest emission, while sTMS-SBA-15 (blue) and TMS-SBA-15 (red) showed decreased

emission. Even though sTMS-SBA-15 revealed larger emission peak than fully

passivated SBA-15, this provides some evidence that the external surface passivation by

the SDA reloading method was effective since greatly reduced adsorption of FloDots was

observed, indicating a passivated external surface. The larger emission thus extra

adsorption of FloDots on the sTMS-SBA-15 sample compared with TMS-SBA-15 is

possibly due degradation of the passivation layer during SDA extraction process with

ethanol which generates ethoxy adducts and silanols from surface bridged siloxanes,

which will be discussed in more detail below (Scheme 3-5). Also since even TMS-SBA-

15 showed small emission peak from FloDots, this implies that FloDots can weakly bind

to the surface even though silanols are capped with TMS groups. Since not all silanols are reactive to silylating agents,[44] these silanols are responsible for the adsorption.
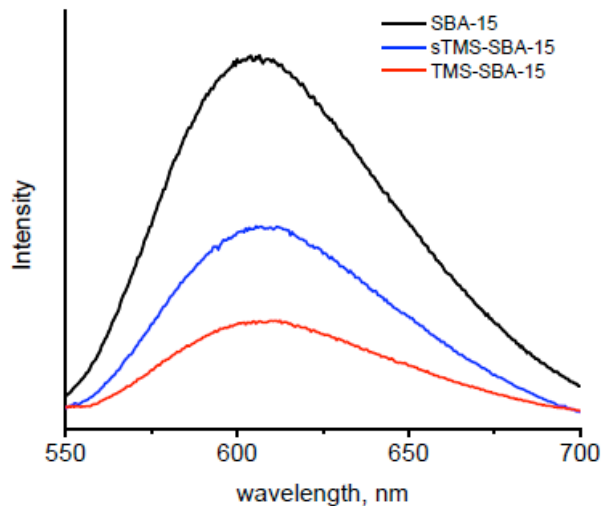
Figure 3-7. **Fluorescence emission scans of a series of SBA-15 materials treated with FloDots. Excitation wavelength = 450 nm. Intensity is normalized by the exact sample mass.**
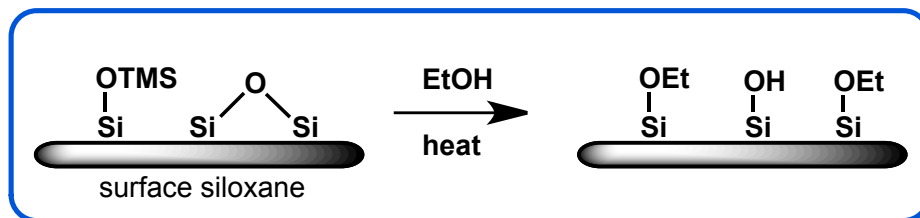
Scheme 3-5. **Ethanol induced ring opening of the surface siloxane**[43, 44]

According to the obtained fluorescence spectra (Figure 3-7), the FloDots test does not seem to provide a definitive answer with regard to the effectiveness of the TMS passivation strategy. In fact, randomly aggregated FloDots were obviously observed on a TEM image of the material with FloDots (Figure 3-8), therefore it seems to be difficult to

give neither quantitative nor qualitative comprehension from this test although the spectra

with the same intensity ratio were reproducible. An additional difficulty may be that the

surface of these materials will have uncapped silanols which absorb FloDots but are not

reactive with alkoxysilyl species for grafting.[45] Hence we turned to other tests as

described below.

0.5 μm
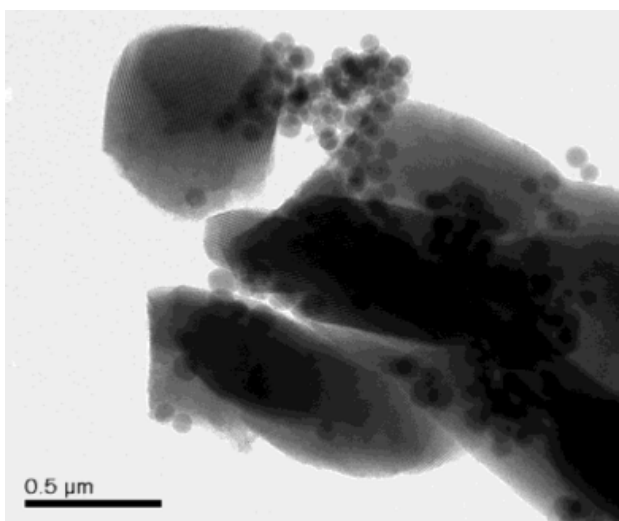
Figure 3-8.   A TEM image of SBA-15 with FloDots[23]

3.2.3 Fluorescence quenching with gold nano particles (GNPs)

In the FloDots test, the samples were treated with our selective passivation

process but not functionalized internally, and therefore the data shown above do not give

any information about the stability of the passivation layer toward the grafting conditions

for introduction of alkoxysilyl groups. A test to evaluate selectively functionalized

materials was invented by Webb[23] which was inspired from Lejeune's work.[46] Thus a

fluorescent dye, pyrenylmaleimide, was covalently attached to the surface thiols of

sTMS-SBA-15-SH and SBA-15-SH, which were then employed in fluorescence

quenching[46] tests with gold nanoparticles (GNPs). The size controlled GNPs cannot

interact with pyrenylmaleimide grafted on internal surface but only with those on the

external surface. Therefore, the sample prepared by selective passivation (sTMS-SBA-

15-SH-pyr), which does not have thiol anchors on external surface should not have

pyrenylmaleimide on the external surface, only the internal surface, and then should not

show fluorescence quenching. The control sample (SBA-15-SH-pyr) which has the

fluorescent species grafted on both the internal and external surfaces should, however,

show a fluorescent emission spectrum with decreased intensity due to the partial

quenching by GNPs interacting with the external surface-bound pyrenyl groups (Scheme

3-6).
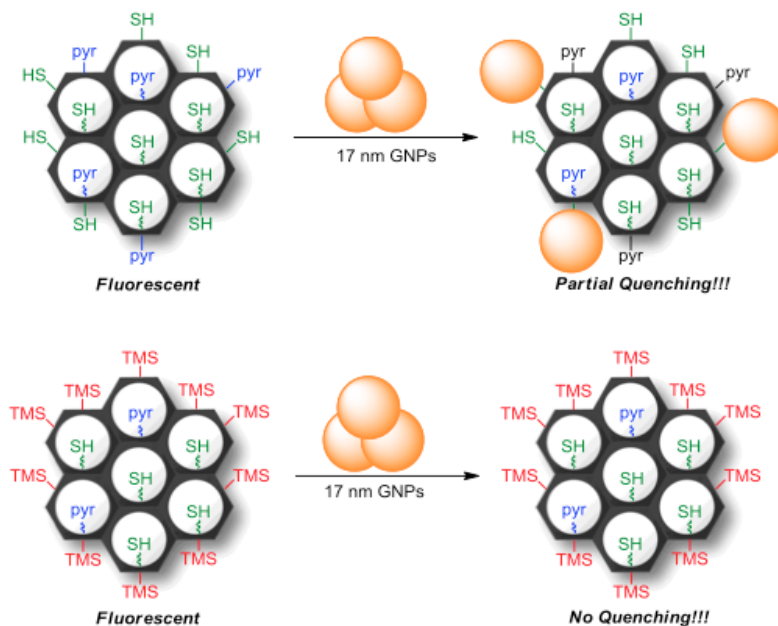
Scheme 3-6.   Fluorescence quenching test with size controlled GNPs[23]

(Pore diameter of SBA-15 is about 8 nm)

GNPs were synthesized with particle size controlled procedure according to literature precedent,[47] and both thiol functionalized SBA-15 materials were treated with pyrenylmaleimide in THF in the presence of triethylamine (Scheme 3-7). Pyrenylmaleimide was covalently attached to thiol anchors on the material to give fluorescent samples, sTMS-SBA-15-pyr and SBA-15-pyr, that showed fluorescence emission spectra due to grafted pyrene.
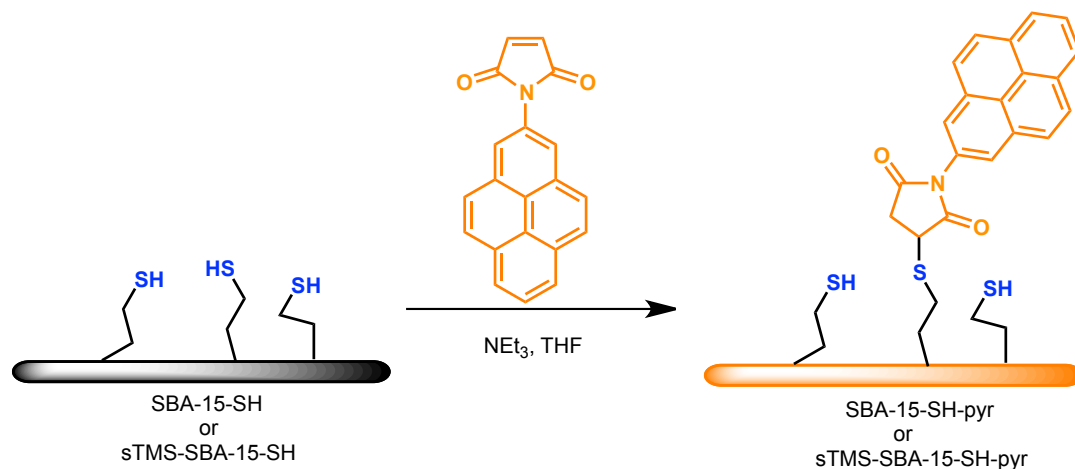
Scheme 3-7. Grafting pyrenylmaleimide on surface thiols (molar ratio of thiol / pyrenylmaleimide = 50 / 1)

The fluorescent emission scanning spectra of the samples are shown in Figure 3-9. Focusing at the normalized intensity at the top of the emission peak (377 nm), SBA-15-pyr showed 2% decreased emission after GNP treatment, while sTMS-SBA-15-pyr showed 7% increased emission. With this result in hand, it was felt that possibly the large size of the nanoparticles relative to immobilized pyrenes on the surface would lead inevitably to poor contact with all of the pyrenes and again an inability to quantify our approach. This theory was strengthened by analysis of the materials by XPS, which showed no signal indicating the presence of gold, (see Appendix). Therefore we finally turned to quantitative solid state NMR in collaboration with Professor Pruski's group at the Ames Lab in the US.
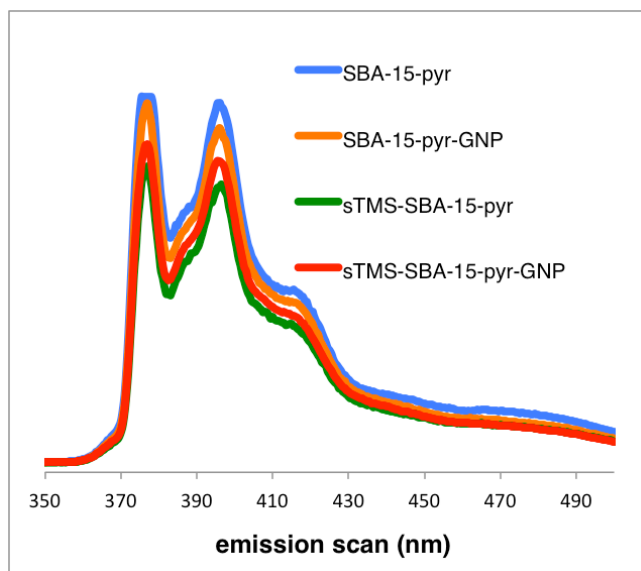
Figure 3-9. Fluorescence emission spectra by GNP test. Excitation at 330 nm, the intensities are normalized with respect to the sample mass.

3.2.4 Quantitative evaluation by solid state NMR

In general, quantitative analysis by using solid state NMR is difficult due to the large baseline noise from anisotropic distribution of the samples, however the recent invention of ultra fast magic angle spinning (MAS) NMR has permitted more reliable analysis and remarkable line widths for SS NMR.[48-51]

A series of SBA-15 samples were analyzed by quantitative solid state NMR (Figure 3-10,

Table 3-2). In sample (a) re-SBA-15, whose mesopores were filled with reloaded P123 surfactants, large Q4-site (-108.1 ppm), Q3-site (-99.1 ppm), and trace amounts of Q2-site silicon (-90.0 ppm) species were observed. In sample (b), which is sample (a)

subjected to silylation conditions as described above, decreased Q2- and increased Q4-site silicon signals were observed, consistent with effective silylation. Unchanged or slightly increased Q3-sites are expected when Q2-site species were capped with single TMS groups, transforming them to Q3 sites (Scheme 3-8).
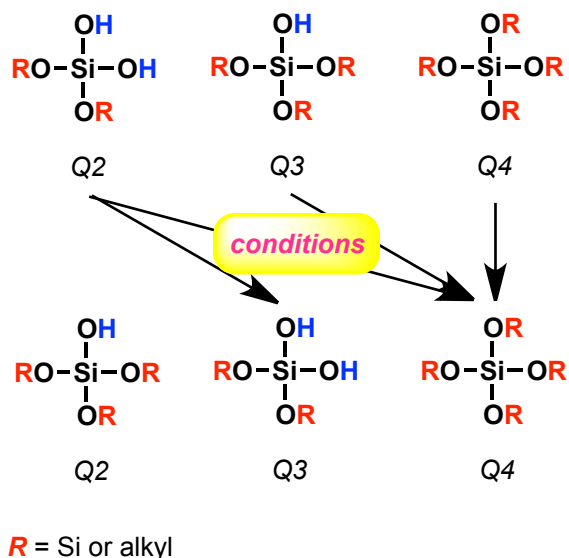
Scheme 3-8.   Transformation of Q-site silicon species during silylation

Simultaneously, almost the same numbers of Q3 sites were transformed to Q4 sites. As expected, a new peak appeared at 15.6 ppm corresponding to the silicon atom of the introduced TMS groups. After this, P123 surfactant still remaining in the mesopores was extracted by hot ethanol. Sample (c) showed further decreased Q3-site intensity and increased Q4-site silicon species, but most importantly, the size of the M-site silicon environment dramatically decreased in intensity. It should be recalled that increased hydrophobicity and carbon content were observed by nitrogen adsorption and elemental

127

analysis so far, thus the sample (c) sTMS-SBA-15 actually has TMS groups present on the surface but these are less than the detection limit by SS NMR in this case. In addition, the change in Q-sites species from (b) to (c) is proposed to result from the formation of ethoxy groups on the surface in hot ethanol media (as shown in Scheme 3-5), and also increased cross linking of the wall structure by hydrothermal treatment.
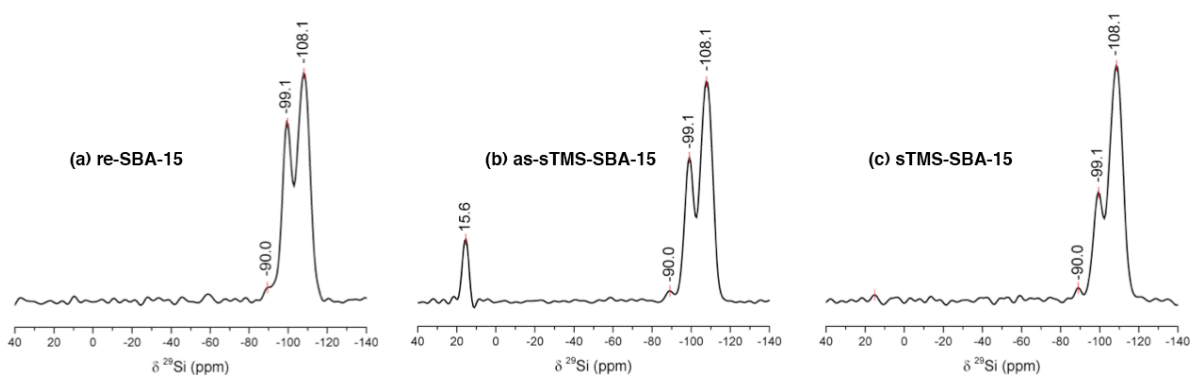
Figure 3-10.   29Si DP-CPMG/MAS spectra: (a) re-SBA-15, NS = 872, S/N = 109; (b) as-sTMS-SBA-15, NS = 296, S/N = 83; (c) sTMS-SBA-15, NS = 296, S/N = 57.

Table 3-2.   Quantitative ^{29}Si DP-CPMG/MAS data in terms of silicon M-, T-, and Q-sites.

Sample	%M	% Q2	% Q3	% Q4	silylation effic. (%)
(a) re-SBA-15	0	4	34	62	0
(b) as-sTMS-SBA-15	9	1	35	64	20
(c) sTMS-SBA-15	0	3	21	76	0

Q-sites were normalized to 100%.

To investigate the rationale for the apparent loss of the TMS groups during the ethanol extraction process, solid state ^{1}H-^{29}Si CP-CPMG-HETCOR was carried out (Figure 3-11). Remarkably, the spectrum revealed that there are two proton peaks that correlate to M-site silicon species, a stronger one at 0.5 ppm and weaker one at -0.5 ppm. Based on this information and also on the fact that the silylation efficiency was much too high in the first estimation, we proposed that the stronger intensity signal results from TMS groups attached to the ends of the surfactant P123, which is not covalently fixed on the material and is thus easily washed out during surfactant extraction process. In fact the 20% efficiency in Table 3-2 (b) implies excess of TMS groups existing on the material since the external surface area is 10% maximum relative to the whole surface area of the material, and even complete silylation of the external surface should not be expected.[32] Thus the weaker peak observed corresponds to TMS groups that were successfully installed on the surface silanols remaining even after the extraction while the strong peak corresponds to silylation of the free OH groups on P123.
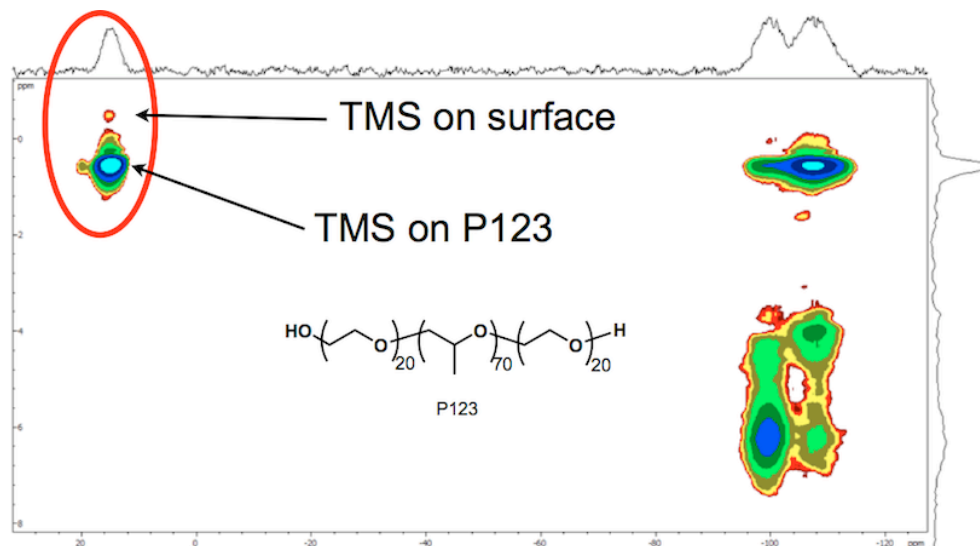
Figure 3-11. ^{1}H-^{29}Si CP-CPMG-HETCOR spectrum of as-sTMS-SBA-15. The vertical axis corresponds to ^{1}H δ (ppm) and the horizontal axis to ^{29}Si δ (ppm).

Since the signal to noise from TMS groups on the material is low, it was hard to quantify this value by ^{29}Si NMR as shown in Figure 3-10 (c). However, solid state ^{1}H NMR permitted us to calculate the number of TMS groups from the peak integral ratio. Thus the passivation efficiency by TMS groups on sTMS-SBA-15 was calculated by ^{1}H DP-MAS NMR using hexamethylbenzene (HMB) as an internal standard (Table 3-3). The quantitative analysis showed that 3 % of silanols on sTMS-SBA-15 were capped with TMS groups. Combining this result with the nitrogen adsorption data, which suggest that the internal surface was not functionalized by any protecting group or functional group, the estimated passivation efficiency of the external surface is 30%, or 1.24 groups

of TMS per nm^2 exist. The key assumption in this calculation is that the external surface represents 10% of the surface area.[52-54]

Table 3-3. **Quantitative data of TMS groups by ^{1}H DP-MAS NMR of sTMS-SBA-15, analyzed with hexamethylbenzene (HMB) as an internal standard.**

Based on ^{1}H Spin-Counting	
TMS groups/nm^2 (overall)	0.124
TMS groups/nm^2 (if ext. only)	1.24
overall silylation effic. (%)	3
ext. silylation effic. (%)	30
mmol of TMS/g	0.16

Even though the passivation efficiency was not 100%, the steric hindrance of TMS groups and the geometry of surface silanols prevented functionalization. It was confirmed by stability tests employing TMS-SBA-15. Solid state ^{13}C and ^{29}Si NMRs of TMS-SBA-15 was measured before and after hot ethanol treatment which was similar our surfactant removal condition. ^{29}Si NMR revealed that there was almost no TMS layer degradation over the hot ethanol process (Figure 3-12), and ^{13}C NMR didn't show growth of new ethoxy peaks (Figure 3-13). Furthermore, TMS'd efficiency of these samples were estimated as 30%, which was as dense as the TMS layer on the external surface of

sTMS-SBA-15. Therefore, sTMS-SBA-15 should have new ethoxy adducts exclusively on internal pore surface without any damage on the external TMS layer. Addition to the stability to hot ethanol tests, TMS-SBA-15 was treated in a standard post-synthesis grafting condition in the presence of MPTMS (Figure 3-14). After the treatment, the sample recovered was isolated by vacuum filtration and was washed with copious amount of toluene, ethanol then acetone. Elemental analysis of the sample showed 0 % sulfur content, thus the TMS layer with 30% TMS'd efficiency was found to be inert to post-synthesis grafting at least toward MPTMS.
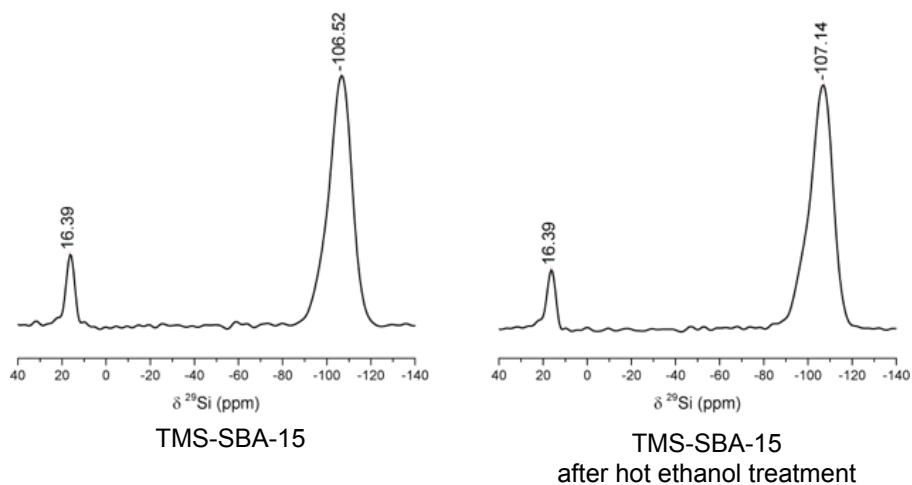
Figure 3-12. ^{29}**Si solid state NMRs of TMS-SBA-15, before (left) and after (right) stirring in ethanol at 85 °C for 48 hours.**
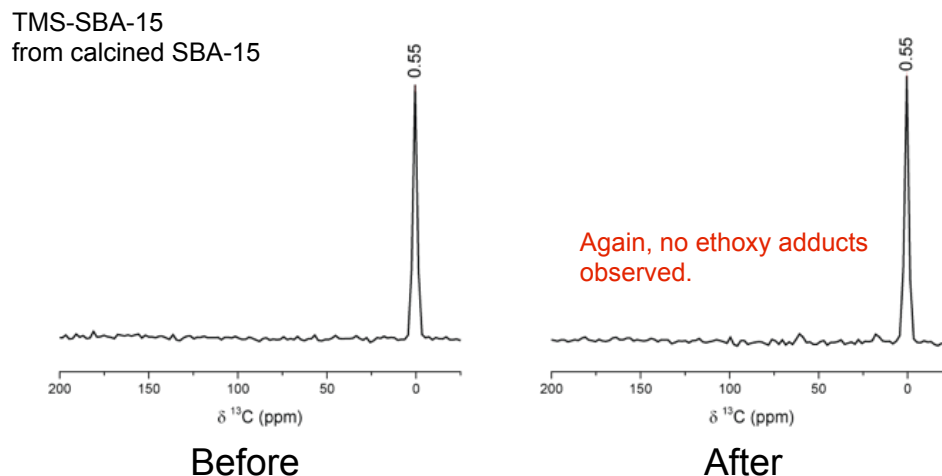
Figure 3-13. ^{13}C solid state NMRs of TMS-SBA-15, before (left) and after (right) stirring in ethanol at 85 ºC for 48 hours.
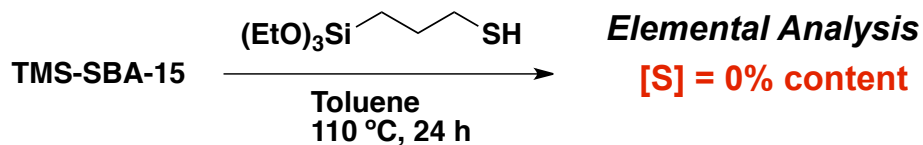
Figure 3-14. Attempted post-synthesis grafting of MPTMS onto TMS-SBA-15

Previous work from the Pruski group, (Figure 3-15)[32] shows a packing model on a two dimensional surface which is estimated to be close to the maximum that the surface can accommodate. This corresponds to 1.8 groups of TMS per nm^2, considering that our sample was estimated to have 1.24 groups per nm^2, this represents a good level of surface coverage according to our stability tests indeed.

Me₃Si(TMS)group
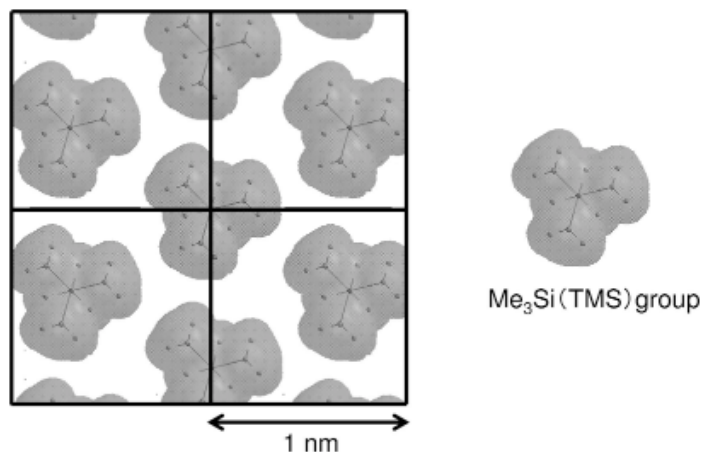
Figure 3-15.   Packing model of TMS groups at the density of 1.8 groups per nm^2. [32]

3.3   Passivation with TBDMS

We also considered the possibility that treatment with hot ethanol might remove

TMS groups. In synthetic organic chemistry, TMS is known as a versatile but relatively

labile protecting group.[55-59] Therefore, employing other protecting groups for the

selective passivation by reloading method was attempted. However, due to the geometry

of the surface silanols, that are mostly similar to tertiary alcohols, the reactivity of bulky

silylating agents was unknown. In fact, even small TMS groups cannot be reacted with

tertiary alcohols under standard conditions, but instead require special conditions such as

TMS triflate with nucleophilic catalysts (Scheme 3-9) or the use of expensive Lewis

acids operating via alternative mechanisms (Scheme 3-10).[60]
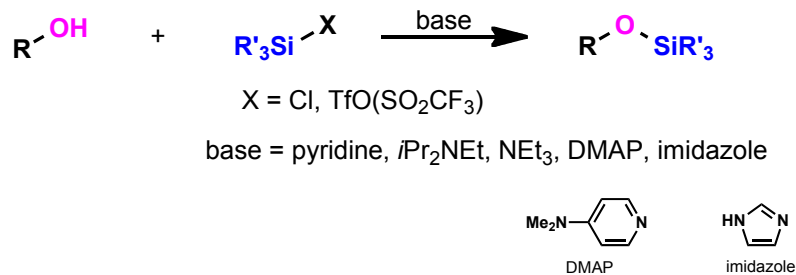
Scheme 3-9. Typical silylating conditions for tertiary alcohols

Scheme 3-10. A unique Lewis acid-catalyzed silylation of bulky alcohols[60]

Among the various silyl ether type protecting groups, tertiary-butyl dimethylsilyl

(TBDMS, or TBS) is a common group that is reasonably stable toward both acid and base.

Importantly, Ritter and co-workers reported that TBDMS-Cl successfully reacts with

TBDMS-OH in the presence of imidazole at room temperature in dichloromethane

(Scheme 3-11), which bodes well for the reaction of surface silanols with this reagent.[61]
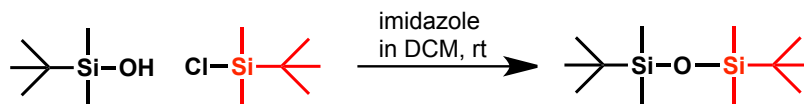
Scheme 3-11. TBDMS capping of a silanol at tertiary alcohol geometry[62]

Thus, employing approximately 2.0 equivalents excess of TBDMS-Cl toward

surface silanols, full passivation of SBA-15 with TBDMS was carried out both on

calcined and extracted materials. We decided to attempt full passivation rather than

selective external passivation since full passivation will give a larger M-site signal which

would be more easily integrated by SS NMR, providing greater accuracy for the

comparison with similar materials after treatment with hot ethanol. Thus a series of

materials were analyzed, before and after passivation with TBDMS-Cl, and silylated

samples were treated in refluxing ethanol for two days after passivation to test the

stability of the silyl protection strategy to the SDA extraction conditions which is two

days on a Soxhlet extractor using ethanol too. The results of ^{29}Si DP-CPMG/MAS

analysis are shown in Figure 3-16.

As expected, SBA-15 itself is comprised of a mixture of Q3 and Q4 sites, with a

higher ratio of Q4-site peaks in the calcined material (Figure 3-16, compared a with d).

SS NMR studies demonstrated clearly that TBDMS groups, (observed as M-sites), were

successfully installed on both calcined and extracted SBA-15 materials (b and e). Since

materials were not positionally grafted, the signal strength was much greater and it was

possible to show that there was no significant degradation of the TBDMS groups after hot

ethanol treatment (compare c and e).
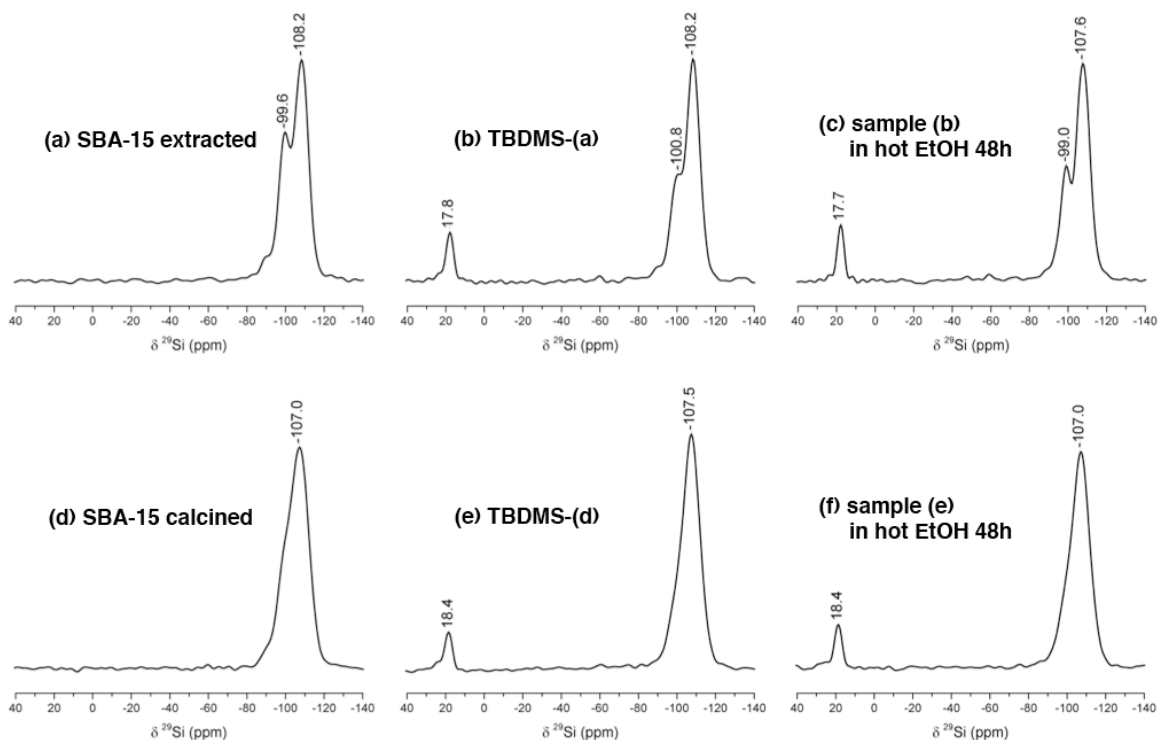
Figure 3-16. ^{29}Si DP-CPMG/MAS spectra obtained for TBDMS test samples

SS ^{13}C NMR studies provided further proof of the stability of TBDMS toward hot

ethanol (Figure 3-17). The spectrum on the left is SBA-15 in which SDA was extracted

prior to passivation, hence ethoxy adducts are present on the surface appearing as a small

peak around 60 ppm. The spectrum on the right is SBA-15, which was calcined to

remove SDA prior to the passivation, therefore this material has not interacted with

ethanol until after it was passivated with TBDMS. Both spectra of silylated materials

before hot ethanol treatment (black) were characterized by peaks at -4, 19, and 25 ppm

for TBDMS and 120 and 135 ppm for imidazole physisorbed on the material. After

ethanol treatment (red), the peaks in aromatic region disappeared thus indicating the

removal of physisorbed imidazole, but most importantly, the size of the TBDMS peaks were not decreased indicating that TBDMS groups were successfully installed on the surface silanols and were not degraded by treatment with hot ethanol. Also no new ethoxy peaks were observed, indicating that TBDMS was effective to protect the surface siloxanes preventing from ring opening or formation of ethoxy adducts even though the estimated TBDMS'd efficiency was 20% thus the samples have more free silanols than TMS-SBA-15.
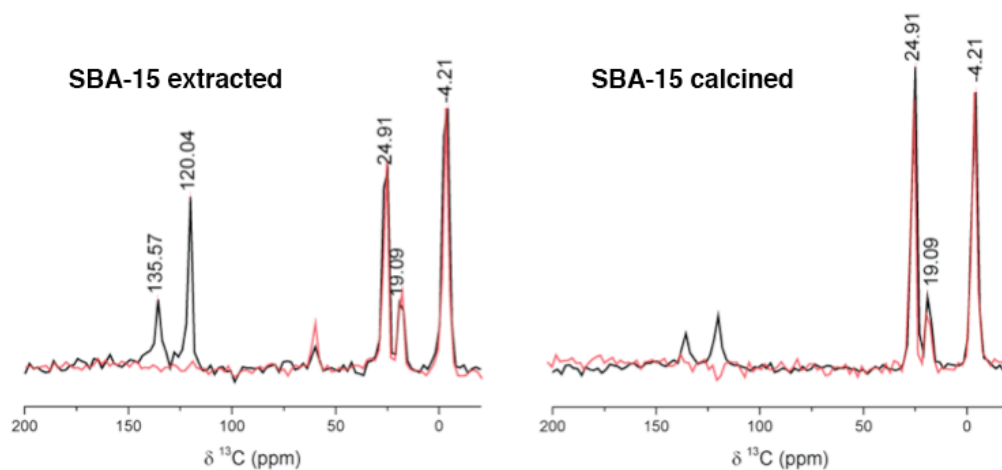
Figure 3-17. Normalized ^{1}H-^{13}C CP/MAS spectra obtained for the extracted and calcined materials before (black) and after (red) hot-ethanol treatment

Thus it is clear that TBDMS is a very effective protecting group for silica surfaces. The only thing that remains to be determined, however, is whether the positional grafting procedure developed with HMDS will be similarly effective with TBDMS-Cl.

Considering the fact that a base has to be employed and organic solvents are needed, this may require some optimization, which is currently underway.

3.4   Direct functionalization on as-sTMS-SBA-15

Since removal of the surfactant with ethanol appeared to be introducing ethoxy and possibility silanol groups on the surface of TMS-protected material, and presumably over the external as well as internal surface, we examined direct functionalization of P123-containing materials with MPTMS in toluene at 110 ºC. These conditions were chosen since the TMS passivation layer should not be degraded by toluene, and thus no new reactive sites should be introduced, and functionalization should only occur if toluene is capable of extracting the P123 simultaneously with silylation by MPTMS. Elemental analysis and nitrogen adsorption data for these samples are shown in Table 3-4.

Table 3-4. **Nitrogen adsorption and elemental analysis data for MPTMS direct grafting samples**

Material	S_{BET}, m^2 g^{-1}	C parameter	C wt%	S wt%
(a)	214	33	-	-
(b)	650	38	14.6	1.54
(c)	729	48	11.0	1.63

Sample (a): grafting MPTMS on as-sTMS-SBA-15, (b): sample (a) after P123 was extracted by placing the sample on Soxhlet extractor with ethanol for 48 hours. (c): grafting MPTMS on s-TMS-SBA-15, then the sample was stirred in ethanol at 85 ºC for 48h. Both surface area and C value were calculated by the BET method.

Sample (a) in Table 3-4 has a surface area of 214 m^2/g, which is significantly larger than as-sTMS-SBA-15 (~19 m^{2}g^{-1}), implying that P123 was partially extracted by the organic solvent. Once surfactant was removed, in sample (b), the presence of sulfur in the material was measured by elemental analysis and determined to be present at significant levels. This suggests that indeed treatment at 110 °C with toluene resulted in at least partial removal of the surfactant permitting internal functionalization without the need for the use of ethanol. Consistent with this, sample (c) has a very similar sulfur content, carbon content and surface area. Thus these results suggest that exposure to

organic solvents at elevated temperatures in the presence of a siloxane functionalizing agent is an effective method for functionalization of the internal surface without the need for ethanol treatment, although the studies using solid state NMR for the details of the materials are still under way.

3.5 Conclusion

A new methodology for selective passivation and functionalization of SBA-15 was demonstrated by the reloading method, such that the mesopores of as-synthesized SBA-15 were further filled with P123, which is denoted as the reloading process. As the internal surface was completely covered by P123, the free external surface was deactivated by HMDS treatment to cap external silanols with TMS. According to quantitative analysis by high resolution solid state NMR, it was estimated that 30% of silanols on the external surface were still protected by TMS even after the extraction of P123 with hot ethanol, and this is the same TMS coverage efficiency with regular TMS-SBA-15 whose stability was confirmed by hot ethanol tests, mimicking the conditions for SDA extraction in the reloading selective functionalization method, and attempted post-synthesis grafting toward MPTMS resulting no MPTMS attached on the material. To avoid unexpected functionalization on the external surface by the presence of defects,

direct functionalization of deactivated SBA-15 without extraction was attempted as well. According to elemental analysis, both MPTMS treated materials before and after the extraction showed almost the same sulfur content, therefore removal of the pore protecting surfactant is not necessary as long as functionalization condition is optimized. Finally, the potential use of TBDMS groups instead of TMS for passivation was described. In spite of the tertiary geometry of the surface silanols, TBDMS-chloride in the presence of imidazole worked effectively to attach TBDMS group covalently on the material. Stability tests of the TBDMS-SBA-15 both extracted and calcined materials showed perfect protection toward hot ethanol. There will be no need to use TBDMS selective passivation if TMS-SBA-15 shows perfect stability as the same as TBDMS-SBA-15, otherwise it will be worthwhile to investigate it as a stronger passivation agent which should be stable toward hydrolysis in both acidic and basic media and thus tolerate further harsh grafting conditions.

3.6　References

1.　　Zhao, D. Y.; Huo, Q. S.; Feng, J. L.; Chmelka, B. F. and Stucky, G. D., *J. Am. Chem. Soc.* **1998,** *120*, 6024.

2.   Zhao, D. Y.; Feng, J. L.; Huo, Q. S.; Melosh, N.; Fredrickson, G. H.; Chmelka, B. F. and Stucky, G. D., *Science* **1998,** *279*, 548.

3.   Kresge, C. T.; Leonowicz, M. E.; Roth, W. J.; Vartuli, J. C. and Beck, J. S., *Nature* **1992,** *359*, 710.

4.   Thomas, J. M.; Harris, K. D. M.; Edwards, P. P. and RSC, *Turning Points in Solid-State, Materials and Surface Science: A Book in Celebration of the Life and Work of Sir John Meurig Thomas*. RSC Pub.: 2008.

5.   Xie, Y. W.; Quinlivan, S. and Asefa, T., *J. Phys. Chem. C* **2008,** *112*, 9996.

6.   Bruehwiler, D.; Ritter, H.; Ramm, J. H.; Dieu, L. Q.; Bauer, C.; Dolamic, I. and Gartmann, N., *Chimia* **2009,** *63*, 8.

7.   Thomas, J. M.; Maschmeyer, T.; Johnson, B. F. G. and Shephard, D. S., *J. Mol. Catal. A-Chem.* **1999,** *141*, 139.

8.   MacQuarrie, S.; Nohair, B.; Horton, J. H.; Kaliaguine, S. and Crudden, C. M., *J. Phys. Chem. C* **2010,** *114*, 57.

9.   Webb, J. D.; MacQuarrie, S.; McEleney, K. and Crudden, C. M., *J. Catal.* **2007,** *252*, 97.

10.   Webb, J.; Macquarrie, S.; McEleney, K. and Crudden, C., *J. Catal.* **2007,** *252*, 97.

11.   Glasspoole, B. W.; Webb, J. D. and Crudden, C. M., *J. Catal.* **2009,** *265*, 148.

12.   Crudden, C. M.; McEleney, K.; MacQuarrie, S. L.; Blanc, A.; Sateesh, M. and Webb, J. D., *Pure Appl. Chem.* **2007,** *79*, 247.

13.   Taguchi, A. and Schuth, F., *Microporous Mesoporous Mater.* **2005,** *77*, 1.

14.   Kruk, M.; Jaroniec, M.; Ko, C. H. and Ryoo, R., *Chem. Mater.* **2000,** *12*, 1961.

15.   Yang, C.-M.; Zibrowius, B.; Schmidt, W. and Schüth, F., *Chem. Mater.* **2003,** *15*, 3739.

16.   Shenderovich, I. G.; Buntkowsky, G.; Schreiber, A.; Gedat, E.; Sharif, S.; Albrecht, J.; Golubev, N. S.; Findenegg, G. H. and Limbach, H. H., *J. Phys. Chem. B* **2003,** *107*, 11924.

17.   Zhao, X. S.; Lu, G. Q.; Whittaker, A. K.; Millar, G. J. and Zhu, H. Y., *J. Phys. Chem. B* **1997,** *101*, 6525.

18.   Johnson, B. F. G.; Raynor, S. A.; Shephard, D. S.; Mashmeyer, T.; Thomas, J. M.; Sankar, G.; Bromley, S.; Oldroyd, R.; Gladden, L. and Mantle, M. D., *Chem. Commun.* **1999**, 1167.

19.   Shephard, D. S.; Zhou, W. Z.; Maschmeyer, T.; Matters, J. M.; Roper, C. L.; Parsons, S.; Johnson, B. F. G. and Duer, M. J., *Angew. Chem., In. Ed.* **1998,** *37*, 2719.

20.   Gartmann, N. and Brühwiler, D., *Angew. Chem., In. Ed.* **2009,** *48*, 6354.

21.   de Juan, F. and Ruiz-Hitzky, E., *Advanced Materials (Weinheim, Germany)* **2000,** *12*, 430.

22.   Lu, A. H.; Li, W. C.; Kiefer, A.; Schmidt, W.; Bill, E.; Fink, G. and Schuth, F., *J. Am. Chem. Soc.* **2004,** *126*, 8616.

23.   Webb, J., *PhD Thesis, Queen's University* **2011**.

24.   Thomas, J. M.; Johnson, B. F. G.; Raja, R.; Sankar, G. and Midgley, P. A., *Acc. Chem. Res.* **2003,** *36*, 20.

25.   Thomas, J. M. and Raja, R., *Acc. Chem. Res.* **2008,** *41*, 708.

26.   Raja, R.; Thomas, J. M.; Jones, M. D.; Johnson, B. F. G. and Vaughan, D. E. W., *J. Am. Chem. Soc.* **2003,** *125*, 14982.

27.   Jones, M. D.; Raja, R.; Thomas, J. M.; Johnson, B. F. G.; Lewis, D. W.; Rouzaud, J. and Harris, K. D. M., *Angew. Chem., In. Ed.* **2003,** *42*, 4326.

28.   Raynor, S. A.; Thomas, J. M.; Raja, R.; Johnson, B. F. G.; Bell, R. G. and Mantle, M. D., *Chem. Commun.* **2000**, 1925.

29.   Thomas, J. M., *Angew. Chem. Int. Ed.* **1999,** *38*, 3588.

30.   Johnson, B. F. G.; Raynor, S. A.; Shephard, D. S.; Mashmeyer, T.; Thomas, J. M.; Sankar, G.; Bromley, S.; Oldroyd, R.; Gladden, L. and Mantle, M. D., *Chem. Commun.* **1999**, 1167.

31.   Bruhwiler, D.; Calzaferri, G.; Torres, T.; Ramm, J. H.; Gartmann, N.; Dieu, L. Q.; Lopez-Duarte, I. and Martinez-Diaz, M. V., *J. Mater. Chem.* **2009,** *19,* 8040.

32.   Hara, K.; Akahane, S.; Wiench, J. W.; Burgin, B. R.; Ishito, N.; Lin, V. S. Y.; Fukuoka, A. and Pruski, M., *J. Phys. Chem. C* **2012,** *116*, 7083.

33.   Inagaki, S.; Ohtani, O.; Goto, Y.; Okamoto, K.; Ikai, M.; Yamanaka, K.; Tani, T. and Okada, T., *Angew Chem Int Ed Engl* **2009,** *48*, 4042.

34.   Asefa, T. and Lennox, R. B., *Chem. Mater.* **2005,** *17*, 2481.

35.   Sun, J. M.; Ma, D.; Zhang, H.; Liu, X. M.; Han, X. W.; Bao, X. H.; Weinberg, G.; Pfander, N. and Su, D. S., *J. Am. Chem. Soc.* **2006,** *128*, 15756.

36.   Zhang, Z.; Dai, S.; Blom, D. A. and Shen, J., *Chem. Mater.* **2002,** *14*, 965.

37.   Huang, X.; Yang, M.; Wang, G. and Zhang, X., *Microporous Mesoporous Mater.* **2011,** *144*, 171.

38.   El Kadib, A.; McEleney, K.; Seki, T.; Wood, T. K. and Crudden, C. M., *Chemcatchem* **2011,** *3*, 1281.

39.   Glasspoole, B. W.; Webb, J. D. and Crudden, C. M., *J. Catal.* **2009,** *265*, 148.

40.   Yao, G.; Wang, L.; Wu, Y.; Smith, J.; Xu, J.; Zhao, W.; Lee, E. and Tan, W., *Analytical and Bioanalytical Chemistry* **2006,** *385*, 518.

41.   Bagwe, R. P.; Hilliard, L. R. and Tan, W., *Langmuir* **2006,** *22*, 4357.

42.   Bagwe, R. P.; Yang, C.; Hilliard, L. R. and Tan, W., *Langmuir* **2004,** *20*, 8336.

43.   Behringer, K. D. and Blumel, J., *Journal of Liquid Chromatography & Related Technologies* **1996,** *19*, 2753.

44.   Blumel, J., *J. Am. Chem. Soc.* **1995,** *117*, 2112.

45.   Zhao, X. S.; Lu, G. Q.; Whittaker, A. K.; Millar, G. J. and Zhu, H. Y., *The Journal of Physical Chemistry B* **1997,** *101*, 6525.

46.   Fousseret, B.; Mougenot, M.; Rossignol, F.; Baumard, J.-F. o.; Soulestin, B.; Boissière, C. d.; Ribot, F. o.; Jalabert, D.; Carrion, C.; Sanchez, C. m. and Lejeune, M., *Chem. Mater.* **2010,** *22*, 3875.

47.   Jana, N. R.; Gearheart, L. and Murphy, C. J., *Langmuir* **2001,** *17*, 6782.

48.   Ma, D.; Deng, F.; Fu, R. Q.; Dan, X. W. and Bao, X. H., *J. Phys. Chem. B* **2001,** *105*, 1770.

49.   Amoureux, J.-P.; Hu, B. and Trebosc, J., *Journal of Magnetic Resonance* **2008,** *193*, 305.

50.   Amoureux, J.-P.; Hu, B.; Trebosc, J.; Wang, Q.; Lafon, O. and Deng, F., *Solid State Nucl. Magn. Reson.* **2009,** *35*, 19.

51.   Mafra, L.; Siegel, R.; Fernandez, C.; Schneider, D.; Aussenac, F. and Rocha, J., *Journal of Magnetic Resonance* **2009,** *199*, 111.

52.   Zhu, H. Y.; Zhao, X. S.; Lu, G. Q. and Do, D. D., *Langmuir* **1996,** *12*, 6513.

53.   Katiyar, A.; Yadav, S.; Smirniotis, P. G. and Pinto, N. G., *J. Chromatogr. A* **2006,** *1122*, 13.

54.   Sayari, A.; Liu, P.; Kruk, M. and Jaroniec, M., *Chem. Mater.* **1997,** *9*, 2499.

55.   Emde, H.; Domsch, D.; Feger, H.; Frick, U.; Gotz, A.; Hergott, H. H.; Hofmann, K.; Kober, W.; Krageloh, K.; Oesterle, T.; Steppan, W.; West, W. and Simchen, G., *Synthesis-Stuttgart* **1982**, 1.

56.   Lalonde, M. and Chan, T. H., *Synthesis-Stuttgart* **1985**, 817.

57.   Muzart, J., *Synthesis-Stuttgart* **1995**, 1325.

58.   Rucker, C., *Chem. Rev.* **1995,** *95*, 1009.

59.   Nelson, T. D. and Crouch, R. D., *Synthesis-Stuttgart* **1996**, 1031.

60.   Blackwell, J. M.; Foster, K. L.; Beck, V. H. and Piers, W. E., *J. Org. Chem.* **1999,** *64*, 4887.

61.   Ritter, D. A.; Kenny, J. D. and Rudolph, A. J., *Clinical Research* **1978,** *26*, A827.

62.   Ritter Ii, G. W. and Kenney, M. E., *J. Organomet. Chem.* **1978,** *157*, 75.

Chapter 4

Chiral Core gel-Star Polymers

(This project was carried out at Sawamoto's research group in Kyoto University, during three months visiting research by the support of GCOE program "Integrated Materials Science", JSPS.)

4.1   Introduction

With our significant interest in heterogeneous catalysis based on silica materials,[1-19] it is important to keep in mind the use of organic materials as supports as well. Organic polymer materials have very long history. The rubber industry started in 1839 by C. Goodyear, although the idea of a polymer as a unique molecule had to wait for the time of Wallace Carothers at DuPont. Prior to this, H. Staudinger proposed the existance of large molecules that monomer units are covalently connected to in 1925.[20] Due to such a long history, it is not surprising that there are an equally large number of organic polymer-supported catalysts, particularly those based on polystyrene.[21-29] More recently, precision polymerization methodologies[30] have been invented and further improved. Among them, living radical polymerization, or Atom Transfer Radical Polymerization (ATRP),[31-40] is one of the most practical technologies that is widely employed in industry

(Scheme 4-1). Alpha-halo carbonyl compounds are common initiators, acting by reversible halogen atom abstraction by a single electron transfer (SET) mechanism which mediates the equilibrium between the active- and dormant-states in the presence of transition metal catalysts (Cu,[31, 32, 37, 41] Ru,[33, 34, 42] Fe,[43-45] Ni[46-49]).
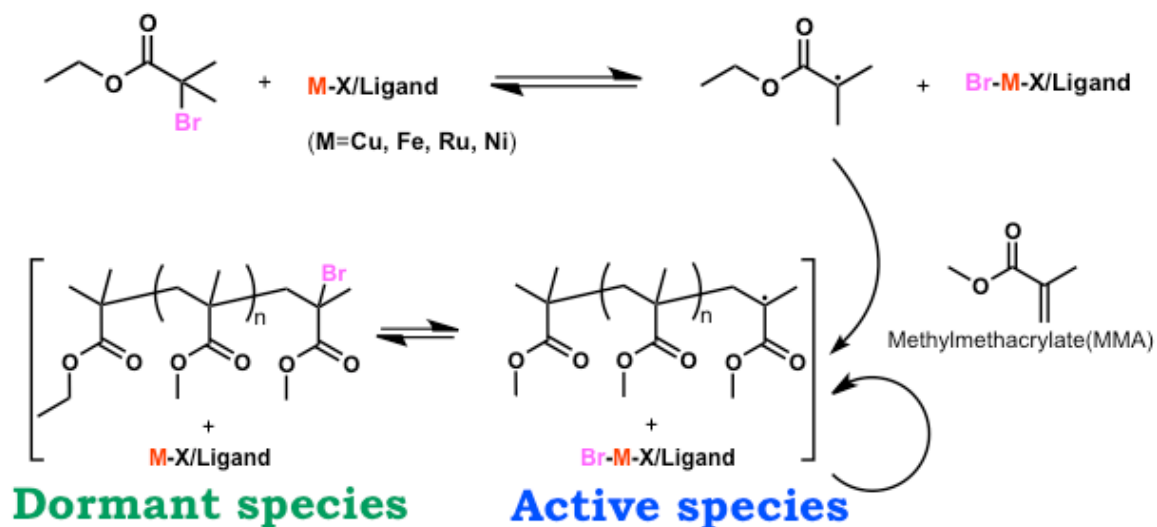
Scheme 4-1.   General example of ATRP

The polymer products synthesized by ATRP process have halogen atoms at the chain ends, and thus they are still able to react with the catalyst to generate active species, to which the another portion of the same or different monomers can be further added to grow the polymer. Thus the polymers themselves can behave as macroinitiators and the polymerization is considered to be "living". Such a precisely controlled polymerization processes permits the synthesis of not only polymers with low polydispersity index (PDI)

and high molecular weight, but also unique structures such as block copolymers,[35] gradient copolymers,[50] and graft polymers[51] (Figure 4-1).

Star polymers[42] are a type of block/graft copolymer which consist of crosslinked core gels surrounded by linear tethers. In the preparation of polymers of this type, linear chain polymers corresponding to the linear tether or arm are synthesized, then the resulting polymer is employed as macroinitiator to react with crosslinking agents, or divinyl monomers. Although linear tethers can be isolated, stored and again placed in the polymerization system by virtue of the living nature of this technique, the star polymers can also be prepared in one pot by employing the same catalyst (Scheme 4-2).[40, 52] Thus, a PMMA core was first prepared in the presence of a ruthenium catalyst, then divinyl monomer was further added to the batch after the MMA conversion reached 90%, which can take up to 48 hours.
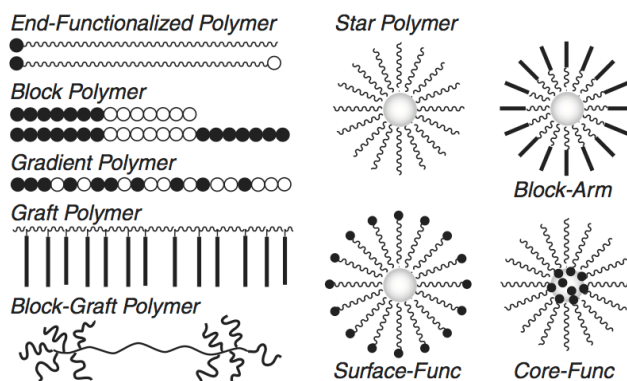
Figure 4-1.   Structure controlled polymers[40]

R−Cl

initiator   monomer   *Living Polimers*

Linear tethers

Core Gel
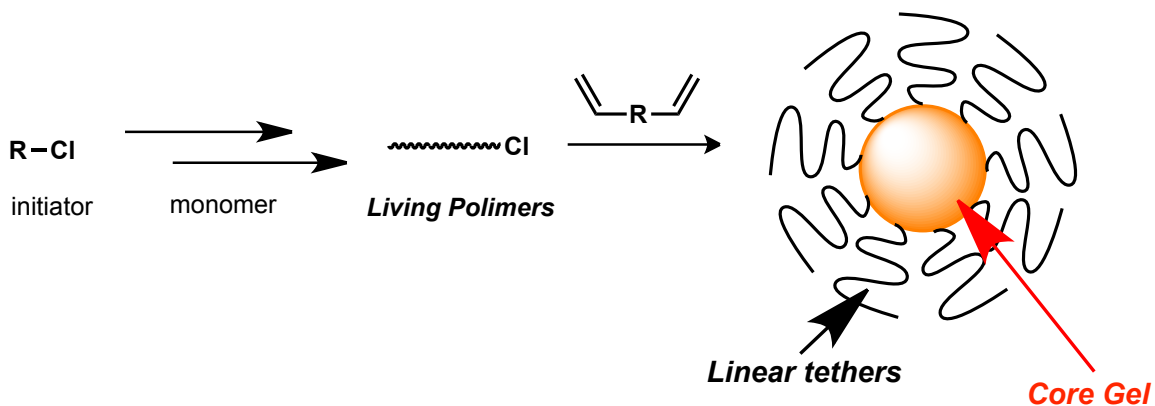
Scheme 4-2.   **General scheme of star polymer synthesis**

4.1.1 Star polymer as homogeneous/heterogeneous catalyst

Among organic materials that are doped with metals to prepare heterogeneous catalysts, dendrimers[53-55] are one of the most attractive polymer materials available since they have a perfectly controlled core and branched structure, thus there is no distribution in the sphere size or molecular weight. However, the synthesis of these materials is incredibly arduous thus star polymers can be attractive alternatives to dendrimers, despite the presence of some inhomogeneity in size.

When star polymers are used as catalyst supports, the catalytically active metal species are typically introduced after the star polymer support is synthesized with functionalities either in the core gel or on linear arms.[56-59] In 2003, Terashima *et al.* reported a one-pot direct preparation of a star polymer containing ruthenium complexes

in the core gel (Scheme 4-3).[52] Thus, employing poly-methylmethacrylate (PMMA) as the macroinitiator, ethyleneglycol dimethylmethacrylate (EGDMA) and *para*-styryldiphenylphosphine (SDP) were copolymerized in the presence of Ru(II) catalyst (RuCl$_2$(PPh$_3$)$_3$) and *n*-butylamine in toluene at 80 °C. Thus the ruthenium complex employed to synthesize the star polymer by ATRP becomes installed in the core gel, where it maintains catalytic activity for other transformations.
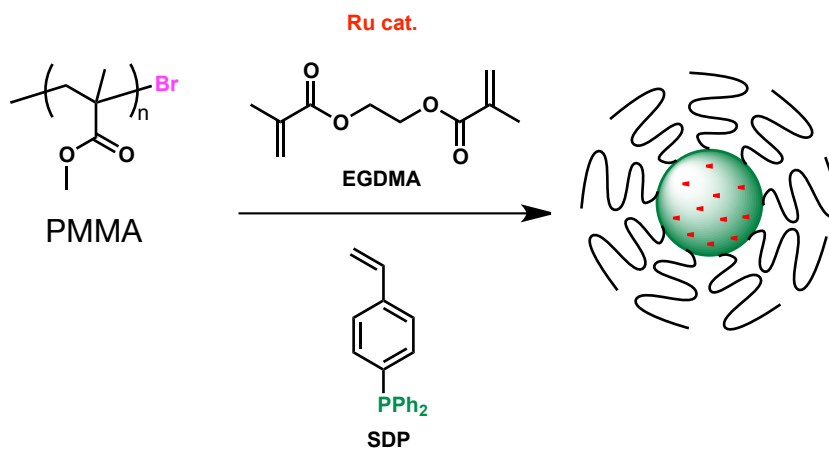
Scheme 4-3.   Direct one-pot synthesis of [Ru]/star polymer

The resulting star polymer-supported ruthenium catalyst was subjected to hydrogen transfer oxidation of 1-phenethylalcohol in basic isopropyl alcohol (Scheme 4-4).
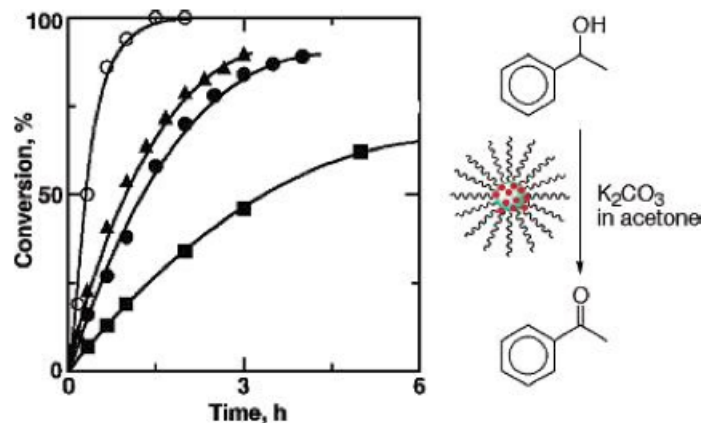
Scheme 4-4. Hydrogen transfer oxidation of 1-phenethylalcohol and substrate conversion. [1-phenylethanol] / [Ru] / [K$_2$CO$_3$] = 10 / 0.010 / 1.0 mmol; star polymers with 31 (black triangle), 58 (black circle), 74 (black square) μmol of Ru/g polymer were employed. Open circles are RuCl$_2$(PPh$_3$)$_3$.[52]

The substrate conversion plots showed that the less ruthenium installed in the core gel, the more reactive the star polymer catalyst was. The total amount of the ruthenium catalyst was fixed in all three batches, however the density of the ruthenium complex was different due to immobilization in the core gel. In this case, the hydrogen transfer is an equilibrium reaction, thus both oxidation and reduction of ketones and alcohols are simultaneously proceeding in the system. With the star polymer catalyst in which the ruthenium complexes are installed in high density, the product ketone, acetophenone, is proposed to interact with the other ruthenium center again to yield reduction product thus the starting alcohol is recovered. Nevertheless it was reported that the supported catalysts

154

with low density catalytic species contributed to increase the reactivity even with the non-equilibrium reactions which supports the huge impact of the diffusion than reverse reaction even when there is the potential for reaching equilibrium.[60, 61]

In the case of the other star polymers whose arms or core gels were further functionalized,[23, 40, 62-69] solubility control by modifying the arms of star polymer is also an important characteristic. The core gel, which is synthesized from divinyl monomers crosslinked randomly, is not soluble in any solvent in general. However the solubility of the star polymer can be controlled by altering the solubility of arms, thus PMMA arms can bring the star polymer into a variety of solvents such as toluene, DMF, and dichloromethane, whereas star polymers with polyethyleneglycol (PEG) arms are soluble in water. In the latter case, the character of thermo-sensitive solubility can also be employed. Star polymers prepared in the same manner as shown in Scheme 4-3 but having PEG arms showed Upper Critical Solution Temperatures (UCST) in organic solvents at 31 °C (Scheme 4-5)[70], such that the PEG star polymer was soluble in the aqueous phase at ambient temperature but in the organic phase at elevated temperature, providing a useful means for catalyst separation and recovery.

This catalyst was subjected to a hydrogen transfer reduction of a ketone in basic isopropyl alcohol. The catalysis proceeded at elevated temperature such that the catalyst

stayed in the organic layer where most of the substrate was soluble. After reaction, the

catalyst was easily separated when it was transferred to the aqueous phase at

temperatures lower than 31 ºC or room temperature, while the product remained in the

organic phase.
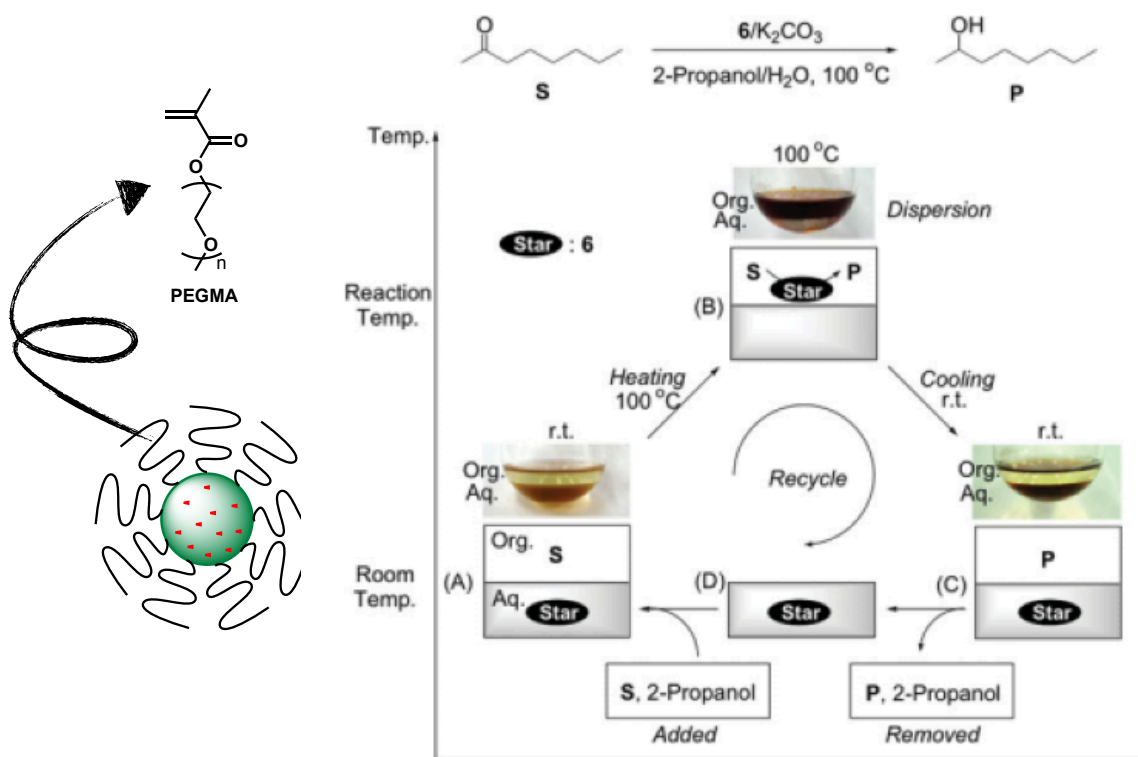
Scheme 4-5. Thermo-sensitive star polymer catalyst and recyclable transfer hydrogenation reduction of a ketone [70]

4.2 Axially chiral divinyl monomers for chiral core-gel star polymers

As discussed in the previous chapters, the advantage of using PMO materials as heterogeneous catalyst supports is their huge surface area and relatively large pore diameter that permits high accessibility to the reactive functionalities on the surface. However, even with such properties of mesoporous silica materials, it is still difficult to overcome the high diffusion thus reactivity of the heterogeneous system, although the insolubility gives the ability of easy separation and recyclability of the catalysts simply by filtration or centrifugation. Solubility controllable star polymers seem to have both advantage of homo- and heterogeneous catalysts, thus high diffusion and easy separation of the catalysts.

Beginning the collaboration with the Sawamoto group, we sought to apply the chirality transfer observed with the axially chiral PMO materials previously reported from our group[12, 13] into the field of start polymers by incorporating axially chiral monomers into the crosslinked space inside the core gel of star polymers by functionalizing these chiral molecules with a cross linkable divinyl group. (Scheme 4-6) Thus it is hoped that the chirality of the chiral dopant will transfer to the bipyridine monomer, such that any asymmetric reaction involving transition metal species bound to the bipyridine ligand might be influenced by the chiral dopant component.
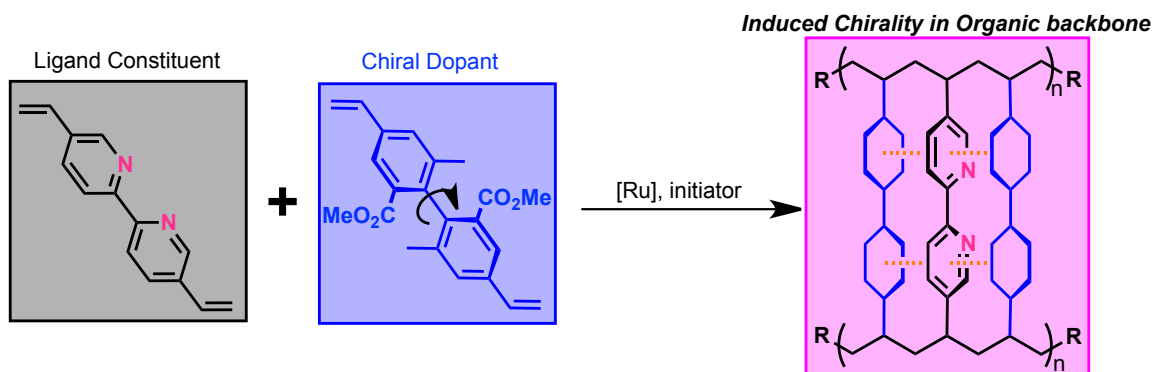
Scheme 4-6.   Chirality transfer in locally ladder shaped polymer (A first proposed theme for the visiting program)

However, the synthesis of the both monomers and the formation of the local ladder shaped-polymer structure might be difficult to accomplish within a three month period, therefore, considerably simplified divinyl monomers were synthesized and converted into chiral star gel polymers (Scheme 4-7). Thus, commercially available BINOL (1,1'-binaphthalene-2,2'-diol) and BINAM (1,1'-binaphthalene-2,2'-diamine) were selected as chiral building blocks for the chiral core gel.
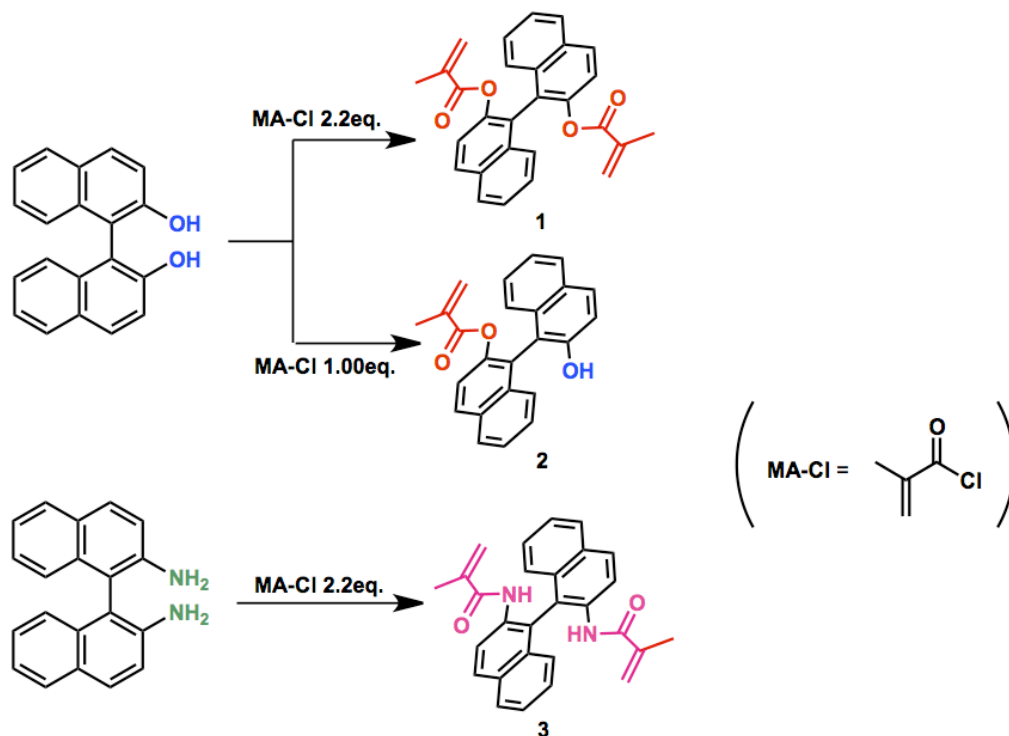
Scheme 4-7.   Chiral binaphthylene monomers

4.2.1 Synthesis of BINOL and BINAM monomers

As shown in Scheme 4-7, hydroxy groups of BINOL or amino groups of BINAM were treated with methacryloyl chloride (MA-Cl) in the presence of triethylamine. BINOL monomers **1** and **2** were relatively easier to synthesize, thus BINOL, triethylamine and MA-Cl were added in THF in this order at room temperature, then the resulting mixture was refluxed for 18 hours. However, BINAM gave multiple species if MA-Cl was added too fast, even at 0 ºC. To suppress the formation of multiple by-products, consequently, a dichloromethane solution of BINAM and Hunig's base was

prepared and stirred well in an ice bath temperature prior to the careful slow addition of

MA-Cl. Stirring for an additional 3 hours as the reaction mixture slowly warmed to room

temperature gave **3** successfully. All three monomers were stored as toluene solutions of

certain calculated concentrations in Schlenk flasks filled with Argon and kept in a

refrigerator at -30 ºC. Other details of syntheses are described in the experimental chapter.

4.3   Results and discussion

4.3.1 Preparation of macroinitiator, PMMA arms

With three chiral monomers in hand, the synthesis of star polymers was attempted.

At first, PMMA-based macroinitiators for the star polymer synthesis were prepared. Thus

MMA was polymerized in the presence of $RuCl_2(PPh_3)_3$ and n-tributylamine, using ethyl

alpha-chlorophenylacetate (ECPA) as the initiator in toluene. Monomer conversion was

monitored by GC employing *n*-octane as the internal standard, and revealed that 90% of

the MMA monomer was consumed in 48 hours (Figure 4-2).
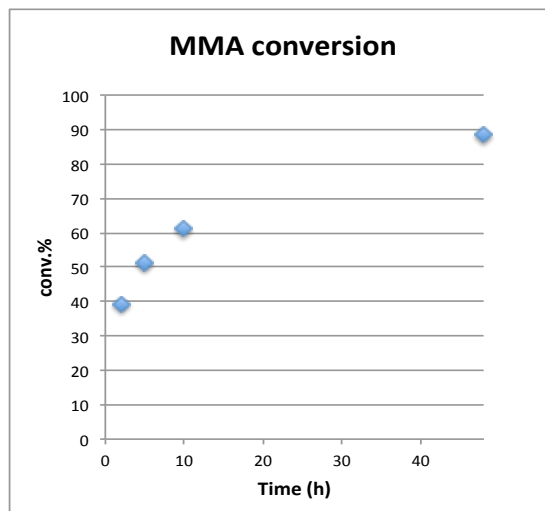
Figure 4-2. Time dependent conversion of MMA in [MMA] / [ECPA] / [Ru] / [nBu$_3$N] = 2000 / 20 / 10 / 40 mM in toluene at 80 ºC. Conversion was calculated from n-octane as the internal standard by GC.

Time dependent GPC data showed that the PDI (M_w/M_n) gets smaller as PMMA chains grow, eventually giving a polymer with PDI = 1.17 and M_n = 12602 (Figure 4-3).
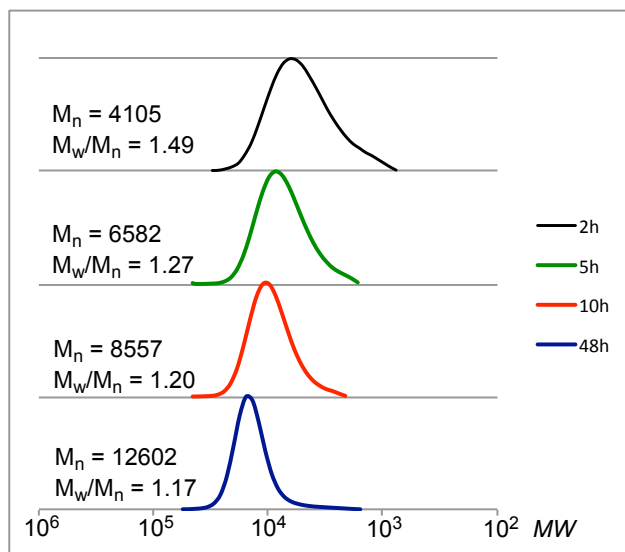
Figure 4-3. Time dependent GPC transition of PMMA arms

4.3.2 PMMA-1-SDP star polymer

All the BINOL and BINAM monomers mentioned below are R enantiomers unless otherwise noted. At first, BINOL-DMA monomer (**1**) was used in place of EGDMA under literature conditions as shown in Scheme 4-3. Thus, the molar ratio of the components were [initiator] / [**1**] / [SDP] / [Ru] = 10 / 200 / 50 / 10 mM in toluene at 80 ºC. ^{1}H NMR of the resulting mixture showed 90% conversion of **1** (internal standard: tetralin) in 48 hours (Scheme 4-8). The absolute weight- average molecular weight (Mw) was determined by GPC to be 57835. This is quite low MW for starpolymers, being simply estimated to have 5 arms at most. To investigate the BINOL monomer incorporation, the CD spectrum of the product polymer was measured.
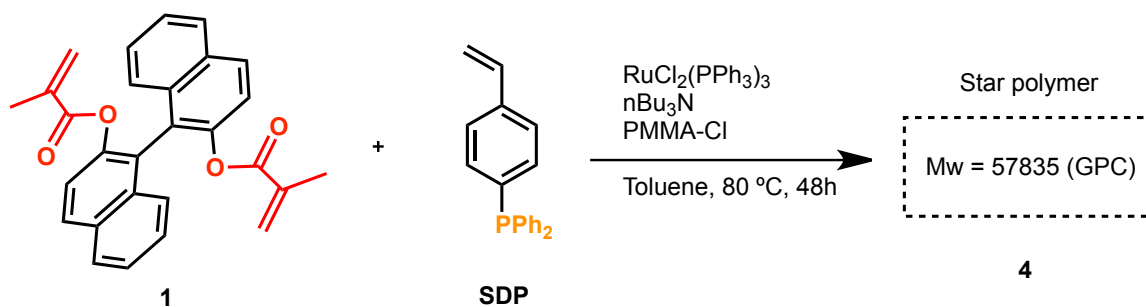
Scheme 4-8.   Attempted synthesis of PMMA-1-SDP star polymer

CD spectra of **4** showed peaks corresponding to (R)-BINOL (Figure 4-4). Sample solutions were prepared in dichloroethane (DCE) at 0.1, 0.01, and 0.001 wt%. The most concentrated one (0.1 wt%, blue) seemed to be saturated for wavelengths less than 320

nm, but did demonstrate that there were no CD signals >320 nm as were observed

previously for π-stacked chiral aggregates in chiral PMO materials from our lab.[13] The

two other diluted samples showed the existance of three other peaks at 280, 250

(shoulder), and 230 nm. It should be noted that the shape of the CD spectrum sometimes

appears as a peak as 250 nm in 0.01 wt% (red), however this is an artifact due to the

saturation. In fact, the more diluted sample (0.001 wt%, green) has no shoulder peak at

250 nm but a λ_{max} at 230 nm. In fact, chiral binaphthyls gave CD signals at 230 and 280

nm.[12]
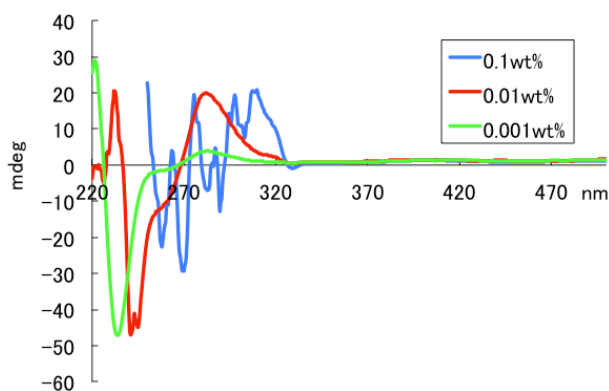
**Figure 4-4.   CD spectra of PMMA-(R)-1-SDP star polymer (4). Sample solutions
were prepared in DCE.**

Considering the monomer conversion, GPC and the CD results, the BINOL

monomer was polymerized and incorporated in the product polymer, however it did not

behave effectively as a crosslinking agent, even though the monomer has divinyl

functionalities. This may imply that the methacrylate moieties on the BINOL monomer

react in an intramolecular cyclization manner, or simply that only one vinyl group polymerized to make a random linear chain attached to the PMMA chain, and another vinyl group remained unreacted. Thus, the chiral monomer and phosphine ligand monomer reacted together to give a random linear polymer rather than a crosslinked gel, however they did contain both the chirality and the ligand functionality therefore the product polymer was employed in the kinetic resolution test for investigating the effect of the remote chirality to the reaction metal center, as described below.

4.3.3 PMMA-3-SDP star polymer
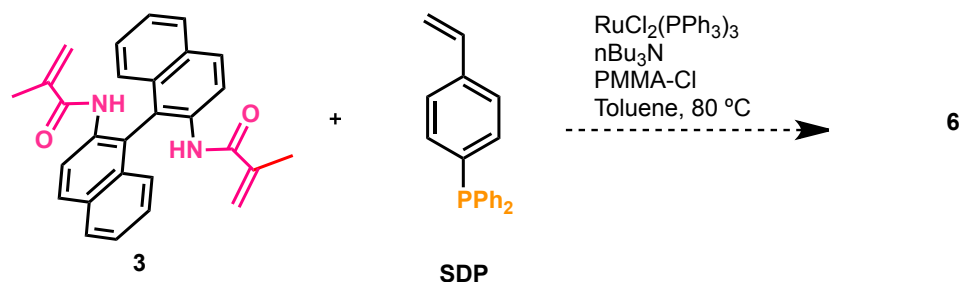
Scheme 4-9.   Attempted synthesis of PMMA-3-SDP star polymer (6). Molar ratio of each component was the same as that employed with 1. Thus [initiator] / [3] / [SDP] / [Ru] = 10 / 200 / 50 / 10 mM.

Divinyl BINAM monomer **3** was then employed under the same conditions employed with **1** (Scheme 4-9). The amine and methacryloyl chloride yield methacryl amide, therefore the reactivity of the monomer was expected to be different from

164

BINOL-DMA **1**. In fact, GPC showed that the macroinitiator remained unreacted such that the polymerization of **3** did not work well (Figure 4-5).
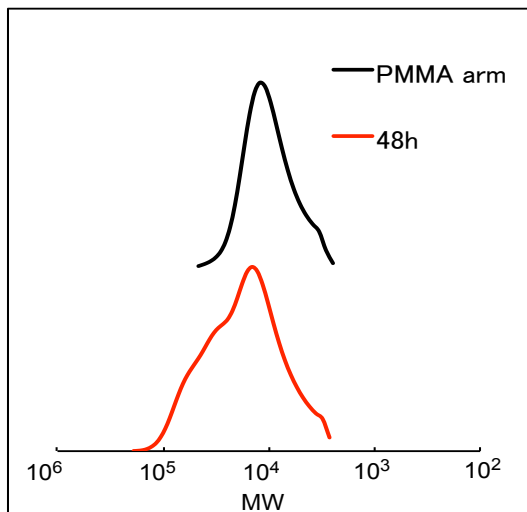
Figure 4-5.   GPC analysis of macroinitiator (black) and attempted preparation of PMMA-3-SDP star polymer (6) after 48 hours of the addition.

Assuming that the low reactivity was caused by the amide strongly coordinating to the ruthenium catalyst and thus behaving as catalyst poison, the polymerization temperature was raised to 100 ºC and then aliquots were monitored by GPC (Figure 4-6). There was no obvious difference compared with the reaction run at 80 ºC, and furthermore, the GPC curve for reactions run at 24 hours (yellow) and 48 hours (brown) showed almost identical distributions. It was suspected that the residual MMA was copolymerizing with **3**, but **3** itself had poor reactivity thus did not react with itself. Hence, conditions were developed where extra MMA was added; [initiator] / [**3**] / MMA

/ [SDP] / [Ru] = 10 / 200 / 200 / 50 / 10 mM in toluene at 80 ºC (Figure 4-7). In this case,

a clear difference, corresponding to growth of polymer was observed in between the

PMMA arm (black) and 24 hours sample (blue), and 48 hours sample (green) although

the 48 hours sample was still bimodal. Unfortunately, the peak corresponding to

unreacted macroinitiators did not disappear even after extended polymerization times up

to 120 hours.
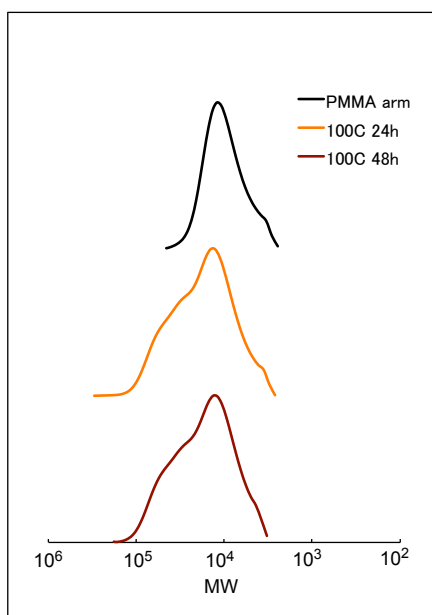
Figure 4-6. **GPC analysis of star polymer aliquots at 100 ºC.**
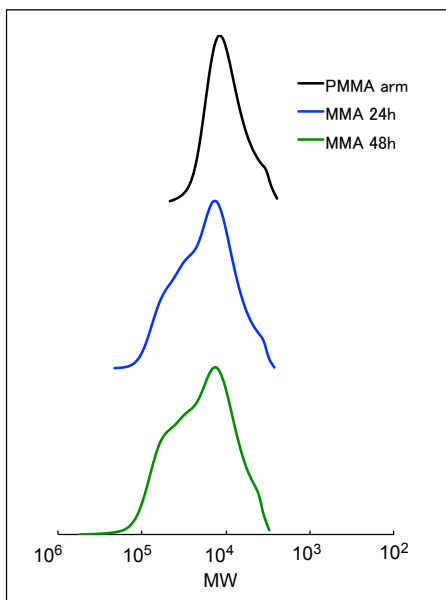
Figure 4-7. **GPC analysis of star polymer aliquots with extra MMA addition.**

Further improvements such as introducing a protecting group on the amide nitrogen of **3** or optimization of copolymerizable monomers are needed to prepare BINAM-crosslinked core gel star polymer **6**, but were outside the time allotted to this project.

4.3.4 PMMA-EGDMA-2-SDP star polymer
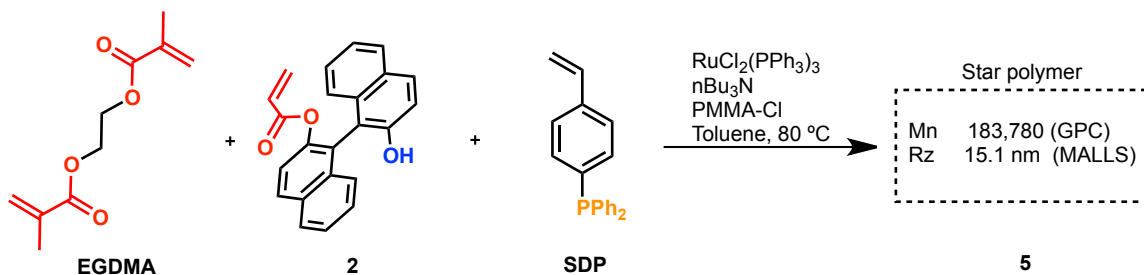
Scheme 4-10. **Synthesis of PMMA-EGDMA-2-SDP star polymer.**

167

Finally, mono vinyl (R)-BINOL monomer **2** was employed as an additive to the PMMA-EGDMA-SDP star polymer (Scheme 4-10). The molar ratio of the components are [initiator] / [EGDMA] / [**2**] / [SDP] / [Ru] = 10 / 200 / 50 / 50 / 10 mM. Conversion of the monomers was observed by ^{1}H NMR analysis of aliquots of the reaction mixture. After 48 hours, both SDP and **2** were almost completely consumed and 90% of EGDMA was also consumed (Figure 4-8). Mw = 155896 by GPC.
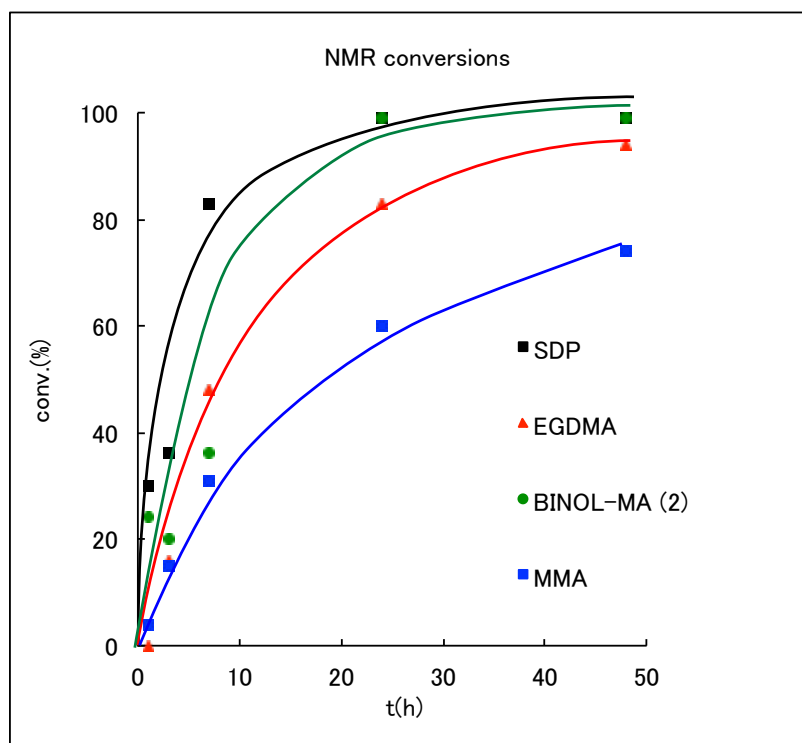
Figure 4-8. **NMR conversion of the monomers in PMMA-EGDMA-2-SDP star polymer 5. Tetralin was employed as internal standard.**

4.3.5 Kinetic resolution in hydrogen transfer oxidation of phenethyl alcohol

Although the exact amount of ruthenium content was not determined, chiral core polymers **4** and **5**, both *R* enantiomers, were used in hydrogen transfer oxidation conditions to verify if the chiral core gel showed any stereoselective partition effects resulting in the kinetic resolution of 1-phenethyl alcohol (Scheme 4-11). To exclude any excess ruthenium that is not immobilized in the core gels, the star polymers were dissolved in toluene and passed through a silica gel column. Labile ruthenium complexes remained on the top of the silica gel column, but those coordinated by SDP in the core gels stayed in the polymer thus eluted in toluene. Even after this process, estimating both **4** and **5** contained all the ruthenium employed at star polymer preparation by ATRP, the catalysts were added to the batch of racemic alcohol, potassium carbonate, in acetone and stirred at 60 ºC. The conversion of alcohol was monitored by the chiral GC. Divinyl BINOL polymer **4** catalyst showed 17% conversion in 48 hours, and monovinyl BINOL star polymer **5** catalyst showed 85% conversion in 7 hours, although both batches gave racemic starting material remaining. Also it should be noted that there is no discussion about the conversion in the batch of **4** and **5** due to uncertain ruthenium loadings as mentioned above.
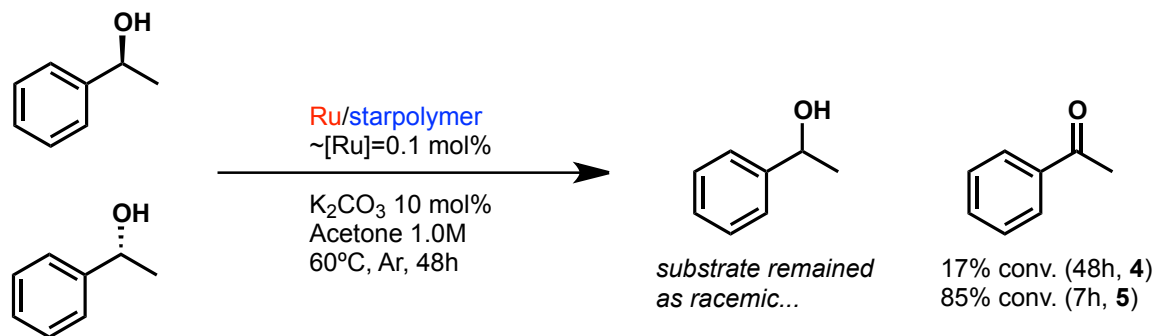
Scheme 4-11. Attempted kinetic resolution of 1-phenethyl alcohol by chiral core gel-star polymer catalyst 4 and 5. Conversions were determined by GC with *n*-octane as the internal standard.

4.4 Conclusion

Three binaphthyl chiral monomers, BINOL-DMA (**1**), BINOL-MA (**2**), and BINAM-DMA (**3**) were synthesized successfully, and attempts made to incorporate them into chiral core gel-star polymers by copolymerizing them with PMMA macroinitiators and SDP. However, employing **1** and **3** in place of EGDMA in the previously reported PMMA-EGDMA-SDA star polymer condition did not give the desired star polymers but employing **2** with EGDMA gave a star polymer containing chiral BINOL units in the core gel. CD spectra indicated that the axial chirality was retained and thus their chiral core gels contain resolved BINOL derivatives. Using these catalysts, kinetic resolution by hydrogen transfer oxidation of racemic 1-phenethyl alcohol was attempted, however the

170

starting alcohol remained racemic after treatment with either polymer catalyst **4** or **5**. This implies, therefore, that the chiral units need to be immobilized closer to the reactive catalyst center somehow, or a greater degree of organization in the nano space in the core gel is necessary to establish asymmetric reaction or chiral separation using chiral core gel-star polymers of this type. Since the BINAM-DMA monomer (**3**) did not polymerize well, the addition of extra MMA to copolymerize **3** increased the conversion of **3**, however not to a sufficient level yet. Protecting the nitrogen atom of the amide group of **3** to avoid catalyst poisoning, or further optimization of co-monomer addition to improve the formation of BINAM core gel are likely necessary.

I mention here again that special thanks should be given to Dr. Takaya Terashima, Dr. Makoto Ouchi, Dr. Mitsuo Sawamoto, and all the other members in Sawamoto's lab, Kyoto University. And I also appreciate the funding for G-COE program, JSPS and the CREATE program from Queen's University.

4.5   References

1.   Motorina, I. and Crudden, C. M., *Org. Lett.* **2001,** *3*, 2325.

2.   Crudden, C. M.; Sateesh, M. and Lewis, R., *J. Am. Chem. Soc.* **2005,** *127*, 10045.

3.   McEleney, K.; Allen, D. P.; Holliday, A. E. and Crudden, C. M., *Org. Lett.* **2006,** *8*, 2663.

4.   Barnes, J.; Dreher, M.; Plett, K.; Brown, R. S.; Crudden, C. M. and Loock, H.-P., *Analyst* **2008,** *133*, 1541.

5.   Nohair, B.; MacQuarrie, S.; Crudden, C. M. and Kaliaguine, S., *J. Phys. Chem. C* **2008,** *112*, 6065.

6.   MacQuarrie, S.; Nohair, B.; Horton, J. H.; Kaliaguine, S. and Crudden, C. M., *J. Phys. Chem. C* **2010,** *114*, 57.

7.   Du, J.; Cipot-Wechsler, J.; Lobez, J. M.; Loock, H.-P. and Crudden, C. M., *Small* **2010,** *6*, 1168.

8.   El Hankari, S.; El Kadib, A.; Finiels, A.; Bouhaouss, A.; Moreau, J. J. E.; Crudden, C. M.; Brunel, D. and Hesemann, P., *Chem. Eur. J.* **2011,** *17*, 8984.

9.   Jayalakshmi, V.; Wood, T.; Basu, R.; Du, J. N.; Blackburn, T.; Rosenblatt, C.; Crudden, C. M. and Lemieux, R. P., *J. Mater. Chem.* **2012,** *22*, 15255.

10.   Seki, T.; McEleney, K. and Crudden, C. M., *Chem. Commun.* **2012,** *48*, 6369.

11.   El Kadib, A.; McEleney, K.; Seki, T.; Wood, T. K. and Crudden, C. M., *Chemcatchem* **2011,** *3*, 1281.

12.   Wu, X. W.; Blackburn, T.; Webb, J. D.; Garcia-Bennett, A. E. and Crudden, C. M., *Angew. Chem. Int. Ed.* **2011,** *50*, 8095.

13. MacQuarrie, S.; Thompson, M. P.; Blanc, A.; Mosey, N. J.; Lemieux, R. P. and Crudden, C. M., *J. Am. Chem. Soc.* **2008,** *130*, 14099.

14. Webb, J. D.; MacQuarrie, S.; McEleney, K. and Crudden, C. M., *J. Catal.* **2007,** *252*, 97.

15. Glasspoole, B. W.; Webb, J. D. and Crudden, C. M., *J. Catal.* **2009,** *265*, 148.

16. Crudden, C. M.; McEleney, K.; MacQuarrie, S. L.; Blanc, A.; Sateesh, M. and Webb, J. D., *Pure Appl. Chem.* **2007,** *79*, 247.

17. Webb, J.; Macquarrie, S.; McEleney, K. and Crudden, C., *J. Catal.* **2007,** *252*, 97.

18. Glasspoole, B. W.; Webb, J. D. and Crudden, C. M., *J. Catal.* **2009,** *265*, 148.

19. Crudden, C. M.; Allen, D.; Mikoluk, M. D. and Sun, J., *Chem. Commun.* **2001**, 1154.

20. Staudinger, H., *Helv. Chim. Acta* **1925,** *8*, 67.

21. Wang, Y.; Wang, X. and Antonietti, M., *Angew. Chem., In. Ed.* **2012,** *51*, 68.

22. Wulff, G. and Liu, J. Q., *Acc. Chem. Res.* **2012,** *45*, 239.

23. Zhang, Y. G. and Riduan, S. N., *Chem. Soc. Rev.* **2012,** *41*, 2083.

24. Diaz, D. D.; Kuehbeck, D. and Koopmans, R. J., *Chem. Soc. Rev.* **2011,** *40*, 427.

25. Framery, E.; Andrioletti, B. and Lemaire, M., *Tetrahedron-Asymmetry* **2010,** *21*, 1110.

26.   Takizawa, S.; Arai, T. and Sasai, H., *J. Synth. Org. Chem. Jpn.* **2009,** *67*, 194.

27.   Popa, D.; Marcos, R.; Sayalero, S.; Vidal-Ferran, A. and Pericas, M. A., *Adv. Synth. Catal.* **2009,** *351*, 1539.

28.   Heitbaum, M.; Glorius, F. and Escher, I., *Angew. Chem. Int. Ed.* **2006,** *45*, 4732.

29.   Canali, L. and Sherrington, D. C., *Chem. Soc. Rev.* **1999,** *28*, 85.

30.   Coates, G. W., *J. Chem. Soc.-Dalton Trans.* **2002**, 467.

31.   Wang, J. S. and Matyjaszewski, K., *Macromolecules* **1995,** *28*, 7901.

32.   Wang, J. S. and Matyjaszewski, K., *J. Am. Chem. Soc.* **1995,** *117*, 5614.

33.   Kato, M.; Kamigaito, M.; Sawamoto, M. and Higashimura, T., *Macromolecules* **1995,** *28*, 1721.

34.   Kamigaito, M.; Ando, T. and Sawamoto, M., *Chem. Rev.* **2001,** *101*, 3689.

35.   Hawker, C. J.; Bosman, A. W. and Harth, E., *Chem. Rev.* **2001,** *101*, 3661.

36.   Chiefari, J.; Chong, Y. K.; Ercole, F.; Krstina, J.; Jeffery, J.; Le, T. P. T.; Mayadunne, R. T. A.; Meijs, G. F.; Moad, C. L.; Moad, G.; Rizzardo, E. and Thang, S. H., *Macromolecules* **1998,** *31*, 5559.

37.   Matyjaszewski, K. and Xia, J. H., *Chem. Rev.* **2001,** *101*, 2921.

38.   Ouchi, M.; Terashima, T. and Sawamoto, M., *Chem. Rev.* **2009,** *109*, 4963.

39.   Kamigaito, M.; Ando, T. and Sawamoto, M., *Chemical Record* **2004,** *4*, 159.

40.   Kamigaito, M., *Polym. J.* **2011,** *43*, 105.

41.   Coessens, V.; Pintauer, T. and Matyjaszewski, K., *Prog. Polym. Sci.* **2001,** *26*, 337.

42.   Ouchi, M.; Terashima, T. and Sawamoto, M., *Acc. Chem. Res.* **2008,** *41*, 1120.

43.   Wakioka, M.; Baek, K. Y.; Ando, T.; Kamigaito, M. and Sawamoto, M., *Macromolecules* **2002,** *35*, 330.

44.   Matyjaszewski, K.; Wei, M. L.; Xia, J. H. and McDermott, N. E., *Macromolecules* **1997,** *30*, 8161.

45.   Zhu, S. M. and Yan, D. Y., *Macromolecules* **2000,** *33*, 8233.

46.   Uegaki, H.; Kotani, Y.; Kamigaito, M. and Sawamoto, M., *Macromolecules* **1997,** *30*, 2249.

47.   Yamamoto, K.; Miwa, Y.; Tanaka, H.; Sakaguchi, M. and Shimada, S., *J. Polym. Sci., Part A: Polym. Chem.* **2002,** *40*, 3350.

48.   Uegaki, H.; Kamigaito, M. and Sawamoto, M., *J. Polym. Sci., Part A: Polym. Chem.* **1999,** *37*, 3003.

49.   Li, P. and Qiu, K. Y., *Polymer* **2002,** *43*, 5873.

50.   Nakatani, K.; Ogura, Y.; Koda, Y.; Terashima, T. and Sawamoto, M., *J. Am. Chem. Soc.* **2012,** *134*, 4373.

51.   Chen, G. H. and Hoffman, A. S., *Nature* **1995,** *373*, 49.

52.   Terashima, T.; Kamigaito, M.; Baek, K.-Y.; Ando, T. and Sawamoto, M., *J. Am. Chem. Soc.* **2003,** *125*, 5288.

53.   Crooks, R. M.; Zhao, M. Q.; Sun, L.; Chechik, V. and Yeung, L. K., *Acc. Chem. Res.* **2001,** *34*, 181.

54.   Lee, J. W.; Kim, J. H.; Kim, B. K.; Shin, W. S. and Jin, S. H., *Tetrahedron* **2006,** *62*, 894.

55.   Mery, D. and Astruc, D., *Coord. Chem. Rev.* **2006,** *250*, 1965.

56.   Mecking, S.; Thomann, R.; Frey, H. and Sunder, A., *Macromolecules* **2000,** *33*, 3958.

57.   Bosman, A. W.; Vestberg, R.; Heumann, A.; Fréchet, J. M. J. and Hawker, C. J., *J. Am. Chem. Soc.* **2002,** *125*, 715.

58.   Slagt, M. Q.; Stiriba, S.-E.; Klein Gebbink, R. J. M.; Kautz, H.; Frey, H. and van Koten, G., *Macromolecules* **2002,** *35*, 5734.

59.   Youk, J. H.; Park, M.-K.; Locklin, J.; Advincula, R.; Yang, J. and Mays, J., *Langmuir* **2002,** *18*, 2455.

60.   Kleij, A. W.; Gossage, R. A.; Klein Gebbink, R. J. M.; Brinkmann, N.; Reijerse, E. J.; Kragl, U.; Lutz, M.; Spek, A. L. and van Koten, G., *J. Am. Chem. Soc.* **2000,** *122*, 12112.

61.   Dahan, A. and Portnoy, M., *Chem. Commun.* **2002**, 2700.

62.   Yoda, H.; Nakatani, K.; Terashima, T.; Ouchi, M. and Sawamoto, M., *Macromolecules* **2010,** *43*, 5595.

63.   Goh, T. K.; Yamashita, S.; Satoh, K.; Blencowe, A.; Kamigaito, M. and Qiao, G. G., *Macromol. Rapid Commun.* **2011,** *32*, 456.

64.   Koda, Y.; Terashima, T.; Nomura, A.; Ouchi, M. and Sawamoto, M., *Macromolecules* **2011,** *44*, 4574.

65.   Terashima, T.; Nomura, A.; Ito, M.; Ouchi, M. and Sawamoto, M., *Angew. Chem., In. Ed.* **2011,** *50*, 7892.

66.   Terashima, T.; Ouchi, M.; Ando, T. and Sawamoto, M., *Polymer Journal (Tokyo, Japan)* **2011,** *43*, 770.

67.   Terashima, T.; Ouchi, M.; Ando, T. and Sawamoto, M., *J. Polym. Sci., Part A: Polym. Chem.* **2011,** *49*, 1061.

68.   Fukae, K.; Terashima, T. and Sawamoto, M., *Macromolecules* **2012,** *45*, 3377.

69. Terashima, T.; Nomura, A.; Ouchi, M. and Sawamoto, M., *Macromol. Rapid Commun.* **2012,** *33*, 833.

70. Terashima, T.; Ouchi, M.; Ando, T. and Sawamoto, M., *J. Polym. Sci., Part A: Polym. Chem.* **2010,** *48*, 373.

Chapter 5

Conclusions

Beginning with the basics and applications of silica-based mesoporous materials including organic/inorganic hybrid material PMOs, the first chapter introduced our previous work in this area, including chiral PMO materials synthesized from axially chiral precursors, whose chiral biphenyl or binaphthyl units are rigidly incorporated in the materials, and thiol functionalized SBA-15 (SBA-15-SH) for palladium scavenging and heterogeneous catalysis. Although our group was not the first to report chiral PMO materials, the phenomenon of transferring chirality in solid state due to π-π stacking reported by us has opened up new possibilities for he use of such PMO materials in catalysis and separation. One of he key possibilities stemming from this work is that small amount of precious chiral monomers can be amplified in the broad nano space of the materials through interactions with other bulk monomers. In fact, the interaction between biphenylene head group-containing liquid crystals and the surface of the chiral PMO does exist, demonstrating chirality transfer to external materials as well. Such phenomena can be accomplished exclusively with PMOs synthesized from rigidly functionalized axially chiral precursors, i.e. direct silylation of the biphenyl or binaphthyl

unit is necessary, although the synthesis of those precursors are much more difficult than previously reported flexible chain-linked precursors. The strategy to prepare fundamentally new chiral PMOs was described in the second chapter, in which rigidly-bridged chiral BINAP PMOs were prepared and used for heterogeneous asymmetric hydrogenations. Quantitative transformations in post-condensation steps implied that most of the ligand functionalities were not buried inside the wall structure but were exposed on the accessible surface domain. The successful complexation of the ruthenium catalyst and the excellent enantioselectivity demonstrated in the hydrogenation reaction revealed that the chiral ligands incorporated in the material did not have to have the polymerization axis exactly on the chiral axis, at least in this case.

In other work from our group, we demonstrated that SBA-15-SH was a superb palladium scavenger and a supported catalyst with long lifetime. TEM analysis of the material showed that palladium was trapped by thiol groups inside the pores and results in the formation of size-restricted nanoparticles, which is critical since the formation of large particles the one of the key mechanisms by which transition metal catalysts lose reactivity. However thiol functionalities are located on both particles' external surface and porous internal surface, and as a result, the use of size-restricted materials is important. In addition to this stabilization effect, mesoporous supported catalysts also

showed drastically improved yield, stereoselectivity, and unique regioselectivity. Again, these supported catalysts were immobilized on both external/internal surface, thus there is still much room for improvement by developing a method to localize functionalities exclusively on the interior pore surface.

Our tactics to accomplish the truly selective functionalization of porous materials are described in the third chapter. This work was based on the work of former PhD student Dr. Jonathan D. Webb, and the key point is the preparation of truly pore-blocked materials by the reloading of surfactant micelles in the pores. Most of the previous attempts at the selective functionalization employed imperfect pore-blocked materials, whereas we further reloaded surfactant micelles to as-synthesized materials followed by optimized passivation in neat HMDS for SBA-15. Multiple analyses by nitrogen adsorption, elemental analysis, and solid state NMR, the last of which was performed in collaboration with Dr. Marek Pruski's group in Iowa State University at Ames, provided convincing information to support our successful selective functionalization.

While chiral PMO materials have been studied in our group, organic polymer–based chiral materials were also studied. The fourth chapter presents chiral star polymers whose core-gels were built up with axially chiral monomers. Phosphine ligand–containing vinyl monomers were copolymerized to construct the core-gel, in which

ruthenium catalysts were installed in the core of the star polymers as the products being polymerized. The main purpose of this work was to observe the chirality transfer effect from the chiral monomers to the catalyst center in the organic polymer core gels by carrying out asymmetric reactions in the chiral space but without chiral ligands, thus the core gels constructed with chiral BINOL or BINAM monomers and ruthenium(II) catalysts. Unfortunately the attempted kinetic resolution did not show any stereospecificity in transfer hydrogenation.

Over several projects, the key concept of employing well defined, nanoscopically ordered catalysts was a common feature. Each domain of science has huge advantage in certain techniques however cross fertilization is critical for truly impactful advances. Hence stimulating those collaborations across the disciplines and inventing new sustainable catalysis or useful materials for humanity will be the biggest objective in my future carrier as a researcher.

Chapter 6

Experimental Procedures

6.1   Experimental procedures for chapter 2

6.1.1 General

2,2'-bis(diphenylphosphino)-1,1'-binaphthyl (BINAP), dichloro (benzene) ruthenium (II) dimer, chloro (1,5-cyclooctadiene) rhodium(I) dimer and (1R,2R)-(+)-1,2-diphenylethylene diamine ((R,R)-DPEN) were purchased from Strem and used without further purification. Triethoxysilane and trifluoromethylsulfonic anhydride were purchased from TCI America. Toluene was obtained dry from a solvent purification system fitted with alumina columns. THF and hexane were freshly distilled from sodium/benzophenone ketyl. Triethylamine was purchased from Aldrich and distilled fresh from CaH_2 prior to use. Isopropanol was dried by storing with activated 4Å molecular sieves under argon then degassed by freeze-thaw technique prior to use. *N,N*-dimethylformamide (DMF), dichloromethane and acetonitrile were purchased dry from EMD and used without any further treatment. Methanol was purchased dry from EMD and degassed by freeze-thaw technique prior to use. Hydrochloric acid was purchased from Fisher scientific and used without further treatment. Hydrogen gas was purchased

from Praxair and used through high-pressure tubing and autoclaves. The substrate for

Table 2-3 entry 6 (methyl 3-oxo-3-(4-methoxyphenyl)propanoate) was synthesized as

reported by Vu *et al.*[1] The other chemicals were purchased from Sigma-Aldrich, Acros or

Alfa Aesar and used without further treatment unless otherwise noted. Nitrogen

adsorption experiments were performed using a Micrometrics ASAP 2010 physisorption

analyzer with nitrogen gas as the adsorbate at 77 K. Samples were degassed at 80 °C for

at least 8 hours and until 10^{-3} mm Hg pressure was maintained. Solid-state CP MAS ^{13}C,

^{29}Si and ^{31}P NMR measurements were recorded on a Bruker Avance 600 spectrometer

operating at 150.9, 119.2 and 243.0 MHz for ^{13}C, ^{29}Si and ^{31}P respectively, and using a

Bruker 5 mm CP MAS probe. A typical spinning rate for CP MAS experiments is 11 kHz.

A 2 ms cross polarization contact time was used to acquire ^{13}C, ^{29}Si and ^{31}P CP MAS

spectra with a repetition delay of 2 s. The number of scans was in excess of 600, 2400

and 3000 for ^{13}C, ^{29}Si and ^{31}P respectively to obtain sufficient signal. ^{13}C, and ^{29}Si MAS

spectra were referenced to tetramethylsilane, and ^{31}P was referenced to phosphoric acid.

TEM images were obtained using a 200keV JEOL 2010 STEM operated in both

transmission and STEM modes. In STEM mode, a Gatan High Angle Annular Dark Field

Detector was used to image the sample. The sample was prepared by placing a small

amount of powder in ethanol and sonicating for 5 minutes. 20 µL of the solution was

pipetted onto a carbon coated, 200 mesh copper grid. Powder X-ray diffraction measurements were run on an automated Siemens/Bruker AXS D5000 diffractometer. The system is equipped with a high power line focus Cu-kα source operating at 50 kV/35mA. A solid-state Si/Li Kevex detector was used for removal of k-beta lines. The diffraction patterns were collected on a theta/2-theta Bragg-Brentano reflection geometry with fixed slits. The slits were set up appropriately for both low- and wide-angle ranges in order to ensure the optimal quality of the diffraction patterns. A step scan mode was used for data acquisition with step size of 0.020 2-theta and counting time of 3.0 s per step for low-theta scans and 1.0 s per step for the wide range scans. The ICPMS was analyzed by Robertson Microlit Laboratories (Ledgewood, NJ, U.S.A.). Centrifugation was performed with a Damon IEC HN-SII.

6.1.2 Synthesis of BINAP-PMO precursors

Diphenyl-[1,1'-binaphthalene]-2,2'-diylester (BINAPO) (8)

This procedure is derived from a literature procedure by Lemaire et al.[2] and the spectra obtained matched those reported. In a 100mL round-bottom flask were placed BINAP (1.0 g, 1.6 mmol) and 8.0mL of CH_2Cl_2. The mixture was cooled in an ice water bath and 4.0 mL of hydrogen peroxide (35%) was then added. The mixture was stirred for 2h. After 50 mL of water was added, the organic layer was separated. The aqueous

layer was extracted with 20 mL of CH_2Cl_2 twice. The combined organic layers were washed with brine, dried over sodium sulfate, and concentrated by rotary evaporation to give a white powder (1.0 g, mmol, quantitative yield). This product was used without further purification. ^{1}H NMR (500 MHz, $CDCl_3$): δ 7.88 (dd, 2H, J = 8, 3.5 Hz), 7.84 (d, 2H, J = 7.5 Hz), 7.73 (dd, 4H, J = 11, 6.5 Hz), 7.35 – 7.94 (m, 12H), 7.22 – 7.32 (m, 8H), 6.79 – 6.86 (m, 4H). ^{31}P NMR (135 MHz, $CDCl_3$): δ 29.48. EI-HRMS (MH$^+$) found 654.1889 m/z (calc. 654.1878).

2,2'-Bis(diphenylphosphinyl)-5,5'-diiodo-1,1'-binaphthyl (9)

This procedure is modified from Olah *et al.*[3] and the spectra obtained matched those reported in the literature.[4] To a solution of BINAPO (**8**) (3.15 g, 4.8 mmol) in MeCN (48 mL) was added Tf$_2$O (4.05 mL, 6.77 g, 24 mmol, 5.0 equiv.) and H_2O (0.44 mL, 24 mmol, 5.0 equiv.). The resulting orange solution was cooled in an ice-bath and then NIS (3.24 g, 14.4 mmol, 3.0 equiv.) was added portion by portion. After 15 min. of stirring in an ice-bath, the mixture was heated at 80ºC for 3 hours. The reaction mixture was quenched with sodium thiosulfate and extracted with CH_2Cl_2. The organic phase was washed with brine and water, dried over sodium sulfate, and concentrated by rotary evaporator. The crude brown oil was chromatographed through a silica gel column

(AcOEt/hexane = 3/1 - 2/1) to give a pale yellow solid. (3.92 g, 90% yield). ^{1}H NMR

(500MHz, CDCl$_3$): δ 8.18 (d, 2H, J = 8.6 Hz), 7.97 (d, 2H, J = 7.2 Hz), 7.73 (dd, 4H, J =

11.7, 7.9 Hz), 7.54 (dd, 2H, J = 11.0, 9.3 Hz), 7.41 (m, 8H), 7.33 (m, 4H), 7.27 (m, 4H),

6.76 (d, 2H, J = 8.5 Hz), 6.51 (t, 2H, J = 7.7 Hz). ^{13}C NMR (125MHz, CDCl$_3$): δ 141.39,

139.44, 135.68, 134.82, 132.71, 132.25, 131.90, 130.36, 130.21, 129.81, 128.77, 128.46,

128.34, 127.26, 99.17. ^{31}P NMR (135 MHz, CDCl$_3$): δ 30.02. mp = 347-348 ºC (decomp).

EI-HRMS (MH$^+$) found 906.9870 m/z (calc. 906.9888).

2,2'-Bis(diphenylphosphinyl)-5,5'-bis(triethoxysilyl)-1,1'-binaphthyl (1)

This procedure was adapted from Masuda *et al.*[5,6] Rh(cod)(CH$_3$CN)$_2$BF$_4$ was

prepared as Collman *et al*. reported[7], but AgBF$_4$ was used instead of Ph$_3$CBF$_4$. This

rhodium catalyst (8.0 mg, 0.021 mmol, 7.6 mol %) and **9** (252.0 mg, 0.278 mmol) were

combined in a small Schlenk tube under argon. DMF (1 mL) was added to the tube

followed by triethylamine (230 μL, 1.65 mmol). This solution was stirred in an ice bath

for 15 min before the addition of triethoxysilane (200 μL, 1.09 mmol). The reaction was

then stirred for 2 hours at 80 °C. The DMF was then removed under high vacuum and the

residue was dissolved in ether. This solution was passed through a plug of celite/charcoal

to remove any residual rhodium and reduced byproduct.[8] The filtrate was then

concentrated to some extent and purified by silica gel flash column chromatography (THF/Hexane = 3/2) very quickly, otherwise most of the product was captured by silica gel. This gave 45.5 mg (0.047 mmol, 17% yield) of **1** as pail yellow oil. Because this compound is sensitive for moisture, it was kept in a flask charged with argon, then stored in a fridge. ^{1}H NMR (400 MHz, CDCl$_3$): δ 8.37 (dd, 2H, J = 8.8, 2.0 Hz) 7.79 (dd, 2H, J = 6.6, 1.0 Hz), 7.74 (dd, 4H, J = 12.2, 7.0 Hz), 7.46 (dd, 2H, J = 11.6, 8.8 Hz), 7.38 - 7.41 (m, 12H), 7.18 (td, 4H, J = 7.6, 2.4 Hz), 6.72 (d, 2H, J = 8 Hz), 6.63 (dd, 2H, J = 8.4, 6.8 Hz), 3.96 (q, 12H, J = 7.0 Hz), 1.31 (t, 18H, J = 7.0 Hz). ^{13}C NMR (100MHz, CDCl$_3$): δ 138.11, 137.49, 132.82, 132.71, 132.34, 132.26, 131.41, 131.09, 130.32, 129.04, 128.45, 128.32, 128.10, 127.98, 124.99, 59.22, 18.58. ^{31}P NMR (135 MHz, CDCl$_3$): δ 28.50. MALDI-HRMS (MH[+]) found 979.3370 m/z (calc. 979.3380).

6.1.3 Material Preparation

This procedure is modified from our previously reported procedure[9]. The molar ratio of the components is Si / Brij 76 / water / HCl / NaCl / EtOH = 1.00 / 0.533 / 600 / 8.40 / 19.0 / 18.4. For example, **5%BINAPO-PMO**: Brij 76 (1.93 g) was dissolved in deionized water (55 mL) and conc. HCl (3.5 mL). This solution was stirred at 60 °C in an

oil bath for 1 hour before the addition of NaCl (5.68 g), then the solution was stirred for a

further 3 hours at the same temperature. To this micelle solution was added an ethanol

solution of siloxane precursors (**1** (250 mg, 0.26 mmol) and 4,4'-

bistriethoxysilylbiphenyl **2** (2.32 g, 4.85 mmol) in 2.8 mL of ethanol) dropwise under

vigorous stirring. The resulting mixture was stirred for 24 hours at 60 ºC, and was aged

for further 48 hours at 90 ºC. The precipitated white powder was recovered carefully by

vacuum filtration using a Kiriyama-funnel, and washed with copious amounts of ethanol,

water and acetone in this order. The surfactant was removed using a Soxhlet extractor

(EtOH with 1% of HCl) for 24 hours. Again, the recovered powder was dried under high

vacuum at 80 ºC overnight, and gave 1.62 g of 5%BINAP-PMO. Nitrogen adsorption

data are given in **Table 2-1**. The amount of BINAP incorporated in the material was

estimated as 0.26 mmol in 1.62 g of the product at highest, thus 0.160 mmol g^{-1}.

6.1.4 Post-grafted Modification

Prior to every step of modification, the material was dried under high vacuum

(0.2 mmHg) at 80 ºC overnight.

Trimethylsilyl (TMS)-capping of free silanols

In a 250 mL round bottom flask, **5%BINAPO-PMO** (1.5 g) was suspended in

dry hexane (60 mL). To this suspension was added hexamethyldisilazane (HMDS, 4 mL,

excess) then stirred for 24 hours at 65 ºC in an oil bath. The material was filtered, washed with copious amounts of ethyl acetate, ethanol and acetone, and then dried under high vacuum (0.2 mmHg) at 80 ºC overnight. 1.5 g of a white powder was recovered. Nitrogen adsorption data are in **Table 2-1**, and solid state ^{29}Si NMR is in **Figure 2-8**.

Reduction of phosphine oxides

This procedure is based on Spencer *et al.*[10] **but it should be noted that extreme high purity of the trichlorosilane is important to prevent the decomposition of the ordered mesoporous structure by acid.** Trichlorosilane packed in an ampule was purchased from Sigma-Aldrich, it was carefully transferred into a Schlenk tube with activated basic alumina under argon atmosphere, then was stored in a fridge. To a suspension of **TMS-capped 5%BINAPO-PMO** (100 mg) in toluene (4.0 mL) was added tributylamine (2.0 mL), triethylphosphite (0.05 mL) and extremely pure trichlorosilane (0.28 mL) under argon. The mixture was stirred for 24 hours at 80 ºC in an oil bath. After cooling the mixture at room temperature, the material was recovered by filtration and washed with copious amount of toluene, ethyl acetate and acetone. Drying this material under high vacuum (0.2 mmHg) at 80 ºC overnight gave **5%BINAP-PMO** quantitatively. Nitrogen adsorption data are in **Table 2-1**, and solid state NMRs are in **Figure 2-9** (^{31}P) and **Figure 6-1** (^{29}Si).
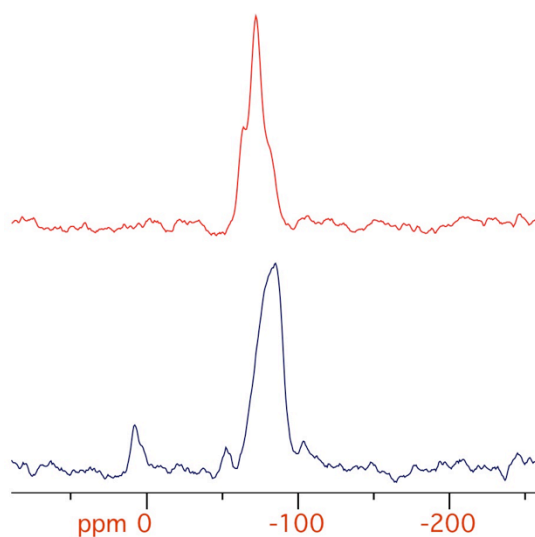
Figure 6-1. Solid state CP MAS ^{29}Si NMR spectra (600MHz, 25ºC, MAS = 10kHz). Before (top) and after (bottom) TMS capping of free silanols. Disappearance of T1 site and increased T3 site, also M site from TMS group are observed.

Ruthenium complexation

This procedure is based on Mashima *et al.*[11] 5%BINAP-PMO (1.50 g) and dichloro benzene ruthenium(II) dimer (30 mg, 0.12 mmol of ruthenium) were placed in a vial with a magnetic stirring bar in a glove box, then a mixture of methanol/benzene (45 mL/5 mL) solution was added. The resulting suspension was stirred for 24 hours at 60 ºC. The material was recovered by filtration, washed with copious amount of methanol and dichloromethane, and dried on a vacuum funnel in a glove box. The amount of the ruthenium doped on this material was determined to be 0.084 mmol g^{-1} by ICPMS elemental analysis, thus the ruthenium was quantitatively immobilized on the material

with ca. 50% of the BINAP binding to the ruthenium(II) catalyst according to the amount

of BINAP incorporated in the material (0.160 mmol g^{-1}) mentioned above. Nitrogen

adsorption data are in **Table 2-1**, solid state ^{31}P NMR is in **Figure 2-9**, and powder XRD

is in Figure **2-11**.

6.1.5 Other material characterization data
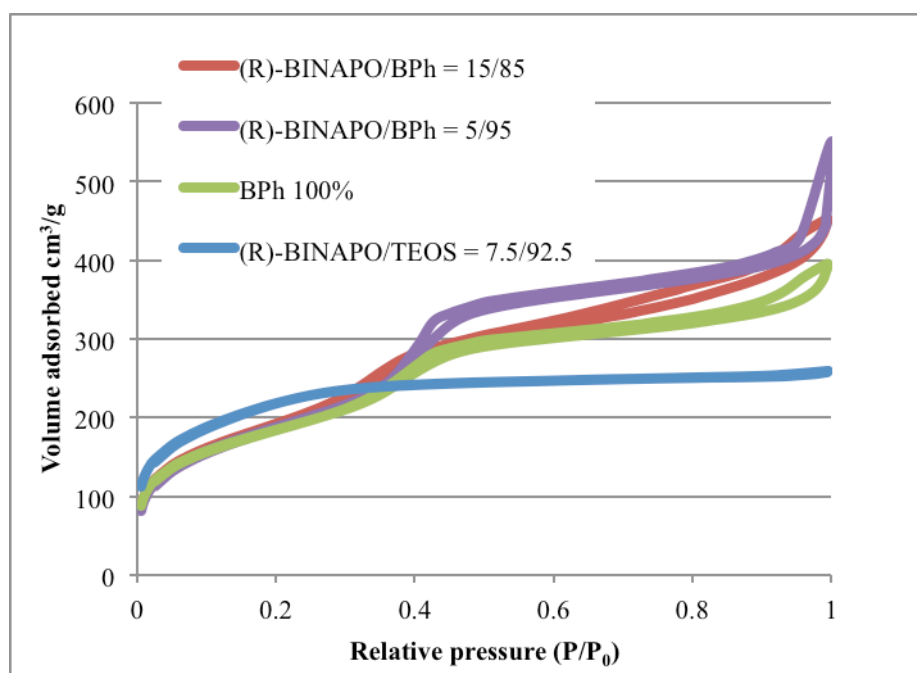
Figure 6-2. **Nitrogen adsorption isotherm plot of a series of BINAPO-PMOs**
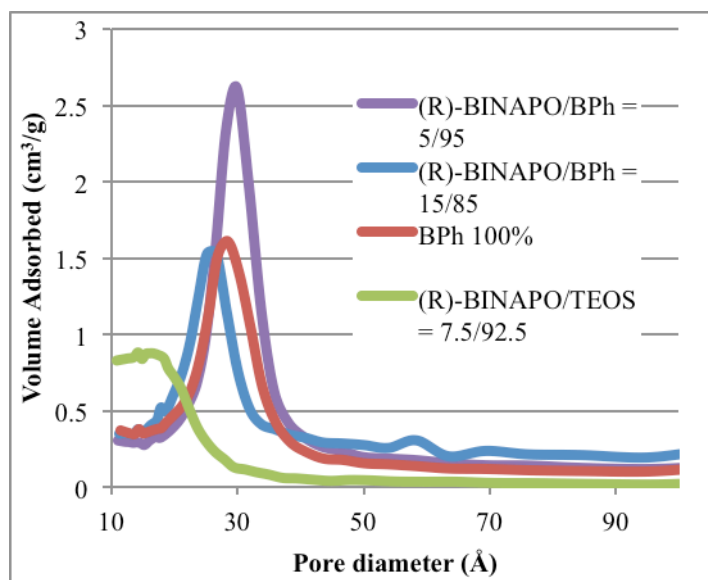
Figure 6-3. BJH adsorption pore diameter distribution of a series of BINAPO-PMOs
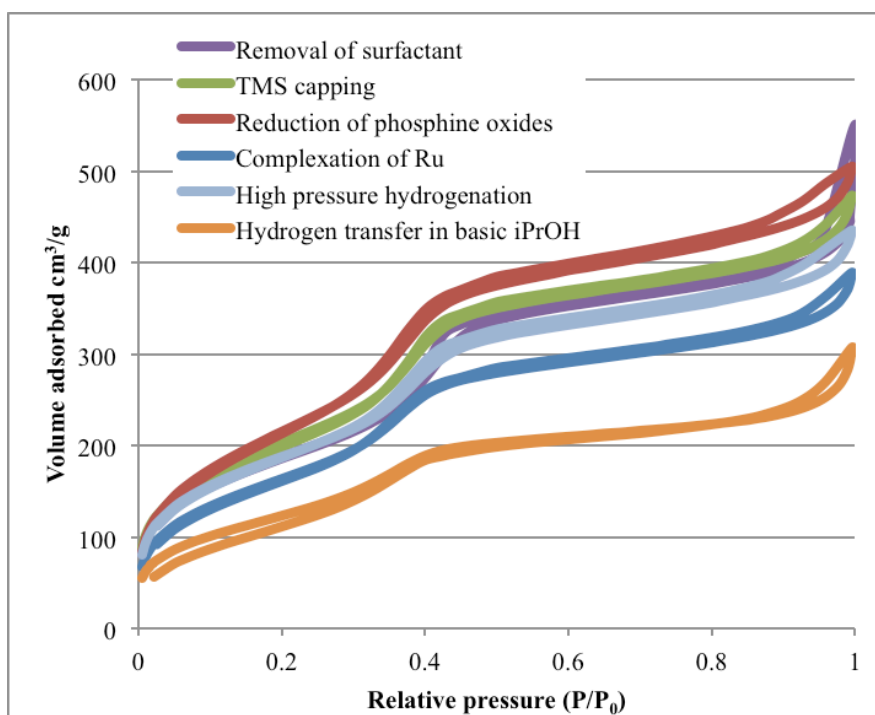
Figure 6-4. Nitrogen adsorption isotherm plots of PMOs over post condensation modifications. All the materials are synthesized from the precursors with molar ratio; (R)-BINAPO/BPh = 5/95.
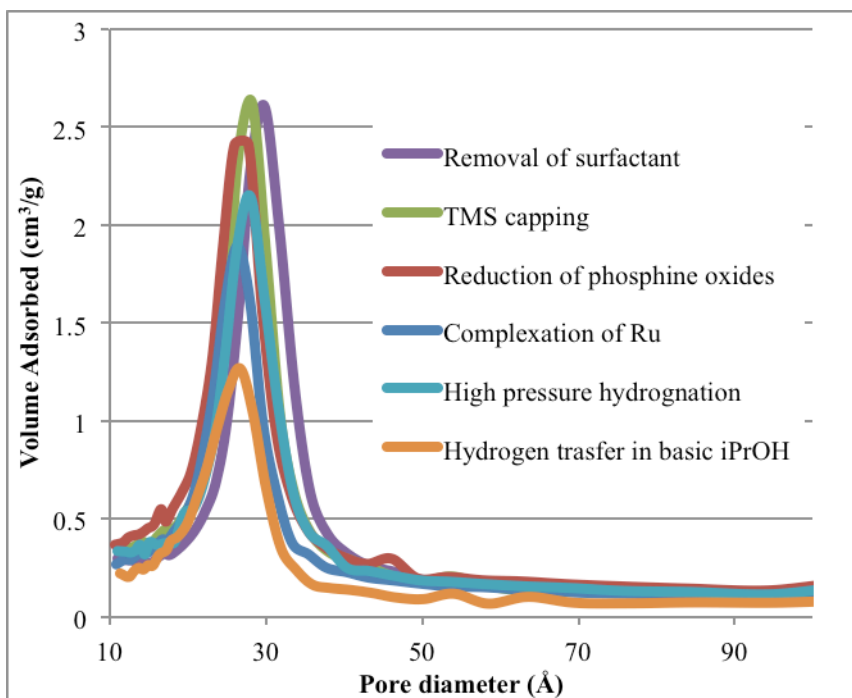
Figure 6-5. BJH adsorption pore diameter distribution of PMOs over post condensation modifications. All the materials are synthesized from the precursors with molar ratio; (R)-BINAPO/BPh = 5/95.

6.1.6 Catalysis Procedures

6.1.6.1 High-pressure hydrogenation

In an inert atmosphere glove box under nitrogen, a 15 mL vial was charged with a magnetic stirring bar and Ru/5%(R)BINAP-PMO (24mg, 2.0 μmol). After being sealed with a rubber septum, the vial was removed from the glove box, and degassed methylacetoacetate (0.21 mL, 2.0 mmol) in methanol (5.0 mL) was added by syringe. The vial was placed in an autoclave and the rubber septum was carefully removed under

Ar flow, then it was purged with hydrogen. After purging, the hydrogen pressure was increased to 600 psi, and the reaction mixture stirred in an oil bath at 50 ºC for 24 hours. After cooling the autoclave to room temperature, the hydrogen was carefully depressurized and the catalyst powder was separated by vacuum filtration. Concentrating the filtrate on a rotary evaporator gave 236 mg (99% yield) of a colorless oil. The spectra obtained were identical with those reported in the literature.[12]

^{1}H NMR (400 MHz, CDCl$_3$) δ: 1.17 (d, J = 6.3, 3H), 2.40 (qd, J = 14.7, 6.1, 2H), 2.94 (br, 1H), 3.65 (s, 3H), 4.14 (dt, J = 6.1, 2.5, 1H). ^{13}C NMR (100 MHz, CDCl$_3$) δ: 22.5, 42.6, 51.7, 64.2, 173.3. SFC (OD-H, 1% MeOH, 2 mL/min, 200 bar, 40 ºC) 4.7, 5.5 min.

ethyl 3-hydroxybutanoate as above ^{1}H NMR (400 MHz, CDCl$_3$) δ: 1.20 (d, J = 6.6 Hz, 3H), 1.25 (t, J = 7.2 Hz, 3H), 2.39 (m, 2H), 3.02 (br, 1H), 4.22 (q, J = 7.2 Hz, 2H). ^{13}C NMR (100 MHz, CDCl$_3$) δ: 14.1, 22.4, 42.7, 55.6, 64.2, 172.9. SFC (OD-H, 1% MeOH, 2 mL/min, 200 bar, 40 ºC) 4.6, 5.7 min.

methyl 3-hydroxypentanoate as above ^{1}H NMR (400 MHz, CDCl$_3$) δ: 0.81 (t, J = 7.5, 3H), 1.42-1.34 (m, 2H), 2.26 (dd, J = 16.4, 9.1, 1H), 2.37 (dd, J = 16.4, 3.1, 1H), 2.99 (br, 1H), 3.56 (s, 3H), 3.79 (dtd, J = 7.2, 3.5, 1.8, 1H). ^{13}C NMR (100 MHz, CDCl$_3$) δ: 9.8,

29.4, 40.7, 51.7, 69.4, 173.5. SFC (OD-H, 1% MeOH, 2 mL/min, 200 bar, 40 ℃) 6.3, 7.1

min.

methyl 3-hydroxy-4-methylpentanoate as above[1]H NMR (400 MHz, CDCl$_3$) δ: 0.96

(dd, J = 11.4, 6.8, 6H), 1.73 (dd, J = 13.0, 6.5, 1H), 2.43 (dd, J = 16.3, 9.6, 1H), 2.53 (dd,

J = 16.3, 2.8, 1H), 3.74 (s, 3H), 3.81 (ddd, J = 9.3, 6.0, 3.1, 1H). ^{13}C NMR (100 MHz,

CDCl$_3$) δ: 17.7, 18.4, 33.2, 38.3, 51.8, 72.8, 173.9. SFC (OD-H, 1% MeOH, 2 mL/min,

200 bar, 40 ℃) 6.2, 6.9 min.

methyl 3-hydroxy-3-(4-methoxyphenyl)propanoate as above ^{1}H NMR (400 MHz,

CDCl$_3$) δ: 1.36-1.20 (br, 1H), 3.77 (s, 3H), 3.90 (s, 3H), 3.98 (m, 2H), 5.15 (m, 1H), 6.97

(d, J = 9.0 Hz, 2H), 7.95 (d, J = 9.0 Hz, 2H). ^{13}C NMR (100 MHz, CDCl$_3$) δ: 24.0, 43.2,

60.7, 68.9, 70.2, 125.5, 125.6, 128.4, 129.2, 129.6, 142.0, 172.2. SFC (OD-H, 20 %

MeOH, 2 mL/min, 200 bar, 40 ℃) 20.0, 22.1 min.

6.1.6.2 Recycling the catalyst

The procedure described above was followed, except that the rubber septum

was not removed when the vial was placed in an autoclave, only a small needle was left

through the septum while running the reaction. After the reaction, the needle was taken

out then this vial and the rubber septum left on during centrifugation for 5 minutes at

2600 rpm. The supernatant was taken out by syringe, and another 5 mL of degassed

methanol was added to rinse the catalyst. The suspension was again centrifuged then the supernatant was taken out. The same manipulation was repeated three times in total. The combined methanol solution was concentrated as above, and a fresh substrate solution in methanol was added to the catalyst to run the second cycle.

6.1.6.3 Transfer hydrogenation

In a 25 mL round bottom flask was placed a magnetic stirring bar, Ru/5%(R)BINAP-PMO (79 mg, 6.7 μmol), potassium carbonate (93 mg, 0.67 mmol) and 4-methoxyacetophenone (1.0 g, 6.7 mmol). The flask was capped with a rubber septum before being purged with Ar. Degassed iPrOH (15 mL) was added by syringe, and then the mixture was stirred at 100 ℃ in an oil bath for 24 hours. After cooling the reaction mixture to room temperature, it was filtered on a Buchner funnel, and washed with copious amounts of ethylacetate. The combined filtrate was washed with brine, dried over magnesium sulfate, and concentrated on a rotary evaporator. ^{1}H NMR of the obtained colorless oil (1.0 g) was measured, and the yield estimated at 87% based on hexamethylbenzene internal standard. In the asymmetric version, (*R, R*)-DPEN (2.8 mg, 13.4 μmol) was at first added with the PMO catalyst and potassium carbonate, purged with Ar, and iPrOH (5 mL) was added by syringe. This mixture was stirred at 50 ℃ in an

oil bath for 1 hour. Then the substrate solution in iPrOH (10 mL) was added to the resulting bright orange mixture. The following procedure was the same as above, except that a filtration through a short Celite plug and a washing with 1M HCl aq. were also performed at work up. ^{1}H NMR of the obtained orange oil (1.0 g) was measured, and the yield estimated at 99% by the internal standard of hexamethyl benzene. The spectra obtained were identical with those reported in the literature.[13]

1-phenylethanol ^{1}H NMR (400 MHz, CDCl$_3$) δ: 1.37 (d, 3H, J = 6.4 Hz), 2.13 (br, 1H), 4.72 (q, 1H, J = 6.4 Hz), 7.19 (m, 5H). ^{13}C NMR (100 MHz, CDCl$_3$) δ: 24.0, 68.9, 112.7, 112.8, 125.6, 129.2, 129.6, 137.0. SFC (OD-H, 1% MeOH, 2 mL/min, 200 bar, 40 ℃) 15.1, 16.6 min.

6.1.7 References for the experimental procedures for chapter 2

1   A. T. Vu, S. T. Cohn, E. S. Manas, H. A. Harris and R. E. Mewshaw, *Bioorg. Med. Chem. Lett.* 2005, **15**, 4520.

2   M. Berthod, C. Saluzzo, G. Mignani, and M. Lemaire, *Tetrahedron: Asymmetry,* 2004**, 15***,* 639.

3   G. A. Olah, Q. Wang, G. Sandford, and G. K. A. Prakash, *J. Org. Chem.* 1993, **58***,* 3194.

4   T. Shimada, M. Suda, T. Nagano, and K. Kakiuchi, *J. Org. Chem.* 2005, **70**,

10178.

5   M. Murata, M. Ishikura, M. Nagata, S. Watanabe, and Y. Masuda, *Org. Lett.* 2002, **4***,* 1843.

6   M. Murata, H. Yamasaki, T. Ueta, M. Nagata, M. Ishikura, S. Watanabe, and Y. Masuda, *Tetrahedron,* 2007, **63***,* 4087.

7   J. P. Collman, J. A. Belmont, and J. I. Brauman, *J. Am. Chem. Soc.* 1983, **105**, 7288.

8   Y. Maegawa, Y. Goto, S. Inagaki, and T. Shimada, *Tetrahedron Lett.* 2006, **47**, 6957.

9   S. MacQuarrie, M. P. Thompson, A. Blanc, N. J. Mosey, R. P. Lemieux, and C. M. Crudden, *J. Am. Chem. Soc.* 2008, **130**, 14099.

10   Based on; H.-C. Wu, J.-Q. Yu and J. B. Spencer, *Org. Lett.* 2004, **25**, 4675.

11   K. Mashima, K. Kusano, N. Sato, Y. Matshumura, K. Nozaki, H. Kumobayashi, N. Sayo, Y. Hori, T. Ishizaki, S. Akutagawa and H. Takaya, *J. Org. Chem.* 1994, **59**, 3064.

12   J.-P. Genêt, V. Ratovelomanana-Vidal, M. C. Caño de Andrade, X. Pfister, P. Guerreiro and J. Y. Lenoir, *Tetrahedron Lett.* 1995, **36**, 4801; A. R. McDonald, C. Muller, D. Vogt, G. P. M. van Klinka and G. van Koten, *Green Chem.* 2008,

10, 424. X. Wan, Y. Sun, Y. Luo, D. Li and Z. Zhang, *J. Org. Chem.* 2005, **70**, 1070.

13   T. Ohkuma, H. Ooka, S. Hashiguchi, T. Ikariya and R. Noyori, *J. Am. Chem. Soc.* 1995, **117**, 2675.

6.2   Experimental Procedures for chapter 3

6.2.1 General

Reagents and solvents were purchased from Aldrich and used as obtained unless otherwise noted. Elemental analysis was performed on a Thermo Scientific Flash 2000 Organic Elemental Analyzer equipped with a CHNS-TCD detector, V_2O_5 was added to sulfur containing samples. Nitrogen adsorption/desorption isotherms were collected at 77 K on a Micrometrics ASAP 2010 instrument. All SBA-15 and MCM-41 samples were degassed at 353 K for at least 6 hours prior to analysis. ^{1}H and ^{13}C NMR spectra were collected on a Bruker Advance 300, 400 or 500 MHz NMR spectrometer as indicated, chemical shifts are reported in ppm and referenced to residual solvent. ^{13}C and ^{29}Si CP-MAS NMR spectra were collected on a 600 MHz NMR spectrometer with spin rates of 10 000 Hz unless otherwise noted. Fluorescence spectra were acquired on a PTI

Fluorimeter equipped with an 814 Photomultiplier Detection System and LPS-220B

Xenon Arc Lamp Power Supply.

Solid state NMR spectra measured in Pruski's lab

^{13}C spectra were obtained using a 400-MHz Varian/Chemagnetics Infinity

spectrometer equipped with a 5-mm Chemagnetics T^3 probe at frequencies of 400.00

and 100.59 MHz for ^{1}H and ^{13}C, respectively, using the following parameters: ^{1}H-^{13}C

CP/MAS: ν_{RFH} = 45 kHz (during excitation, CP, and TPPM decoupling); ν_{RFC} = 55 kHz

(during excitation and CP); τ_{CP} =2ms; τ_{RD} =1.5s; NS=2000. For all samples, the ^{29}Si

spectra were obtained using a 400-MHz Varian/Chemagnetics Infinity spectrometer

equipped with a 5-mm Chemagnetics T^3 probe at frequencies of 400.00 and 79.46 MHz

for ^{1}H and ^{29}Si, respectively, using the following parameters: ^{29}Si DP-CPMG/MAS: ν_{RFSi}

= 55 kHz (during excitation and CPMG pulses); ν_{RFH} = 45 kHz (during TPPM

decoupling); n_{CPMG} = 10 echoes (only 3 used); τ_{CPMG} = 10 ms; τ_{RD} = 300 s; NS = 296.

^{1}H-^{29}Si CP/MAS: ν_{RFH} = 45 kHz (during excitation, CP, and TPPM decoupling); ν_{RFSi} =

55 kHz (during excitation and CP); τ_{CP} = 7.5 ms; τ_{RD} = 1 s; NS = 2000. The spectra for

proton spin-counting were obtained using a 600-MHz Varian spectrometer equipped with

a 1.6-mm Varian T^3 probe at a frequency of 599.6023864 MHz for ^{1}H using the

following parameters: ^{1}H DP/MAS: ν_{RFH} = 100 kHz (excitation pulse); τ_{RD} = 5 and 3 s

for the HMB standard and sample 2, respectively; NS = 4. The two-dimensional ^{1}H-^{29}Si

correlation spectrum was obtained using a 600-MHz Varian spectrometer equipped with

a 1.6-mm Varian T^3 probe at frequencies of 119.1142280 and 599.5998896 MHz, for ^{29}Si

and ^{1}H, respectively, using the following parameters: ^{1}H-^{29}Si CP-CPMG-HETCOR:

v_{RFSi} = 100 kHz (during excitation and CPMG pulses) and 94 kHz (during CP); v_{RFH} = 10,

60, and 100 kHz (during spinal-64 decoupling, CP, and excitation, respectively); n_{CPMG} =

49 echoes (45 were used); τ_{CP} = 15 ms; τ_{CPMG} = 4 ms; τ_{RD} = 1 s; NS = 300. A sample

spinning rate of v_R = 10 kHz was used for all experiments, with the exception of the

correlation experiment, which was obtained at v_R = 40 kHz. Any deviations from the

values listed above are explicitly specified in the relevant figure caption. Deconvolution

of the ^{29}Si DP-CPMG/MAS spectra was performed using three echoes and a global

Gaussian fit.

6.2.2 A series of SBA-15 materials

6.2.2.1 SBA-15

The condensation procedure was adapted from Stucky et al.[1] 4.0 g of P123 was

weighed into a 500 mL glass jar equipped with a magnetic stirring bar, 40 mL of distilled

water and 5.0 mL of conc. HCl was added and the resulting mixture was stirred at 40 °C

in an oil bath for approximately 4 hours until the mixture became homogeneous. To this solution, TEOS (9.0 mL) was added via syringe over a period of 1 min to the mixture, which was stirred vigorously at 40 °C for another 24 hours followed by at 80 °C for 48 hours. The as-synthesized material was recovered by filtration without washing and dried on a vacuum funnel for 1 hour. The surfactant of asSBA-15 was removed by Soxhlet extraction with ethanol for 48 hours or calcination in an oven at 550 ºC for 6 hours. The recovered material was further dried under 2 mmHg at 80 ºC in a flask overnight prior to any catalysis use or analysis.

6.2.2.2 SBA-15-SH

In a 10 mL round bottom flask equipped with a magnetic stirring bar, 200 mg of SBA-15 was added and charged with argon followed by an addition of 2.0 mL of toluene. To the suspension, 0.2 mL of MPTMS was added and the resulting mixture was stirred at 100 ºC in an oil bath for 24 hours. After cooling the mixture at room temperature, the material was recovered by vacuum filtration, washed with copious amounts of toluene, ethanol and acetone, and finally dried on a vacuum funnel for 15 min. The recovered material was further dried under 2 mmHg at 80 ºC in a flask overnight prior to any catalysis use or analysis.

6.2.2.3 reSBA-15

In a 250 mL glass jar, 20 g of P123 was dissolved in 70 mL of ethanol by vigorously stirring the mixture at 40 ºC. To the resulting solution was added 5.0 g of asSBA-15 and the suspension was stirred for 24 hours at room temperature. The material was recovered by vacuum filtration without washing, and was dried on a vacuum funnel for 1 hour. The recovered material was further dried under 2 mmHg at 80 ºC in a flask overnight prior to the following modifications.

6.2.2.4 sTMS-SBA-15

In a 250 mL round bottom flask equipped with a magnetic stirring bar, 5.0 g of reSBA-15 was added and the flask purged with argon. To the flask, 50 mL of HMDS was added and then the resulting suspension was stirred at room temperature for 3 hours. The material was recovered by vacuum filtration, washed with copious amounts of hexane, and dried on a vacuum funnel for 15 min. The surfactant was removed by Soxhlet extraction with ethanol for 48 hours. The recovered material was further dried under 2 mmHg at 80 ºC in a flask overnight prior to the following modifications.

6.2.2.5 sTMS-SBA-15-SH

In a 10 mL round bottom flask equipped with a magnetic stirring bar, 200 mg of sTMS-SBA-15 was added and the flask charged with argon followed by an addition of 2.0 mL of toluene. To the suspension, 0.2 mL of MPTMS was added and the resulting mixture was stirred at 100 ºC in an oil bath for 24 hours. After cooling the mixture to room temperature, the material was recovered by vacuum filtration, washed with copious amounts of toluene, ethanol and acetone, and finally dried on a vacuum funnel for 15 min. The recovered material was further dried under 2 mmHg at 80 ºC in a flask overnight prior to any catalysis use or analysis.

6.2.3 FloDots test

6.2.3.1 Preparation of FloDots

This procedure is adapted from Tan *et al.*[2] In a 20 mL dram vial equipped with a magnetic stirring bar, 7.5 mL of cyclohexane, 1.8 mL of 1-hexanol, 1.66 g of Triton® 100-X, 340 µL of distilled water, and 120 µL of dichloro tri(2,2'-bipyridyl) ruthenate 0.115 M aqueous solution were added, and the resulting bright orange solution was stirred vigorously for 10 min at room temperature. To this solution was added 100 µL of TEOS, followed by vigorous stirring for 10 min, and then 60 µL of 30% NH_3 aq. was

added. After 12 hours of stirring at room temperature, another 50 µL of TEOS was added

followed by 30 min of stirring again, and 66 µL of 3(trihydroxysilyl)propyl

methylphosphonate sodium salt 42 wt% aqueous solution was added and the resulting

mixture was stirred further 12 hours at room temperature. A half portion of this solution

was transferred to another 20 mL dram vial, and then 12.5 mL of EtOH was added to

both vials. Both were shaken well. These vials were centrifuged at 2000 rpm for 10 min,

and the supernatant was discarded. The precipitate was dispersed in 7.5 mL of tBuOH :

H_2O = 1 : 1 using a sonicator for 30 sec, and the resulting orange solution was again

centrifuged at 2600 rpm for 10 min. **The supernatant is the stock solution** employed at

the test, thus the supernatant was carefully transferred to a clean vial wrapped with

aluminum foil, and was kept under dark.

6.2.3.2 Differential adsorption of FloDots

In a 20 mL dram vial was added 35 mg of the SBA-15 samples and dispersed in

4.5 mL of tBuOH / H_2O = 1 / 1 solution. To this suspension was added 0.5 mL of the

FloDots stock solution as described above, and the vial was shaken well by hand, and left

stand overnight. The vial was centrifuged for 5 min at 2600 rpm, and the supernatant was

discarded. The residual solid was suspended in 2 mL of H_2O / EtOH = 4 / 1 solution with

150 mL of CTAB. The mixture was heated gently to dissolve CTAB, and then topped up

with water. The solid was recovered by vacuum filtration, and washed with water, EtOH, and hexane. In a vial was added 5 mg of the air-dried sample which was suspended in 3.5 mL of DMF. The fluorescence spectra of the materials were collected by stirring the sample in a quartz cuvette (10 mm) at the excitation wavelength λ_{ex} = 450 nm and the emission range at 500 – 700 nm with a step size and residence times of 0.5 nm and 1 sec respectively. Fluorescence spectra of the materials are shown in **Figure 3-7**.

6.2.4 Fluorescence quenching by size controlled gold nano particles (GNPs)

6.2.4.1 Preparation of size controlled GNPs

The original procedure was reported by Murphy and co workers.[3] A 20 mL aqueous solution containing 0.25 mM $HAuCl_4$ and 0.25 mM trisodium citrate was prepared in an Erlenmeyer flask. To the solution was added 0.6 mL of ice-cold, freshly prepared 0.1 M $NaBH_4$ aqueous solution dropwise with stirring. The solution turned pink immediately after adding $NaBH_4$, indicating particle formation. The particles in this solution were used as seeds within 2-5 h after preparation. In a 200 mL flask, 0.25 mM $HAuCl_4$ aqueous solution was prepared, to which was added 6.0 g of solid cetyltrimethylammonium bromide (0.08 M final concentration), and the resulting mixture

was heated until the solution turned a clear orange color. The solution was cooled to room temperature and used as a stock growth solution. Three 50 mL Erlenmeyer flasks were labeled A, B, and C. In set A, 7.5 mL of growth solution was mixed with 0.05 mL of freshly prepared 0.1 M ascorbic acid aqueous solution. To the solution was added 2.5 mL of seed solution dropwise with stirring. Stirring continued for 10 min after the solution turned wine red. Particles prepared this way were spherical with a diameter of 5.5 ± 0.6 nm. Similarly, 9 mL of growth solution and 0.05 mL of 0.1 M ascorbic acid solution were mixed as set B, and 1.0 mL of seed solution was added while vigorously stirring. Stirring continued for 10 min. The solution's final color was deep red. Particles prepared this way were spherical with a diameter of 8.0 ± 0.8 nm. The particles prepared here were used as seeds in set C, 30 min after preparation. In set C, 9 mL of growth solution was mixed with 0.05 mL of 0.1 M ascorbic acid solution, and 1.0 mL of the seed solution prepared in set B was added while stirring vigorously. Stirring was continued for 10 min. The final color of the solution was reddish brown. Particles prepared in this way were roughly spherical with a diameter of 17 ± 2.5 nm. This solution was used in the attempted fluorescence-quenching test.

6.2.4.2 Preparation of pyrenyl-functionalized SBA-15-SH

To a 10.00 mL volumetric flask was added pyrene-maleimide (3 mg, 0.01 mmol) and THF diluting up to 10 mL to give a 1.0 mM solution. To a 20 mL dram vial was added SBA-15-SH (50 mg, 0.06 mmol S at 1.2 mmol S/g) and THF (1 mL). To the suspension was added the pyrene-maleimide (1.0 mL, 1.0 μmol) stock solution which was prepared above, followed by triethylamine (50 μL). The reaction mixture was allowed to stand overnight at room temperature and the solution was decanted. The material was recovered by filtration and washed with copious amounts of THF and hexanes. The material was dried under vacuum at room temperature.

6.2.4.3 Fluorescence measurements

The fluorescence spectra of the materials were collected by stirring the sample at the excitation wavelength $\lambda_{ex} = 330$ nm and the emission range at 350 – 600 nm with a step size and residence time of 0.5 nm and 1 sec respectively. For the analysis, 3 mg of silica was weighed out in a dram vial and was suspended in DMF (10.0 mL). A portion (0.5 mL) of the silica solution was transferred to a quartz cuvette (10 mm) fitted with a stir bar, and the suspension was diluted to 3.5 mL with DMF. Fluorescence spectra of the materials are shown in **Figure 3-8**.

6.2.4.4 XPS analysis of GNP/SBA-15-SH-pyr samples

Table 6-1. XPS analysis of GNP/SBA-15-SH-pyr samples

GNPs on	Bonding energy / eV of detected elements		
	S(2p)	Si(2s)	C(1s)
A. sTMS-SBA-15/SH-pyr	163.86	154.28	-
B. SBA-15/SH-pyr	162.97	153.84	291.99
C. sTMS-SBA-15	-	154.14	-

6.2.5 TBDMS passivation of SBA-15

In a 20 mL glass vial, SBA-15 (200 mg), TBDMS chloride (200 mg, 1.32 mmol), imidazole (90 mg, 1.32 mmol) and dichloromethane (4 mL) were added and sealed with a screw Teflon cap. The mixture was stirred at 50 ºC on a heating stir-plate for 24 hours. The powder was recovered by vacuum filtration, washed with copious amounts of dichloromethane and dried on a funnel. 140 mg of the powder was recovered. Solid state NMRs are shown in **Figure 3-12** and **Figure 3-13**.

6.2.6 Direct functionalization on as-sTMS-SBA-15

In a 20 mL glass vial, as-sTMS-SBA-15 (200 mg), MPTMS (0.2 mL), and toluene (2.0 mL) were added and sealed with a screw Teflon cap. The mixture was stirred at 100 ºC on a heating stir-plate for 24 hours. The powder was recovered by vacuum filtration, washed with copious amounts of toluene and hexane and then dried on a funnel. 100 mg of the powder was recovered. Physical characteristic data from nitrogen adsorption are shown in **Table 3-4**.

6.2.7 References for the experimental procedures for chapter 3

1.   Zhao, D. Y.; Huo, Q. S.; Feng, J. L.; Chmelka, B. F. and Stucky, G. D., *J. Am. Chem. Soc.* **1998**, *120*, 6024.

2.   Bagwe, R. P.; Hilliard, L. R. and Tan, W., *Langmuir* **2006**, *22*, 4357.

3.   Jana, N. R.; Gearheart, L. and Murphy, C. J., *Langmuir* **2001,** *17*, 6782.

6.3   Experimental Procedures for chapter 4

6.3.1 General

Reagents and solvents

Methyl methacrylate (MMA, Tokyo Kasei, >99%) was dried overnight over calcium chloride, and purified by double distillation from calcium hydride before use.

Ethylene glycol dimethacrylate (EGDMA, Aldrich, >98%) was distilled from calcium hydride and stored in ampules as toluene solution before use. 4-Styryldiphenyl phosphine (SDP)[1] was prepared according to the literature. $RuCl_2(PPh_3)_3$ (Aldrich, >97%) was used as received and handled in a glovebox (M. Braun Labmaster 130) under a moisture- and oxygen-free argon atmosphere (H_2O < 1 ppm, O_2 < 1 ppm). Toluene was dried overnight over calcium chloride and distilled from sodium/benzophenone ketyl. *n*-Octane and tetralin were dried overnight over calcium chloride and were distilled twice from calcium hydride. *n*Bu_3N (Aldrich, >98.5%) and K_2CO_3 (Wako, >99.5%) were used as received. 1-Phenylethanol was distilled from calcium hydride before use. Acetone (Wako, for Organic Synthesis Grade, H_2O < 50 ppm) was degassed before use by freeze-thaw-pumping technique.

Measurements

The MWD, M_n, and M_w/M_n ratios of the polymers were measured by GPC in DMF containing 10 mM LiBr at 40 °C (flow rate: 1 mL/min) on three linear-type polystyrene gel columns (Shodex KF-805L; exclusion limit = $5 \cdot 10^6$; pore size = 20–1000 Å; 0.8 cm i.d. x 30 cm) that were connected to a Jasco PU-980 precision pump, a Jasco RI-930 refractive index detector, and a Jasco UV-970 UV/Vis detector set at 256 nm. The columns were calibrated against 13 standard PMMA samples (Polymer

Laboratories; M_n = 200–1200000; M_w/M_n = 1.06–1.22) as well as MMA monomer. The weight-average molecular weight (M_w) of the star polymers was determined by MALLS in DMF at 40 °C on a Dawn EOS instrument (Wyatt Technology; Ga-As laser, λ = 690 nm). The refractive index increment (*dn/dc*) was measured in DMF at 40 °C on an Optilab DSP refract meter (Wyatt Technology; λ = 690 nm, c < 8.0 mg/mL). ^{1}H NMR spectra were recorded in CD_2Cl_2 at 25 °C on a JEOL JNM-LA500 spectrometer, operating at 500.16 MHz. UV-Vis spectra were recorded in DCE at room temperature on Shimadzu MultiSpec-1500. ^{1}H and ^{13}C NMR spectra were recorded in $CDCl_3$ at room temperature on a JEOL JNM-LA500 spectrometer operating at 500 and 125 MHz respectively.

6.3.2 Synthesis of monomers

[1,1'-binaphthalene]-2,2'-diyl bis(2-methylacrylate) (1)

In a round bottom flask equipped with a magnetic stirring bar and a three-way stopcock, BINOL (1,1'-bi-2-naphthol, 1.0 g, 3.49 mmol) was weighed out and then the flask was filled with nitrogen. THF (17 mL) and triethylamine (1.07 mL, 7.68 mmol) were added and the resulting mixture was stirred at room temperature. To the solution was added methacryloyl chloride (0.676 mL, 6.99 mmol) dropwise, and then the mixture was stirred at 75 ºC in an oil bath for 14 hours. The reaction mixture was cooled to room

temperature, and then was poured into water with drops of NH₃ aq. in a flask. The mixture was extracted with DCM and was washed with water and brine, dried over MgSO₄, filtrated and concentrated by using rotary evaporator. The residual colorless oil was passed through a silica gel column with Hexane / Ethylacetate = 3 / 1 eluent to yield 1.45 g (97% yield) of the product. ^{1}H NMR (500 MHz, CDCl₃) δ ppm 1.60 (s, 6 H) 5.32 (t, J = 1.43 Hz, 2H) 7.48 (ddd, J = 7.99, 4.65, 3.58 Hz, 2H) 7.53 (d, J = 8.60 Hz, 2H) 7.95 (d, J = 8.11 Hz, 2H) 5.66 (t, J = 1.40 Hz, 2H) 7.33 (dd, J = 4.29, 0.95 Hz, 4H) H) 8.01 (d, J = 8.58 Hz, 2H).

2'-hydroxy-[1,1'-binaphthalen]-2-yl methacrylate (2)

In a round bottom flask equipped with a magnetic stirring bar and a three-way stopcock, BINOL (1,1'-bi-2-naphthol, 500 mg, 1.75 mmol) was weighed out and then the flask was filled with nitrogen. THF (10 mL), triethylamine (0.267 mL, 1.93 mmol) were added and the resulting mixture was stirred at 0 ℃ in an ice bath for 5 min. To the solution was added methacryloyl chloride (0.169 mL, 1.75 mmol) dropwise, then the mixture was stirred at room temperature for 10 hours. The reaction mixture was poured into water with drops of NH₃ aq. in a flask. The mixture was extracted with DCM and was washed with water and brine, dried over MgSO₄, filtered and concentrated by using rotary evaporator. The residual colorless oil was passed through a silica gel column with

214

Hexane / Ethylacetate = 3 / 1 eluent to yield 367.3 mg (59% yield) of the product. ^{1}H NMR (500 MHz; CDCl$_3$): δ 8.09 (d, J = 8.8, 1H), 7.98 (d, J = 8.2, 1H), 7.87 (d, J = 9.0, 1H), 7.83-7.81 (m, 1H), 7.51 (ddd, J = 8.2, 6.7, 1.5, 1H), 7.47 (d, J = 8.9, 1H), 7.36 (ddd, J = 8.4, 6.8, 1.4, 1H), 7.32-7.29 (m, 3H), 7.24 (ddd, J = 8.4, 6.9, 1.4, 2H), 7.09-7.07 (m, 1H), 5.71 (quintet, J = 1.1, 1H), 5.33 (quintet, J = 1.5, 1H), 1.61 (dd, J = 1.5, 1.0, 3H)

N,N'-([1,1'-binaphthalene]-2,2'-diyl)bis(2-methylacrylamide) (3)

In a round bottom flask equipped with a magnetic stirring bar and a three-way stopcock, BINAM (1,1'-binaphthyl-2,2'-diamine, 122.5 mg, 0.431 mmol) was weighed out and then the flask was filled with nitrogen. DCM (4.0 mL), triethylamine (0.132 mL, 0.948 mmol) were added and the resulting mixture was stirred at 0 °C in an ice bath for 5 min. To the solution was added methacryloyl chloride (0.091 mL, 0.948 mmol) dropwise, and then the mixture was stirred at room temperature for 3 hours. To the reaction mixture was diluted with water and extracted with ethylacetate. The organic layer was washed with diluted NH$_3$ aq. and brine, dried over MgSO$_4$, filtered, and concentrated by using rotary evaporator. The residual colorless oil (170 mg, 94% yield) was diluted in toluene as a 700 mM solution and then was used in polymerization without further purification. ^{1}H NMR (500 MHz; CDCl$_3$): δ 8.71 (d, J = 9.0, 2H), 8.08 (d, J = 9.1, 2H), 7.96 (d, J = 8.2,

2H), 7.46 (ddd, J = 8.1, 6.9, 1.2, 2H), 7.32 (ddd, J = 8.4, 6.9, 1.4, 4H), 7.17 (dd, J = 8.5,

0.8, 2H), 5.14 (s, 2H), 5.08 (t, J = 0.7, 2H), 1.53 (t, J = 1.1, 6H)

6.3.3 General synthetic procedure for starpolymers by ruthenium catalyzed Living radical polymerization[2]

The PMMA arms were synthesized as DP = 100 condition, thus MMA (2.0 M),

ECPA (20 mM), $RuCl_2(PPh_3)_3$ (10 mM) and nBu_3N (40 mM) in toluene at 85 ºC.

Crosslinking was carried out in one pot to the batch of PMMA arm polymerization when

the MMA conversion reached to 90%, in 48 hours. EGDMA (200 mM), SDP (50 mM)

and another portion of $RuCl_2(PPh_3)_3$ (10 mM) in toluene was added. Thus, in a 20 mL

Schlenk flask equipped with a magnetic stirring bar and a three-way stopcock, 52.4 mg of

$RuCl_2(PPh_3)_3$ was carefully weighed out using a globe box. To this flask was added 3.28

mL of toluene, 0.291 mL of n-octane (internal standard for GC), 0.546 mL of nBu_3N

(400mM toluene solution), 1.163 mL of MMA and 0.177 mL of ECPA (620 mM toluene

solution), and the resulting mixture stirred at 85 ºC in an oil bath. The MMA conversion

was monitored by the GC. When the MMA conversion was confirmed as 90%, in another

Schlenk flask equipped with a three-way stop cock, 23.01 mg of $RuCl_2(PPh_3)_3$ was

weighed out carefully and then 0.797 mL of toluene, 0.024 mL of tetralin (internal

standard for NMR), 0.256 mL of EGDMA (1872.49 mM toluene solution) and 0.119 mL

of SDP (1000.8 mM toluene solution) were added. The second mixture was swirled in an oil bath at 85 ºC for a few seconds, and the dark red solution was transferred to the first flask by a syringe under strong argon flow through the three-way stopcock. The conversions of EGDMA and SDP were monitored by the GC and ^{1}H-NMR respectively. EGDMA was substituted by the same molar amount of mono- and divinyl-monomers for synthesizing the other starpolymers containing chiral core gels.

6.3.4 Hydrogen transfer oxidation reaction

The reaction was performed by the syringe technique under argon in a baked three-necked round bottom flask equipped with a three-way stopcock, a reflux condenser, and a magnetic stirring bar. In the flask was placed 300 mg of star polymer (~0.01 mmol Ru) and 138 mg of K_2CO_3 (1.0 mmol), 10 mL of acetone and 1.21 mL of 1-phenylethanol (10 mmol) was added at room temperature under argon. The flask was placed in an oil bath at 65 °C. In predetermined intervals, aliquots were removed by syringes for measurement of conversion by gas chromatography.

6.3.5 References for the experimental procedures for chapter 4

1.   Rabinowitz, R.; Marcus, R.; Pellon, J. *J. Polym. Sci., Part A,* **1964**, *2*, 1241.
2.   Terashima, T.; Kamigaito, M.; Baek, K.-Y.; Ando, T. and Sawamoto, M., *J. Am. Chem. Soc.* **2003**, *125*, 5288.